

Ludwig-Maximilians-Universität München
Fakultät für Geowissenschaften
Department für Geographie

MASTERARBEIT
Umweltsysteme und Nachhaltigkeit
Monitoring, Modellierung und Management

Wissenschaftliche Arbeit zur Erlangung des akademischen Grades Master of Science

Radar Interferometry as a technique for mapping peatland surface deformation around energy development infrastructure in Northern Alberta

Radarinterferometrie als Methode zur Kartierung der
Oberflächenverformung von Moorlandschaften im Bereich von
Energieentwicklungsinfrastruktur in Nord-Alberta

Betreuer:
Prof. Dr. Ralf Ludwig

Mitbetreuung:
Prof. Dr. Greg McDermid
(University of Calgary)

Prof. Dr. Scott Ketcheson
(Athabasca University)

Verfasser:
Niklas Daniel Heiß
Reutenbergstraße 16, 87784 Westerheim
Niklas.Heiss@campus.lmu.de / nickhot@web.de
Matrikelnummer: 11721477

Abgabedatum:
21.06.2023

Acknowledgement

First and foremost, I want to thank my supervisor Prof. Ralf Ludwig at Ludwig-Maximilians-University Munich, who made the internship at University of Calgary (UofC), Canada possible in the first place. He was instrumental in the execution of this project and he and his team with Verena Garcia and Yueli Chen supported me with their advice and valuable suggestions throughout the whole process of this master thesis.

I also would like to thank Prof. Dr. Greg McDermid, who warmly integrated us into his team at UofC and the Boreal Ecosystem Recovery and Assessment (BERA) project. This was the beginning of a sensational and productive time. Besides the possibility to plan and execute an own project with your support, I would like to explicitly thank you for letting me get a taste of various research projects and deep insights into applied research like the drone studies on the Athabasca Glacier or the Reclamation work on Ya Ha Tinda Ranch. Those are great memories that remain.

Prof. Dr. Scott Ketcheson played a major role in conducting and organizing my fieldwork on the ASPEN lease. Thanks for your support with all problems and challenges and your scientific advice.

I want to thank everyone within the Applied Geospatial Research Group and the BERA project. Dr. Julia Linke for all the organizational support, Alejandro Caguao, Sean Hillson, Hunter Jackson, Sara Heerema and Cameron Torrance for the constructive discussions and for welcoming us so wholeheartedly in Calgary, Dr. Richard Zeng and Maverick Fong for the IT support, and especially Dr. Irina Terenteva & Tony Terenteva, Lelia Weiland & Joseph Tuffner for always inspiring me in all kinds of matter.

Marlis Hegels, Jasper Koch, Patrick Klotz – it was a blast working, living and traveling together. Thanks for the conversations, help and fun hours. Simply an awesome time with you.

My stay in Canada was funded by Mitacs Globallink, the BERA project, the University of Calgary and the Ludwig-Maximilians-University (LMU) Munich.

Culminating 6 years of study in geography at LMU, I take this opportunity to thank all the people that have accompanied me through this amazing time marked by achievements,

field trips and experiences that will be remembered a lifetime long. Thanks to my father for his financial support and to my brother for being the best since times immemorial.

I would like to end the words of acknowledgement with a quote that helps me through life and comes from the best carpentry boss:

Goat id, gait's id!

(Geht nicht, gibt es nicht! – Everything is possible)

Abstract

This study presents an in-depth examination of the surface deformation of boreal peatlands around energy development infrastructure with focus on edge effects on mineral-filled resource access roads, an area of strong scientific interest due to their vulnerability to hydrological changes. In this thesis Interferometric Synthetic Aperture Radar (InSAR) techniques are employed, namely Persistent Scatterer Interferometry (PSI) and Small Baseline Subset (SBAS) to determine and characterize the effects of anthropogenic impacts on the complex boreal peatland environments in Aspen, northeast of Fort McMurray, Alberta, Canada.

A key revelation of this study is the evident discrepancy between the PSI and SBAS timeseries, with differences of the two methodological approaches outweighing distinctions among diverse ecosites and between upstream and downstream side of the Aspen Road. Factors such as inadequate spacing and data resolution contribute to this limitation and highlight the necessity of careful interpretation as well as prudent methodological choices.

The examination of the 2021 dataset, where both methodological approaches show a similar pattern underscores the potential of InSAR to extract valuable information. Despite the qualitative character of results, the statistical robustness for quantification of the surface deformations remains challenging.

The conducted research further demonstrates the utility of velocity maps, especially based on the SBAS results. It offers detailed spatial characteristics, especially in vegetated areas, where PSI technique struggles due to incoherence. This reinforces the value of using complementary InSAR methods in capturing comprehensive range of surface deformation. The yearly velocity analysis reveals spatial patterns that can be connected to the level of functionality of the installed culverts.

In conclusion, the potential and complexities of employing InSAR techniques on edge effects in monitoring boreal peatland surface deformation are recognized. The findings underscore the potential of InSAR methods to contribute valuable insights, aid planning and decision-making as well as monitoring the integrity or disturbances in the boreal wetlands of northern Alberta.

Table of Contents

Acknowledgement	II
Abstract	IV
List of Figures	VI
List of Tables	VIII
List of Acronyms	IX
1. Introduction	1
1.1 Motivation and State of the Art	1
1.2 Research Objectives	4
1.3 BERA Project	5
2. Materials and Methods	7
2.1 Study Area	7
2.2 Data	11
2.2.1 Sentinel 1	11
2.2.2 Meteorological Data	14
2.2.3 Groundwater Level Data and Culverts	16
2.3 InSAR Methods	20
2.3.1 Persistent Scatterer Interferometry Workflow	22
2.3.2 Small Baseline Subset Workflow	26
2.3.3 Post-Processing in RStudio	29
3. Results	31
3.1 PSI and SBAS Timeseries Analysis	31
3.2 Focus on 2021 Data	44
3.3 Spatial Distribution of Yearly Velocity Rates of West Orbit Track Data	46
4. Discussion	52
5. Conclusion and Outlook	60
References	62
Appendix	X

List of Figures

Figure 1: Oil Sands Areas in Alberta (AOS). The deposit areas are marked with orange and the surface minable areas with purple. The area is categorized into Peace River, Athabasca and Cold Lake deposits. Most of the area is in Alberta's boreal forest (King and Yetter, 2011).3

Figure 2: BERA project diagrams of the Remote Sensing (upper) and Carbon Dynamics (lower) theme complex. Each theme addresses strategic priorities that are coupled with one or more tactical deliverables. In red is marked where this thesis contributes to the goal and interferes with the high priority targets (adapted BERA 2023).6

Figure 3: Overview of the Aspen study area. In the left top corner, the Aspen Road connects to the East Athabasca Highway. The blue crosses mark the effective installed culverts (scouted in June 2023), the orange crosses the semi-effective culverts and the red crosses the ineffective culverts. The Bog polygons are in green hatched, the fen ones in orange cross hatched. In the East on the large vegetation cleared area the weather station is installed. The groundwater wells installed by Dr. Scott Ketchesons lab from Athabasca University are symbolized with blue droplets. GCS WGS 1984 is applied.8

Figure 4: Ecosite types in the study area. It shows the wetland classification provided by Imperial. The culverts and groundwater wells are symbolized by crosses and droplets respectively. The polygons of the Bog and Fen are located north and south of the road and named B1 for Bog north and B2 for south, as well as F1 and F2 for the fens. Spatial reference: NAD 1983 UTM Zone 12N.9

Figure 5: Ascending Sentinel 1 orbit tracks 49 (West), 78 (East) and 151 (Middle) covering the AOI (yellow). The figure is north oriented (ASF 2023a).12

Figure 6: Descending Sentinel 1 orbit track 79 covering the AOI (yellow). The figure is north oriented (ASF 2023a).12

Figure 7: Kearl Weather Station data from 2019 to 2022 in the snow free study period from May to October (inclusive). X-axis is the time, y-axis on the left side displays the temperature amplitude in °C. On the second y-axis (right) the precipitation amount in mm is displayed. The red line represents daily average temperature, in blue bars the daily precipitation amounts are visualized (data provided by Imperial, 2022).16

Figure 8: Timeseries of water table depth of 4 selected groundwater wells in the study area. The surface is defined as 0 and below surface as negative values. The values are in centimetres The groundwater wells are MART2_5 (blue), MART4_NC_2 (light blue), MART3_EC_3 (lime-green), MART1_5 (forest-green). The light-blue line shows the confidence interval, smoothed line and non-smoothed line.16

Figure 9: In-depth focus on culverts label and position and the selected groundwater wells (green). The culverts are classified, following table 3, as effective (blue), semi-effective

(orange) and ineffective (red). The map shows the analysis relevant culverts. Spatial reference: GCS WGS 1984.....	17
Figure 10: Images of culverts EC11 – effective, EC7 semi-effective and EC6 – ineffective. The left column shows the upstream side and the right column the downstream one (Photos taken by Dr. Scott Ketecheson and Lelia Weiland in June 2023).	19
Figure 11: Example baseline plot for (a) the PSI and (b) the SBAS method based on the data from 2022 East Orbit track.....	21
Figure 12: TOPSAR Split Operator for the Master images. Example is chosen from the Middle Orbit. Selected Options are VV polarization, the IW2 subswath and the bursts 2 to 5 in order to cover the AOI.	23
Figure 13: PSI workflow for processing Sentinel-1 images with SNAP, SNAP2StaMPS and StaMPS (based on Mancini et al.(2021)).....	25
Figure 14: Workflow diagram of the SBAS approach. Processes are in light blue, the used parameters and properties in light yellow brown.	28
Figure 15: Timeseries plots for PSI and SBAS method results for the years 2019 – 2022. The plots are created for each Ecosite, respectively B1, B2 (for the Bog north and south of the road) and F1, F2 (for the Fen north and south of the road). The orbit tracks are represented by the colours green = West, yellow = Middle, and magenta = East, if the orbit track data is available in the specific year. On the x-axis the timeline is shown with explicit dates of the image acquisition. The y-axis shows the mean LOS displacement value of all valid pixels within a ecosite shapefile in mm.	42
Figure 16: Timeseries 2021 focus on statistical parameters. West, Middle, East orbit track timeseries data of the SBAS method are merged and displayed with boxplot diagrams. Median = black horizontal line in box, mean = red cross, mean \pm standard deviation = horizontal whiskers, median \pm 1.5 IQR = length of vertical whiskers, extent box = IQR, outlier = black dots, trend of this merged timeline = purple dashed line with confidence interval.	44
Figure 17: Displacement differences over time. In green is the difference between shapefile mean values of B1 – B2, in blue for F1-F2.	46
Figure 18: Spatial distribution of yearly LOS rates in mm generated from West Orbit track data. The SBAS results are illustrated from 2019 till 2022. The PSI only for 2019. The Figure shows velocity rates from -100 mm/year to +80 mm/year. The scale is on all graphs identical. Symbology: Blue = Water Mask, White shapefile = road, Ecosite Shapefile border = black, ineffective Culverts = red cross, effective culvert = blue cross. Spatial reference: NAD 1983 UTM Zone 12N.....	51

List of Tables

Table 1: Overview of the data availability the various orbit tracks of Sentinel 1 covering the AOI during the snow free period. Data has been retrieved through ASF API.....	13
Table 2: Statistical weather station data from Kearl (black) and Aspen (blue) through the study period. Note that the Aspen station has been installed in September 2020 (Data provided by Imperial).....	14
Table 3: Culvert overview. Name, function and description of culverts within the study area Aspen. (Data provided by Dr. Scott Ketcheson, June 2023).	18
Table 4: Statistical parameters of PSI timeseries analysis, namely R^2 , RMSE and retrieved from the Mann-Kendall timeseries trend test τ . If the τ result is statistically significant with p-value < 0.05 its cell is marked in light yellow.	42
Table 5: Statistical parameters of SBAS timeseries analysis, namely R^2 , RMSE and retrieved from the Mann-Kendall timeseries trend test τ . If the τ result is statistically significant with p-value < 0.05 its cell is marked in light yellow.	43
Table 6: Statistical parameters of the 2021 merged orbit track data timeseries, calculated with the SBAS method. τ and p-value are calculated with the Mann-Kendall test.	46

List of Acronyms

ABMI	Alberta Biodiversity Monitoring Institute
AOI	Area Of Interest
AOS	Alberta Oil Sands
ASF	Alaska Satellite Facility
BERA	Boreal Ecosystem and Recovery and Assessment
BS	Shrubby Bog
BWc	Wooded coniferous Bog
C	Carbon
DEM	Digital Elevation Model
DS	Distributed Scatterer
ESA	European Space Agency
FS	Shrubby Fen
FWc	Wooded coniferous Fen
GNSS	Global Navigation Satellite System
InSAR	Interferometric SAR
IQR	Inter-Quartile Range
LMU	Ludwig-Maximilians University
LOS	Line of Sight
MintPY	Miami InSAR time series software in Python
NAD83	North American Datum
NASA	National Aeronautics and Space Administration
PSI	Persistent Scatterer Interferometry
RMSE	Root Mean Square Error
SAR	Synthetic Aperture Radar
SBAS	Small Baseline Subset
SNAP	Sentinel Application Platform
StaMPS	Stanford Method of Persistent Scatterers
TOPSAR	Terrain Observation with progressive Scans SAR
UofC	University of Calgary
UTM	Universal Transverse Mercator
WT	Water table

1. Introduction

1.1 Motivation and State of the Art

Peatlands, defined as wetland ecosystems with >40 cm of organic matter, are an integral part of the boreal landscape, important reservoirs of global terrestrial carbon (C) and are strongly linked to hydrological processes from the pore space to landscape scale (Plach et al., 2017; Price, 2003; Willier et al., 2022). They provide essential ecosystem and landscape functions, including being key to flood storage and desynchronisation, groundwater recharge and discharge, dissipating erosive forces and playing major roles as habitat for other biota (Howie and Hebda, 2018; Plach et al., 2017; Price, 2003; Willier et al., 2022). Water supply, driven by Water Table (WT) depth and soil moisture, influences environmental parameters like soil temperature, vegetation composition and microbial communities and activity (Plach et al., 2017). The peatlands of Western Canada cover 365 157 km² and store 2.1% of the world's terrestrial C (Vitt et al., 2000). 30% of the boreal region of Canada on average is covered by peatlands (Downing and Pettapiece, 2006, p. 46).

As the Alberta Oil Sands (AOS), representing one of the world's largest oil deposits, are located in the boreal area, this natural system is impacted by numerous anthropogenic disturbances, mostly through energy development infrastructure (Canadian Association of Petroleum producers, 2022 (CAPP), Figure 1). The AOS industrial operations necessitate a variety of facilities and transformation on the landscape for open pit mining and in situ extraction techniques, since much of the deposits are too deep for surface mining. Those industrial activities threaten peatland integrity in boreal forests and include the construction of seismic lines (petroleum-exploration lines), pipelines, powerlines, well pads and interconnecting resource access roads (Roberts et al., 2022; Willier et al., 2022). Although resource access roads occur in many areas of the boreal forest, they are particularly dense in the province of Alberta due to the AOS. The construction process raises the road above the peat surface and involves initial clearing of the vegetation, in some cases placing surficial soil layers, geotextile and stockpiling of excess materials, before placement of the mineral fill layer, which can be several meters thick (Plach et al., 2017; Saraswati et al., 2020b; Saraswati and Strack, 2019). These roads can have considerable effects on local hydrology when constructed in peatlands as they cause

hydrological disruption, especially when built perpendicular to flow direction. Acting as dams, they limit the hydrological connection between fragmented parts of the peatland and therefore block surface and subsurface water flow, leading to bilateral flooding and drying (Saraswati and Strack, 2019; Willier et al., 2022).

These disturbances lead to changes in the hydrological regime, resulting in diverse effects on vegetation. The upstream side of the road experiences more flooding, causing mortality or stunted growth in woody vegetation due to poor oxygen conditions in the root zone (Saraswati et al., 2020a). Conversely, the downstream side may suffer from a prolonged drop in the WT, leading to deeper root systems, increased growth in woody plants and inducing a positive feedback drying loop that would enhance the ecosystem impact of infrastructure within wetlands (Saraswati et al., 2020b; Willier et al., 2022). These hydrological impacts likely vary between peatland types, depending on hydromorphic setting and directionality of water flow relative to the orientation of the constructed road. Other authors anticipate mitigation of those edge effects through improved road building and adequate culvert installation (Willier et al., 2022), whereas in long-term it is evident that the upstream side of the road will experience flooding (Bocking et al., 2017; Ducks Unlimited Canada, 2016, p. 15; Willier et al., 2022). On a large scale, the wetlands of Canada play a major role in C sequestration and storage with their C balance being driven by their hydrological regime. Any resource management activity that disrupts the ability to sequester C must come under increased scrutiny and those impacts and effects must be understood in their full extend (Ducks Unlimited Canada, 2016).

Peatland surfaces are particularly dynamic and move in response to changes in the mass of water, gas and organic matter stored within the peat body (mire breathing). This rising and lowering of the surface is one of the key self-regulating feedback mechanisms providing resilience and maintaining function during periods of hydrological stress and is based on a poro-elastic mechanical response to ecohydrological processes. Changes are caused by both seasonal and long-term environmental change (Alshammari et al., 2020; Bradley et al., 2021; Howie and Hebda, 2018). The subject of this study is the change caused by the resource access road built during 2017 – 2019 in ASPEN on the Imperial Oil Resources Limited's (herein Imperial) in-situ lease (referred to as 'Aspen') 45 km northeast of Fort McMurray. As field-based techniques to measure surface deformation are not cost-

effective over large areas and long time periods, the remote sensing technique of interferometric synthetic aperture radar (InSAR) is a promising alternative (Alshammari et al., 2020; Hoyt et al., 2020; Tampuu et al., 2020).



Figure 1: Oil Sands Areas in Alberta (AOS). The deposit areas are marked with orange and the surface minable areas with purple. The area is categorized into Peace River, Athabasca and Cold Lake deposits. Most of the area is in Alberta's boreal forest (King and Yetter, 2011).

“Remote Sensing data can greatly contribute to the monitoring task by providing timely, synoptic, cost-efficient and repetitive information about the status of the Earth’s surface” (Atzberger, 2013).

Recent developments in the use of Satellite InSAR to measure seasonal oscillation of peatland surface at the site or landscape scale have shown to be highly diagnostic of peatland character and condition (Alshammari et al., 2020; Bradley et al., 2021; Hoyt et al., 2020; Marshall et al., 2022; Tampuu et al., 2020). As proposed methods to measure the surface deformations there are the persistent scatterer (PS) and distributed scatterer (DS) approaches as well as mixed forms. Though coherence and interferometric phase are two major products of InSAR processing, the data of low coherence are usually, in PS and DS approaches, considered to prove little or no value. Nevertheless, Tampuu et al. (2020) use the temporal and spatial variation of coherence to provide useful information about

hydrological conditions and vegetation cover, allowing delineation of the area inundated with surface water and distinguishing different wetland types and assessing short and long-term changes. Several studies show that time series InSAR analysis has the potential to characterise seasonal mire breathing and long term trends, which are important for assessing the WT dynamics, restoration success or to improve spatial models of material flow and gas exchange in northern temperate peatlands (Alshammari et al., 2020, 2018; Crosetto et al., 2016; Howie and Hebda, 2018; Hoyt et al., 2020; Izumi et al., 2022; Khodaei et al., 2023; Lanari et al., 2007; Marshall et al., 2022; Mohammadimanesh et al., 2018; Tampuu et al., 2020; Zhou et al., 2019). The edge effects of a resource access road disturbing a peat in the boreal region have been examined by several studies, but have not yet been fully explored (Elmes et al., 2021; Liu et al., 2015; Plach et al., 2017; Saraswati et al., 2020a; Saraswati and Strack, 2019). To the authors knowledge there is no study trying to assess the extent and magnitude of access road edge effects using satellite InSAR methods.

This thesis focuses on applying radar remote sensing timeseries analysis of said resource access roads and their edge effects. Understanding provides information that can be used to inform road planning and mitigation strategies in peatlands, as well as inform buffer size considerations when assessing the effects of roads on their surrounding area.

1.2 Research Objectives

As stated, there is an immediate and critical research need in the analysis of edge effects of disturbances in wetlands caused through development of infrastructure. The Aspen Road is an opportunity to evaluate the temporal response of a wetland structure and function over time and represents a unique possibility to produce the first information of this kind in the region. Subsequently a timeseries remote sensing approach is used from 2017 to 2022, taken only the snow-free period into account, to clarify the two objectives:

- 1) Apply and compare two radar remote sensing techniques, Persistent Scatterer Interferometry (PSI) and Small Baseline Subset (SBAS), for characterizing surface deformation in boreal peatlands.

- 2) Assess and quantify the spatial and temporal extent of energy development infrastructure, with focus on mineral-filled resource access roads, on surface deformation within various wetland types in northern Alberta.

1.3 BERA Project

This thesis was conducted within the Boreal Ecosystem and Recovery Assessment (BERA) project. The project is a multi-sectoral research partnership of academic institutions, private sector companies, a public sector division and a not-for profit organization. The project focuses on roads, well pads, seismic lines, forest-harvest areas, and other elements of anthropogenic footprints in the boreal forest of Alberta. The central goal is to understand the impacts and effects of those anthropogenic and especially industrial disturbance on natural ecosystem dynamics. It is aimed for the development of strategies for restoring those disturbed landscapes in a system under climate change pressure. A disturbance is defined as an event that causes a change in the physical characteristics and properties of a environment and disrupts the ecosystem (Bartels et al., 2016). The main objectives associated with industrial disturbance are promoting a return to forest cover, restoring natural carbon dynamics, maintaining wildlife habitat and enhancing woodland caribou habitat, a species-at-risk in Alberta (BERA 2023; Filicetti et al., 2019). There are four teams within BERA: Vegetation, Soils and Ecohydrology, Humans and Wildlife, and Remote Sensing (RS). The thesis is part of the work of the remote sensing team (project code RS3.1) and is strongly connecting to the Soils and Ecohydrology team through the WT parameter. The focus of the RS team is to develop workflows and planning tools to assist management and research activities associated with assessment and monitoring of disturbances and restoration. The Carbon dynamics team goal is to understand and quantify the impact of various factors on ecosystem C dynamics as well as identifying the effects of disturbances on soil C cycling and vegetation composition, in order to develop best practices for the recovery of natural C dynamics (BERA 2023). The process diagrams of the RS and Carbon dynamics team depict a subset of the high-priority targets. The key areas of focus and interactions within this study are indicated by the red markings (Figure 2).

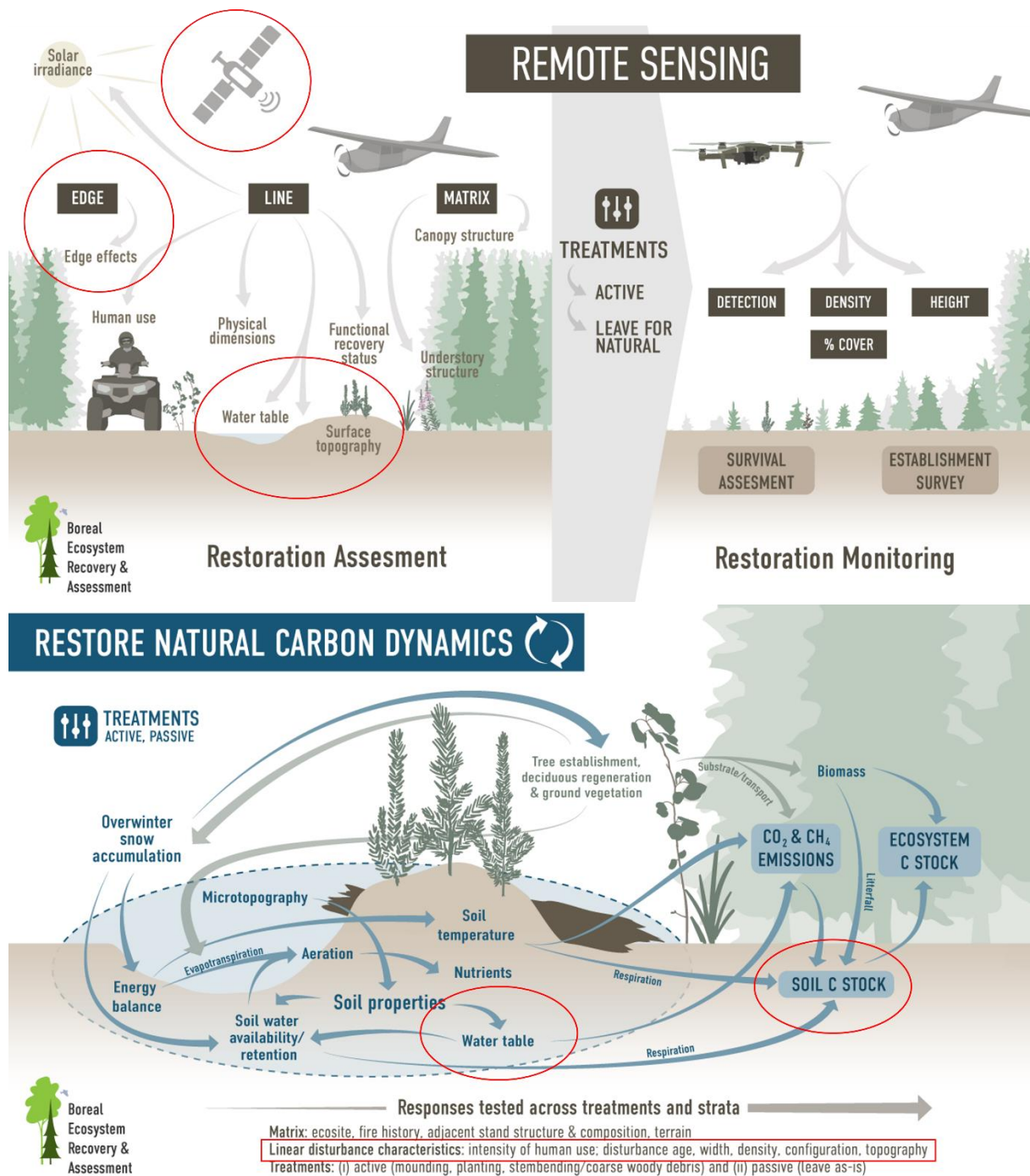


Figure 2: BERA project diagrams of the Remote Sensing (upper) and Carbon Dynamics (lower) theme complex. Each theme addresses strategic priorities that are coupled with one or more tactical deliverables. In red is marked where this thesis contributes to the goal and interferes with the high priority targets (adapted BERA 2023).

2. Materials and Methods

2.1 Study Area

The study area is located about 45 km northeast of Fort Mc Murray, Alberta and connects to the East Athabasca highway (Figure 3). The Imperial lease is called Aspen and consists of 75% wetland cover making it an ideal area to evaluate wetland response to energy industry development. The Aspen facility contains a relatively new access road, where the vegetation was cleared before 2017 and therefore peat has already been compressed. According to Sentinel 2 images from ESA Copernicus Sentinel-Hub the mineral layer has been added in the winter season 2018/2019 between November and February. In addition to the road construction, in the surrounding area typical in-situ infrastructure at various stages of construction, including cleared but not yet constructed well pads and road sections have been built. The project framework is a \$2.6 billion investment to develop 75,000 barrels per day of bitumen production (Imperial, 2018). The project got ramped down in March 2019 due to market uncertainty.

Figure 3 displays the AOI encompassing the Aspen lease, the road infrastructure and the placement of groundwater wells installed in August 2021 and the meteorological station, installed in September 2020. There is a second weather station northwest on the Kearn lease. The map indicates the location of effectively and ineffectively installed culverts in red and blue crosses.

According to Alberta Parks (2015), the study area is situated in the boreal forest natural subregion. The plant communities are largely determined by the presence of wetland ecosystems or drier upland regions. The wetland classification map (Figure 4) shows the different wetland types and the shapefiles used for this study. The study differentiates between a bog and a fen, and the polygons are drawn north and south of the road for each ecosite type. The shapefiles cover an area in between 250 and 300 m of distance from the road in perpendicular direction. This is done analogously to the positioning of the groundwater wells. From now on it is referred to the various ecosites as B1 and B2 for the bog north and south of the road and F1 (north) and F2 (south) for the fen. The bog shapefiles consist of a shrubby bog (BS) and a wooded coniferous bog (BWc). The fens subtypes have similar classifications, namely shrubby fen (FS) and wooded coniferous fen (FWc).

Aspen study area

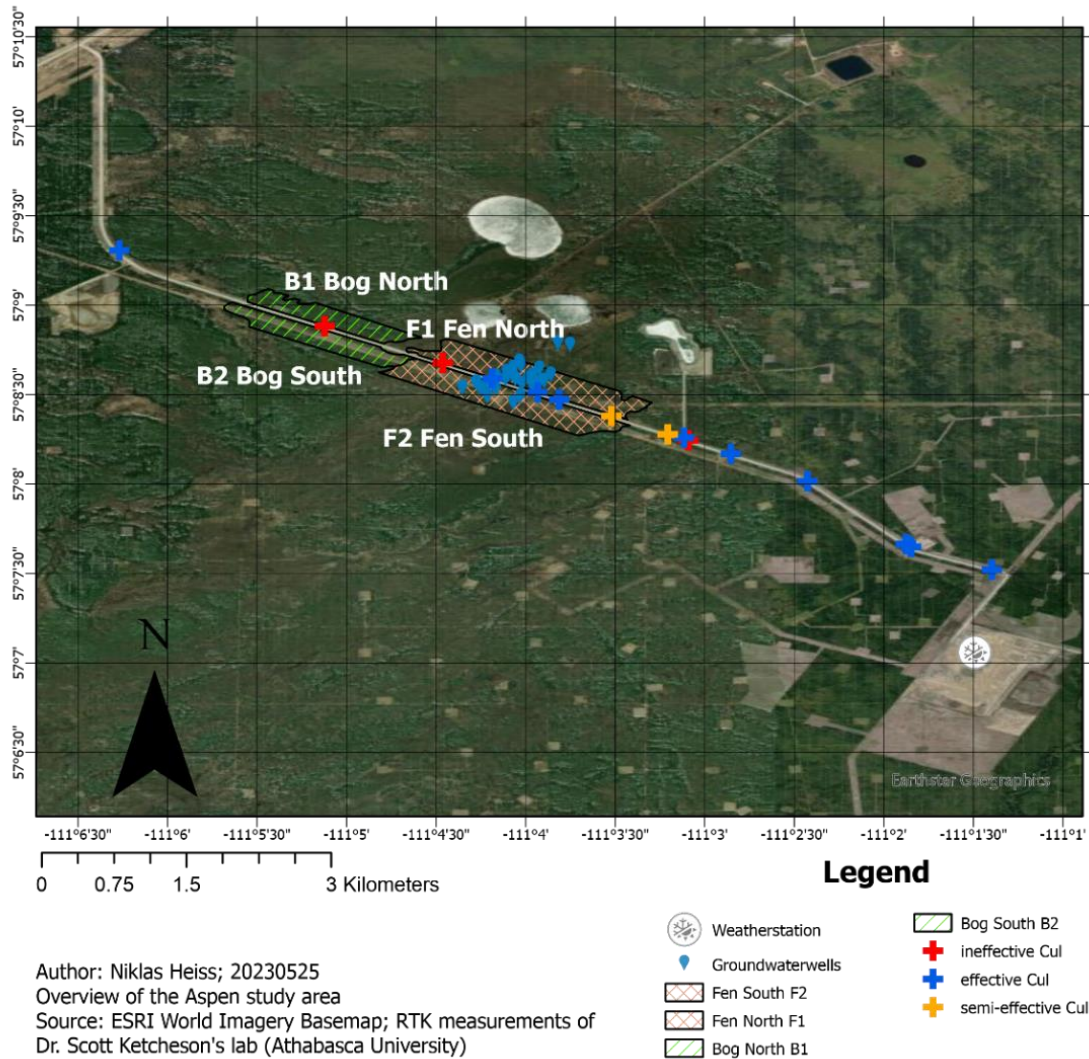
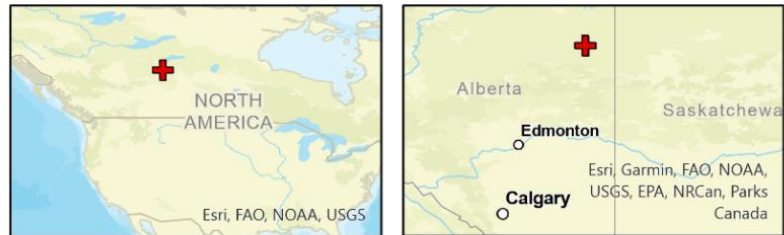


Figure 3: Overview of the Aspen study area. In the left top corner, the Aspen Road connects to the East Athabasca Highway. The blue crosses mark the effective installed culverts (scouted in June 2023), the orange crosses the semi-effective culverts and the red crosses the ineffective culverts. The Bog polygons are in green hatched, the fen ones in orange cross hatched. In the East on the large vegetation cleared area the weather station is installed. The groundwater wells installed by Dr. Scott Ketcheson's lab from Athabasca University are symbolized with blue droplets. GCS WGS 1984 is applied.

AOI Ecosites with Fen & Bog shapefiles for analysis

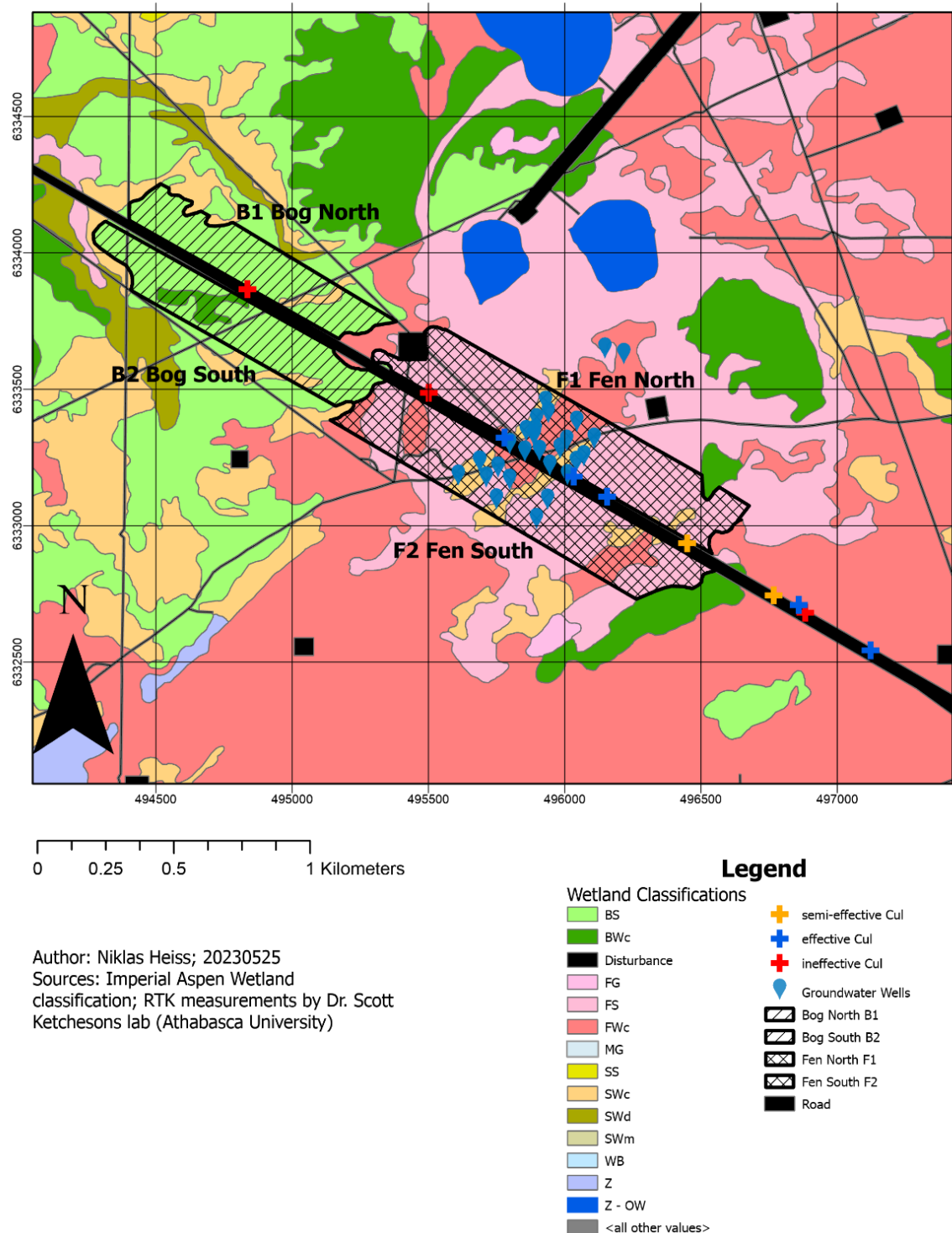


Figure 4: Ecosite types in the study area. It shows the wetland classification provided by Imperial. The culverts and groundwater wells are symbolized by crosses and droplets respectively. The polygons of the Bog and Fen are located north and south of the road and named B1 for Bog north and B2 for south, as well as F1 and F2 for the fens. Spatial reference: NAD 1983 UTM Zone 12N.

A bogs ground surface is composed of peat and is isolated from surface water and groundwater influences due to elevation; it is typically >40 cm above the WT. Elevation of the ground surface can result from the accumulation of peat and as a result bogs are ombrogenous systems fed exclusively by precipitation (Government of Alberta, 2015). Bogs are permanent wetlands as their moisture levels are effectively maintained by the capillary action of *Sphagnum* mosses. The primary production exceeds decomposition. Wooded bogs are defined by a tree cover >25 % by coniferous species, predominantly black spruce. The trees tend to be small, stunted, and rarely reaching heights greater than ten metres. Common Labrador Tea is the predominant understory shrub, interspersed by cranberry species. Shrubby bogs have >25 % shrub cover and less than 25 % tree cover. Most shrubs are less than one metre tall. Shrub and ground cover species are similar in wooded and shrubby bogs (Ducks Unlimited Canada, 2016; Government of Alberta, 2015).

Fens are minerogenous peatlands, meaning they receive water from a variety of sources as precipitation, groundwater and/or surface and subsurface flows. Fens are permanently saturated wetlands and have fresh to slightly brackish water. The vegetation is typically dominated by sedges. When present, shrubs are one to two metres tall. Many vascular plants commonly found in fens are not typically for bogs like various sedges species, tamaracks and willows. The wooded fen is defined similarly as the wooded bog, but the WT is typically less than 20 cm below the ground surface and black spruce and tamarack dominate the treed stratum. Understory shrubs are birches and willows. Shrubby fens have the same cover definition as shrubby bogs, but the WT is within 10 cm of the ground surface. Common species include various birch and willow types and the shrubs reach one to two metres, which makes them taller than the ericaceous shrubs that dominate bogs (Ducks Unlimited Canada, 2016; Government of Alberta, 2015).

2.2 Data

2.2.1 Sentinel 1

Mission

Sentinel 1 is a Synthetic Aperture Radar (SAR) mission, which provides continuous all-weather day and night imagery at C-band. It is in a near-polar, sun synchronous orbit with a 12-day repeat cycle for a single satellite and has a right looking flight attitude. The mission is based on a constellation of two identical satellites, Sentinel 1A and 1B with a 180° orbital phasing difference. 1A was launched in 2014, 1B in 2016 and in the two-satellite constellation the repeat cycle can deliver a six-day repeat cycle at the equator. The center frequency is 5.405 GHz and there are four different operating modes characterised with different spatial resolutions and coverages. The modes are Stripmap, Interferometric Wide Swath Mode (IW), Extra Wide Swath Mode and Wave. Over land they primarily operate in IW and allow combining a large swath width, 250 km, with a moderate geometric resolution, 5 m by 20 m. Interferometry is ensured by sufficient overlap. The IW mode images three sub-swaths using Terrain Observation with Progressive Scans SAR (TOPSAR). The incidence angle is between 29° – 46° and the polarization is HH+HV, VV+VH, HH, VV. The Level-1 products are generally available, intended for most users and are produced in Single Look Complex (SLC) or Ground Range Detected. The SLC product consists of focused SAR data, geo-referenced using orbit and attitude data from the satellite. For IW each sub-swath consists of a series of bursts, which are re-sampled to a common pixel spacing grid and therefore ensures that interferometry between pairs of products acquired multiple repeat periods apart can be performed (ESA, 2023, 2021, 2015, 2012).

Used data and orbits

For this study, Level 1 SLC data in mode IW is used. The AOI is covered by the orbit tracks 49 (West), 78 (East) and 151 (Middle), from now on referred to as West, East and Middle in respect of their position to the AOI (Figure 5). The West orbit track is available through the whole study period from 2017 to 2022, the East orbit track starting in 2021 and the Middle one until the end of Sentinel 1B in December 2021. Table 1 gives an overview of the respective snow-free periods used for analysis and the available Sentinel 1 A/B scenes orbit-track-wise for the study period. In order to provide the possibility of a plausibility check based on different viewing geometries the ascending flight direction is used as it

covers the AOI with three orbit tracks, whereas descending only covers one (Aslan et al., 2019). Furthermore, the only descending orbit track covering the AOI is track 79 and was based on satellite Sentinel 1B, which results in a data coverage lasting only until the end of the mission in December 2021 (Figure 6). The snow free period for each year has been obtained through the ESA Sentinel-hub, where a manual check of Sentinel 2 imagery provides the information.



Figure 5: Ascending Sentinel 1 orbit tracks 49 (West), 78 (East) and 151 (Middle) covering the AOI (yellow). The figure is north oriented (ASF 2023a).



Figure 6: Descending Sentinel 1 orbit track 79 covering the AOI (yellow). The figure is north oriented (ASF 2023a).

Table 1: Overview of the data availability the various orbit tracks of Sentinel 1 covering the AOI during the snow free period. Data has been retrieved through ASF API.

YEAR	START	END	IMG ASC ORBITS				IMG DES ORBIT
			TOTAL	WEST 49	MIDDLE 151	EAST 78	71 (only S1B)
2022	01.May	10.October	19	11	0	8	0
2021	01.May	28.October	45	15	15	15	30
2020	03.May	10.October	35	13	12	10	28
2019	07.May	07.October	24	12	12	0	25
2018	05.May	04.October	21	10	11	0	24
2017	2.May	06.October	18	7	11	0	26
		Total	162	68	61	33	(Descending image number = tile north + tile south)

2.2.2 Meteorological Data

In the AOI vicinity there are two meteorological stations called Aspen and Kearl, named after the AOS lease, they are placed on. Aspen is close to the study site and located east of the road on the large vegetation cleared area (Figure 3). It is collecting data since 25. September 2020. The Kearl station is 27 km northwest of the AOI at the Kearl lake. Its data covers the whole study period.

The climate in the study area is classified as Dfc following the Köppen climate classification. It is a subarctic climate with cold winters, no dry season and cool summers. The mean temperature exceeds the 10 °C isotherm in 1-4 months (Malberg, 2002, p. 287f.). The daily average temperature since 2017 was -15.65 °C in January and 18.1 °C in July. Mean summer (snow-free period, May to October) precipitation amounts to 292 mm according to the Kearl station (Table 2). Note, that the precipitation measurements of the Kearl Station for the whole study period in 2020 have been substituted by the Aurora station in Fort McMurray due to a malfunctional sensor.

Table 2: Statistical weather station data from Kearl (black) and Aspen (blue) through the study period. Note that the Aspen station has been installed in September 2020 (Data provided by Imperial).

Year	Mean Temperature January (°C)		Mean Temperature July (°C)		Yearly Precipitation sum (mm)	
2017	-12.1		18.8		111	
2018	-17		17.8		308	
2019	-17		17		259	
2020	-15.7		18		563	
2021	-12.3	-12.5	19.2	17.9	271	271
2022	-19.8	-20.2	18.8	16.9	242	224

The Kearl Weather Station data retrieved since 2019, the year of adding the mineral filled layer to the road, are shown below (Figure 7). The data of the station at Aspen as well as the data from 2017 – 2019 can be found in the Appendix.

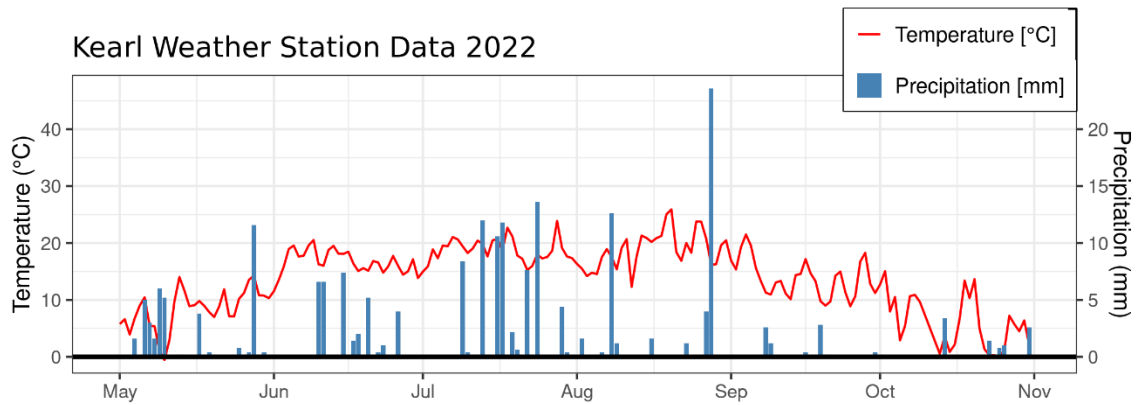
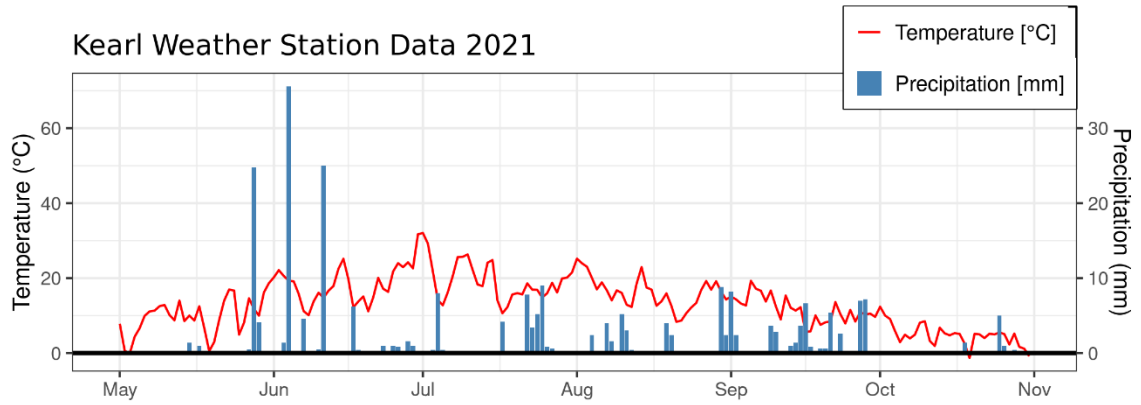
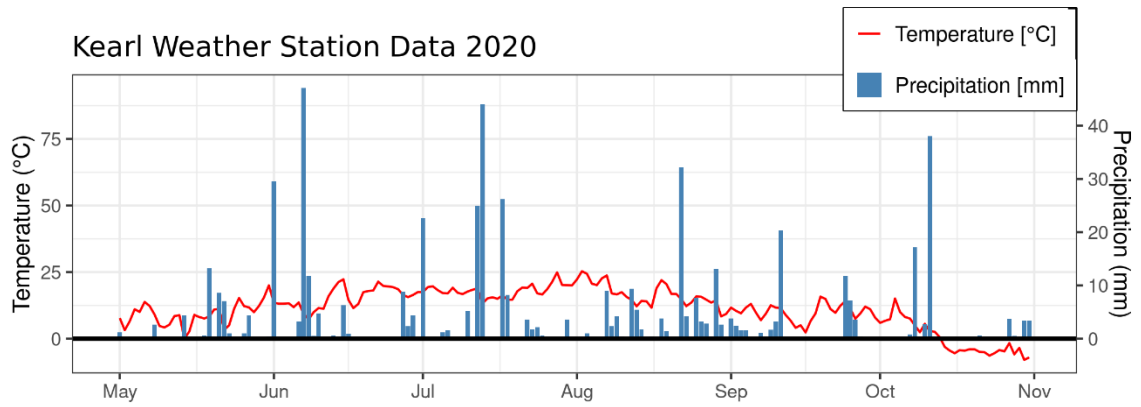
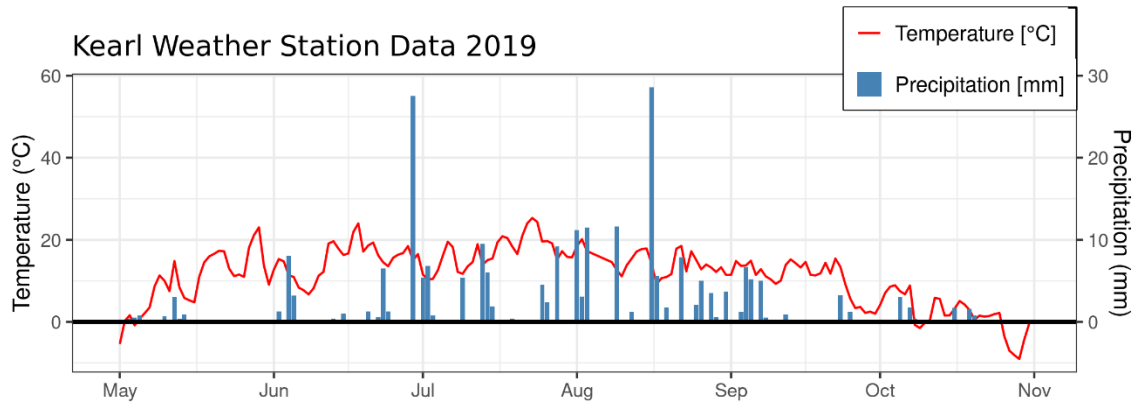


Figure 7: Kearl Weather Station data from 2019 to 2022 in the snow free study period from May to October (inclusive). X-axis is the time, y-axis on the left side displays the temperature amplitude in °C. On the second y-axis (right) the precipitation amount in mm is displayed. The red line represents daily average temperature, in blue bars the daily precipitation amounts are visualized (data provided by Imperial, 2022).

2.2.3 Groundwater Level Data and Culverts

The groundwater wells have been installed in August 2021 for scientific monitoring purposes. These wells are strategically placed in four transects, each consisting of six wells bisecting the road. In order to establish a reference, two additional wells were installed to the north of the road at an approximate distance of 450 m. To collect data on WT depth 6-hourly interval data is logged at each monitoring well. Figure 8 illustrates the data of four chosen wells, with two of them located downstream (south) of the road and two upstream. The WT depth is represented in negative values relative to the surface, with zero defined as the surface level over the available data period. Positive values indicate depths above the surface, negative below the surface. One of the wells, referred to as MART4_NC_2 (T4_2) is displayed with the confidence interval, a smoothed line, and a non-smoothed line to effectively depict the amplitude and variability of the data. The raw data has been extracted from the well sensors in September 2022 using the WinSitu5 software. Additionally, the piezometric data has been corrected for barometric pressure variations.

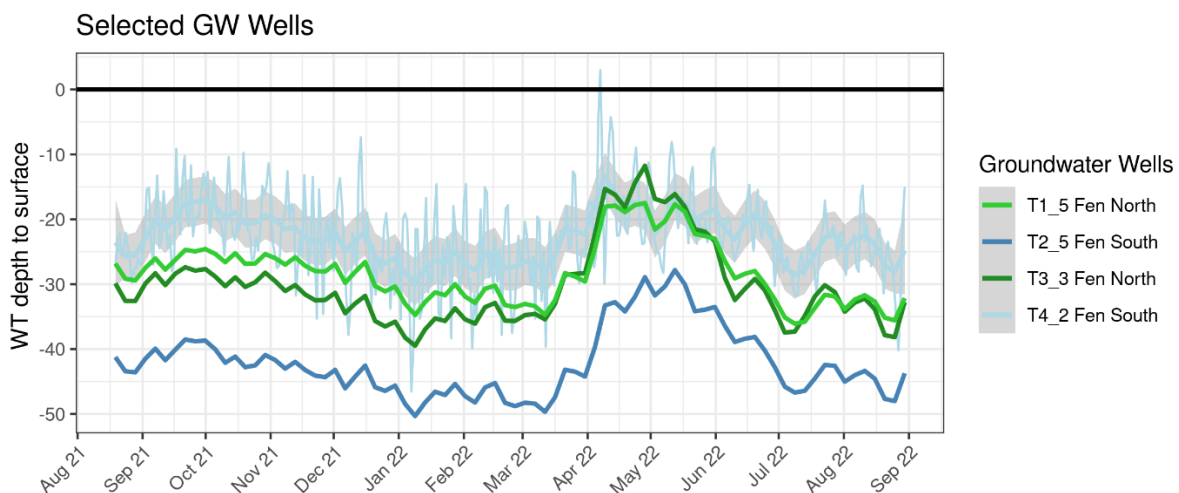


Figure 8: Timeseries of water table depth of 4 selected groundwater wells in the study area. The surface is defined as 0 and below surface as negative values. The values are in centimetres. The groundwater wells are MART2_5 (blue), MART4_NC_2 (light blue), MART3_EC_3 (lime-green), MART1_5 (forest-green). The light-blue line shows the confidence interval, smoothed line and non-smoothed line.

Within the designated study area, a total of 15 culverts have been installed to address the restoration of the subsurface and surface waterflow between upstream and downstream sides of the road, as well as to mitigate the hydrological barrier (Figure 9). However, the

effectiveness of these culverts varies significantly. The culverts have been comprehensively scouted on June 4, 2023, conducted by Dr. Scott Ketcheson and Lelia Weiland (Table 3, Figure 10). Figure 10 provides visual documentation of the upstream and downstream side of an effective culvert (EC11), a semi-effective (EC7) and an ineffective culvert (EC6), revealing their functional performance, which will vary in response to hydrological conditions.

EC11 is an effective functioning culvert. It provides a sufficient streamflow from the upstream to the downstream side. The upstream side of EC7 shows deep ponds, while the flow is limited. EC6 shows almost no flow but could be effective at very high WT levels. In the background some smaller ponds can be detected but the culverts level is too high to re-establish subsurface flow.

In-depth focus on Culverts & Groundwater-wells

Author: Niklas Heiss, 20230612,
Data provided by Dr. Scott Ketcheson's Lab,
ESRI Imagery Background Map

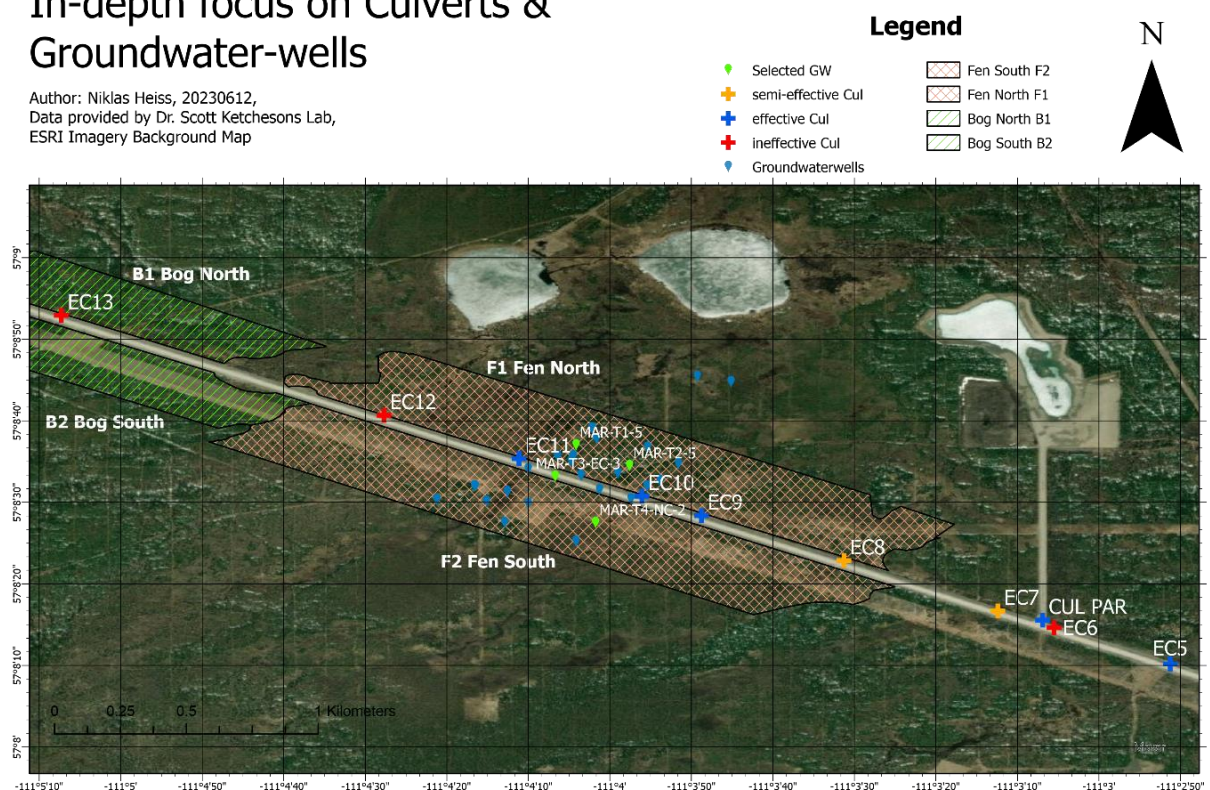


Figure 9: In-depth focus on culverts label and position and the selected groundwater wells (green). The culverts are classified, following table 3, as effective (blue), semi-effective (orange) and ineffective (red). The map shows the analysis relevant culverts. Spatial reference: GCS WGS 1984.

Table 3: Culvert overview. Name, function and description of culverts within the study area Aspen. (Data provided by Dr. Scott Ketcheson, June 2023).

Name	Function	Description
EC1	effective	
EC2	effective	Culvert is parallel to the road on the north side and leads to EC3.
EC3	effective	
EC4	effective	Low flow but flowing.
EC5	effective	
EC6	ineffective	Almost no flow. Effective at very high flow conditions
CUL_PAR	effective	Parallel to the road on the north side. Water rerouting to the West instead to EC6.
EC7	semi-effective	Flows, but deep ponds on upstream side. No ponds on downstream side.
EC8	semi-effective	Shallow and narrow on upstream side. Nothing on downstream side.
EC9	effective	Low flow. Very ponded on both sides.
EC10	effective	Low flow. Ponding on both sides
EC11	effective	
EC12	ineffective	Draining the lakes on the north side. Very low flow. Big ponds on the north side.
EC13	ineffective	
EC14	effective	



Upstream	Downstream
Culvert EC11 - effective	
	



Figure 10: Images of culverts EC11 – effective, EC7 semi-effective and EC6 – ineffective. The left column shows the upstream side and the right column the downstream one (Photos taken by Dr. Scott Ketechedson and Lelia Weiland in June 2023).

2.3 InSAR Methods

The basic principles of SAR and InSAR can be obtained e.g. from Bamler and Hartl, 1998; ESA, 2007; Jansing, 2021; Rosen et al., 2000. Time series InSAR is a powerful geodetic technique to derive the temporal evolution of surface deformation from a series of repeated SAR images. It is widely used to monitor seasonal and long-term line-of-sight (LOS) deformation of the Earth's surface. The decorrelation of the SAR signal, the atmospheric delay and the phase unwrapping error limit the accuracy and precision of the received surface displacement. Decorrelation is mainly caused by changes of the surface backscatter characteristics over time and by the non-ideal acquisition strategy of SAR satellites (Alshammari et al., 2018; Hanssen and Van Leijen, 2008; Hoyt et al., 2020; Izumi et al., 2022; Tampuu et al., 2020; Yunjun et al., 2019).

To overcome the limitations associated with SAR satellites, including the revisit time of 6 to 12 days (temporal baseline) and the orbit separation (spatial baseline) between repeat acquisitions, two groups of InSAR time series techniques have been developed: PSI methods and distributed scatterer (DS) methods (Yunjun et al., 2019). The PSI methods focus on the phase-stable point scatterers as a function of time, where it is assumed that there is a single dominant scatterer in a resolution cell. It attempts to solve two problems simultaneously. First, coherent scatterers need to be identified, whose phase history is dominated by the geometry between satellite and scatterer, rather than physical changes within the scatterers' resolution cell. Second, for scatterers deemed coherent, parameters, such as their relative geometric height, their displacement behaviour in time, atmospheric delay factors and integer phase ambiguities, need to be reliably estimated (Alshammari et al., 2020; Hanssen and Van Leijen, 2008). For this reason, the PSI is less likely to succeed over forest canopies or densely vegetated areas. In the PSI method a single master image is chosen to create the interferograms, in this study for each snow-free season, which allows reduction of noise contribution of the master image prior to phase unwrapping as it is present in all interferograms (Figure 11, left; Ma et al., 2021).

The second method uses a DS approach, which relaxes the strict limit on the phase stability and includes areas that are affected by decorrelation through the exploitation of the redundant network of interferograms. There are two categories of methods proposed based on the interferogram network for deformation inversion. The first one uses all

possible interferograms of employed SAR SLC images (full network approach). The second one uses parts of all possible interferograms characterised by small spatio-temporal baseline thresholds, called Small Baseline Subset (SBAS), which is used in this study (Alshammari et al., 2020; Izumi et al., 2022). It was first proposed by Berardino et al. (2002) and uses multi-master images (Figure 11, right; Li et al., 2022)

If InSAR methods can produce reliable and diagnostic time series over peatland, the technique would enable a new view and understanding of peatland surface motion and its relationship to condition and hydrology on a landscape scale. It would become a powerful tool for peatland monitoring across whole catchments, regions and countries. But there is a key barrier of applying InSAR to quantify peatland dynamics: the mismatch between large scale of observations, accuracy and precision of InSAR and small-scale field measurements. This makes it extremely difficult to validate the accuracy of the results. The main problem is to cover a resolution cell of 40 x 40 m, as considered in this study, with appropriate transects and point measurements (Alshammari et al., 2020). This is one of the reasons for choosing the ascending Sentinel 1 flight direction, as it covers the AOI with three different orbit tracks and therefore with three different looking geometries. The results can still be valuable if the concerns about absolute accuracy are abandoned and the focus shifted on whether the characteristics of the InSAR time series can be used to quantify the peatland condition, in effect using the InSAR time series as an operationally defined measure or proxy. This works under the premise, that the results are representative of the surface motion and that in turn surface motion is representative of peat condition (Alshammari et al., 2020). In this study both, the PSI and SBAS method approaches are applied.

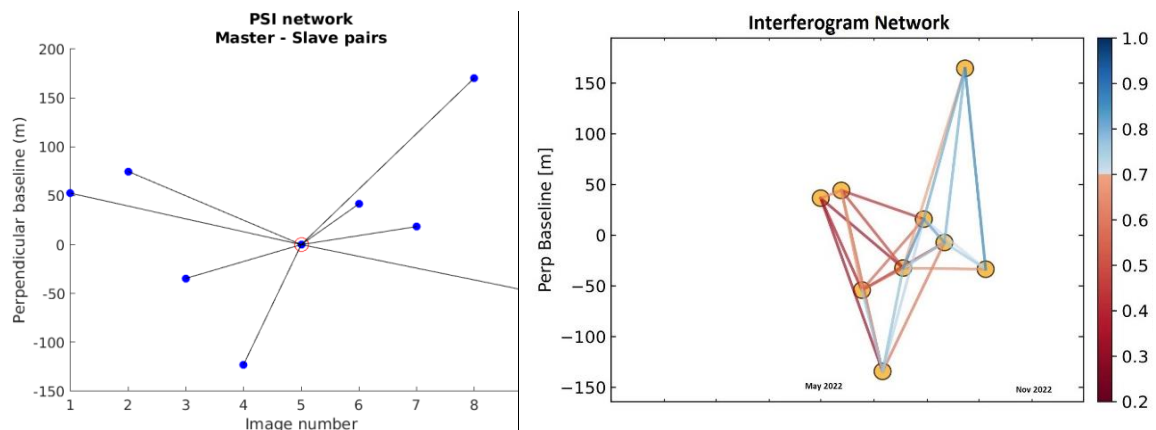


Figure 11: Example baseline plot for (a) the PSI and (b) the SBAS method based on the data from 2022 East Orbit track.

2.3.1 Persistent Scatterer Interferometry Workflow

The PSI is a powerful advanced InSAR technique able to measure and monitor displacements of the Earth's surface over time with high accuracy. Hooper et al. (2004) proposed a novel PS selection using characteristics of phase, which is suitable to find low-amplitude natural targets with phase stability. This work originated the most widely used software package StaMPS (Stanford method for Persistent Scatterers)(Delgado Blasco et al., 2019; Hooper et al., 2018).

The workflow used in this study follows the SNAP2StaMPS proposed by Blasco & Fomelis together with A. Hooper (2018) to automate the pre-processing of the Sentinel-1 SLC data and their preparation for ingestion to StaMPS. The pre-processing is based on using free software SNAP (Sentinel Application Platform by ESA) and SNAP2StaMPS python scripts, followed by the StaMPS processing in MATLAB. All the processes are conducted in a VirtualBox Linux Ubuntu 22.0 environment as recommended by several authors and the GitLab and ESA SNAP Forum community (Blasco et al., 2018; Hooper et al., 2018; Serco Italia SPA, 2020). The workflow is performed individually for each year and each orbit track. The complete processing steps are visualized in Figure 13.

Pre-processing with SNAP and SNAP2StaMPS

First, the data is downloaded via the Alaska Satellite Facility API using python and considering only the snow-free period (see Table X) and ascending mode images. To select the ideal master image the SNAP InSAR Stack Overview function is used. The function minimises the distribution of the perpendicular baseline values and tries to maximize the expected stack coherence of the interferometric stack. This should lead to improved visual interpretation of the interferograms and assist quality assessment. Once the master is selected, its sub-setting is done via the TOPSAR Split operator, where the Subswath is chosen for each orbit track in order to cover the AOI, and the number of Bursts is reduced to a minimum to still cover the AOI in full extend, but to reduce computation time and power (Figure 12). The VV polarisation is selected, and the orbit files get applied to provide accurate satellite position and velocity information.

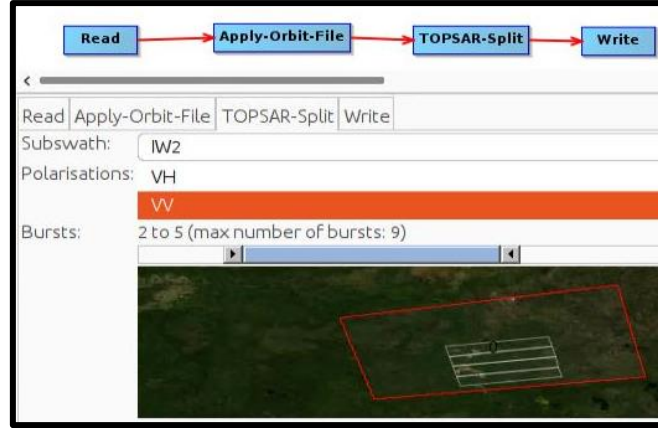


Figure 12: TOPSAR Split Operator for the Master images. Example is chosen from the Middle Orbit. Selected Options are VV polarization, the IW2 subswath and the bursts 2 to 5 in order to cover the AOI.

To run the next steps in an automated way, the snap2stamps includes a *project.conf* file, where all necessary user inputs, e.g., AOI coordinates, computational power, folder paths are defined. Before the co-registration of master and slave images, the slaves must be split, and their orbit information updated analogously to the master image before. The co-registration of each slave image with the master image is performed with the Back-Coding operator using the Digital Elevation Model (DEM) and the orbital parameters. The SRTM DEM with three arc-second (~ 90 m) spatial resolution was used, because the differences in the results to the one arc-second product were negligible, but the implementation and computational time is more efficient with the three arc-second products. This is followed by the debursting process, which resamples the IW SLC product to a common pixel spacing grid in range and azimuth and merges the bursts to a continuous image. Now the complex interferogram can be computed with subtraction of the flat-earth phase. The flat-earth phase is the phase present in the interferometric signal due to the curvature of the reference surface. The last pre-processing step is to remove the topographic phase information. The operator first “radarcodes” the DEM and then subtracts it from the complex interferogram (Blasco et al., 2018; Serco Italia SPA, 2020).

Summed up, the pre-processing steps consist of forming a stack of co-registered single-master interferograms. The final step before ingestion of the data into StaMPS for PSI processing is the estimation of the amplitude dispersion index. The D_A value describes the amplitude stability, which is used to pre-select pixels and therefore reduces the number of pixels for the phase analysis. It is calculated as:

Equation 1	$D_A = \frac{\sigma_A}{\mu_A}$
	(Mancini et al., 2021; Serco Italia SPA, 2020)

Where σ_A is the standard deviation and μ_A is the mean of a series of amplitude values. The range is recommended between 0.40 and 0.42. In this study 0.42 is used as more pixels are selected for phase analysis (Blasco et al., 2018; Serco Italia SPA, 2020).

Processing with StaMPS

The processing with StaMPS is based on various parameters, which can be adjusted and controlled. Only the ones that have been changed for this study are mentioned as mostly the default setting has been used. The first step of StaMPS is to load in the data into formats required for PS processing and storing them in the MATLAB workspaces. Then the phase noise is estimated in an iterative process for each candidate pixel in every interferogram. Pixels are selected based on their noise characteristics. These pixels are then weeded, dropping those that are due to signal contribution from neighbouring ground resolution elements and those deemed too noisy. Following, the wrapped phase of the selected pixels is corrected for spatially uncorrelated look angle (DEM) error. Once the PS selection is done, the phase can be unwrapped, and the spatially correlated errors estimated. This estimates the total DEM (look angle) error, and the master atmosphere and orbit error. The last step of StaMPS, atmospheric filtering has not been carried out, as no atmospheric data of the study area was available. It could improve the quality of the results, but is not necessary for the process to work (Blasco et al., 2018; Mancini et al., 2021; Serco Italia SPA, 2020). The results are exported in *.csv format and are visualized and further analysed in RStudio.

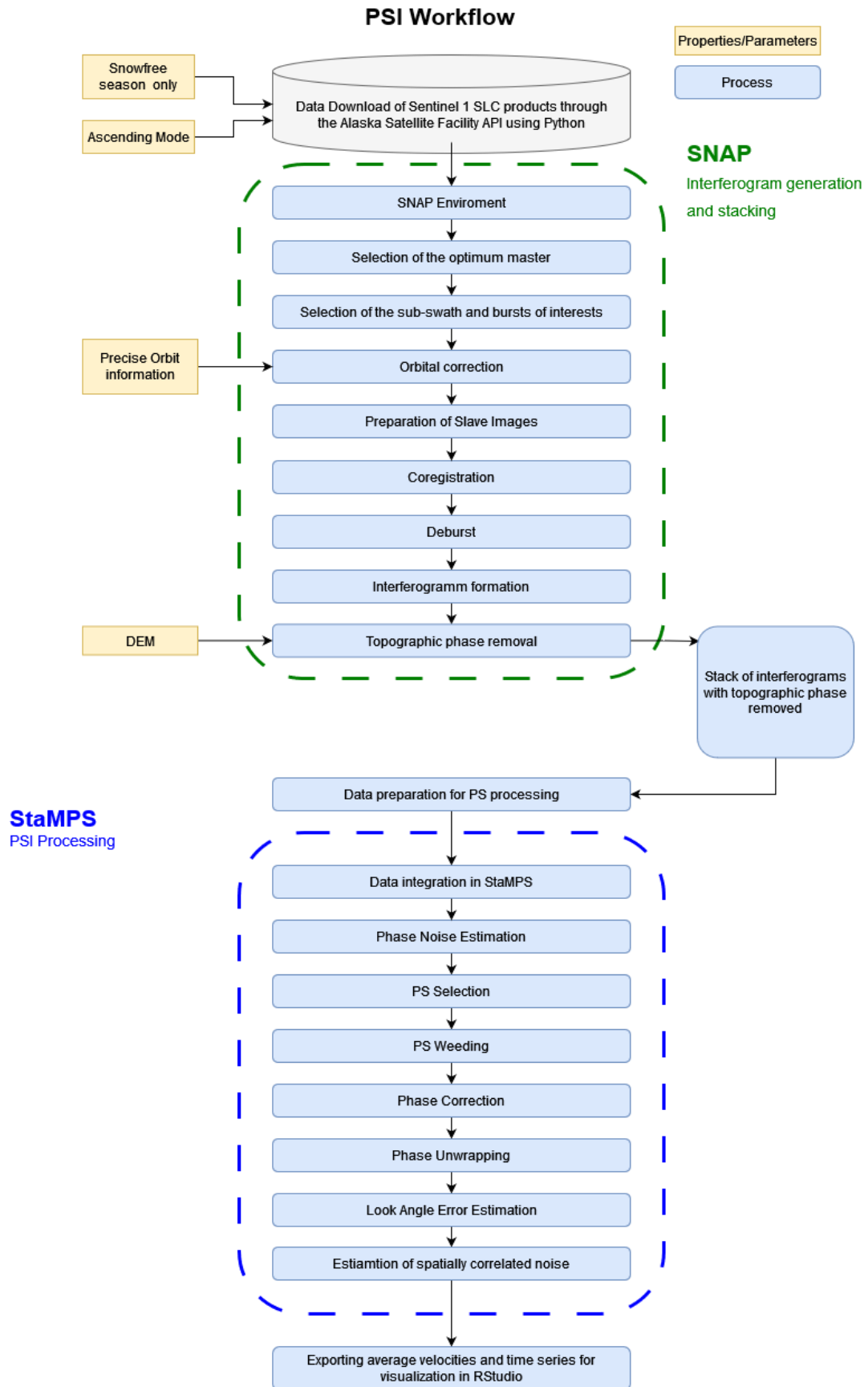


Figure 13: PSI workflow for processing Sentinel-1 images with SNAP, SNAP2StaMPS and StaMPS (based on Mancini et al.(2021)).

2.3.2 Small Baseline Subset Workflow

The ASF offers On-Demand processing of Sentinel-1 datasets to generate InSAR products directly in the Data Search – Vertex portal. ASF uses cloud computing to efficiently calculate the data and afterwards enable the download in a short time period after submitting. For this method the SBAS interface has been used, which is designed to compile a series of InSAR pairs that cover a certain time period. After importing the AOI shapefile into the search tool, the filters are set to SLC file type and IW beam mode. The SBAS criteria filters include options to refine the result list of interferogram pairs. The first one is the overlap threshold. It can be a quick and easy way to remove low-value pairs from the time series. The filter is not applied in this study as each orbit track is analysed separately and within one track there is sufficient overlap, and the AOI is always fully covered. However, there is one exception in 2017 on the middle track in the image taken on the 1st of July, which has a data gap and is not covering the AOI, wherefor it got manually excluded. The second SBAS criteria is the date filter, which restricts the pairs that fall within the specified date range. The applied time periods are listed in Table 1. Next, the baseline tolerances are adjusted. Thresholds for perpendicular (spatial) and temporal baseline are 300 m and 48 days respectively. The perpendicular baseline is the perpendicular distance between sensor locations during acquisitions in meters, whereas the temporal one is the time between acquisitions in days. To properly monitor surface deformation, the perpendicular baseline for acquisitions should be very small to maximize the coherence of the phase measurements. To determine topography, slightly different vantage points are required. Sensitivity to topography depends on the two baselines, the sensor wavelength, the distance between the satellite and the ground, and the sensor look angle. After manually checking the InSAR pairs they have been submitted for InSAR Gamma SLC processing with the MintPy option setting, as the SBAS analysis is performed using the MintPy software. That includes DEM, Look Vectors and Wrapped Phase. The Looks option is set to 10 x 2 as it defines the resolution and pixel spacing of the output products. The chosen option results in pixel spacing of 40 m, whereas the default 20 x 4 reduces the spatial resolution to 80 m (Alaska Satellite Facility, 2023b (ASF), ASF 2023a).

The InSAR time series analysis is conducted using the Miami InSAR time series software in Python (MintPy), which was developed by the Rosenstiel School of Marine and

Atmospheric Science (RSMAS) geodesy group at the University of Miami (Park and Hong, 2020; Yunjun et al., 2019). It reads the stack of interferograms (here the ASF output) and the geometry files. It references them to the same coherent pixel (referent point), which has been placed by the algorithm randomly among pixels with high spatial coherence and a threshold of ≥ 0.85 . Then it calculates the phase closure, which involves assessing the consistency of the phase measurements, and estimates the unwrapping errors. MintPy then inverts the (subset) network of interferograms into time series, calculates the temporal coherence to evaluate the quality of inversion, corrects DEM errors and in a final step estimates the surface velocity in LOS. Positive values represent motion towards the satellite, which would equal an uplift for pure vertical motion. The parameters for this process can be adapted but are used mostly in the default settings. In order to exclude outliers affected by decorrelation, pixels with a coherence lower than 0.5 are masked out. The pixel selection criterion is relaxed as not only the pixels that are coherent in all interferograms are used, but also pixels with fewer interferograms as long as a predefined number of other interferograms is available for each SAR acquisition (1 by default). This reduces the sensitivity of the network inversion result to the few very low coherent interferograms in a redundant network, giving robust and consistent spatial coverage (Park and Hong, 2020; Yunjun et al., 2019). The MintPy time series analysis results are saved in HDF5 format data and plotted and analysed further in RStudio (Figure 14).

SBAS Workflow

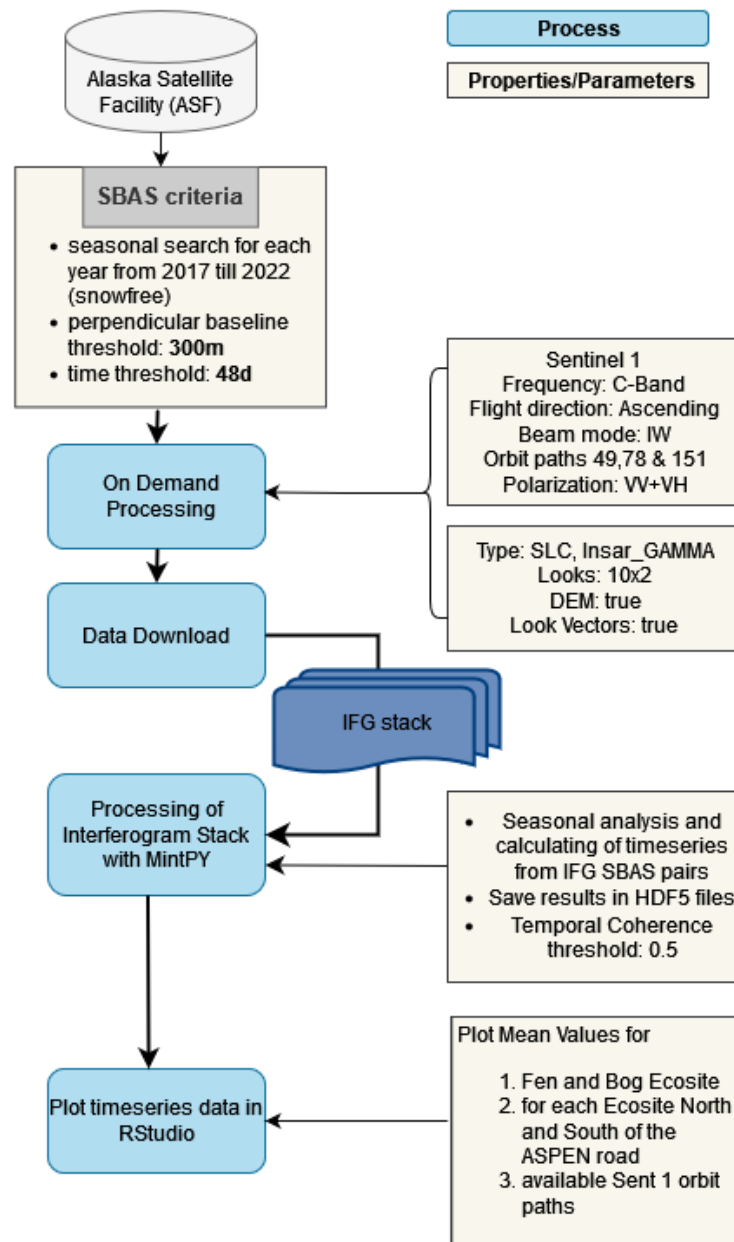


Figure 14: Workflow diagram of the SBAS approach. Processes are in light blue, the used parameters and properties in light yellow brown.

2.3.3 Post-Processing in RStudio

In this study, the post-processing stage was guided by a multifaceted analytical approach, using different statistical methods to explore the depth and breadth of the generated results and analysed data through PSI and SBAS methods. The specific post-processing steps undertaken in RStudio (v 4.1.2) are:

- 1) First a comprehensive timeseries analysis is executed. The mean values for each timestep within the study period were computed for each ecosite shapefile under both methodologies. These mean values were utilized instead of median values due to their propensity to weigh “outliers” more heavily. Noteworthy in this context is, that statistical outliers not necessarily be erroneous or extraordinary data. For instance, the edge effects of the road, which is one focus of the study, can occur as a gradient regarding the distance from the road in hydrological disturbed peatlands. This effect is better accounted for by the mean. Moreover, the discrepancies between median and mean values in this analysis proved to be marginal, as demonstrated in the focus on year 2021 plots that provide a detailed and focused lens on statistical parameters. The timeseries were plotted with a trend for each orbit track and statistical parameters such as the coefficient of determination (R^2), the root mean square error (RMSE) as well as the p-value and τ derived from the Mann-Kendall trend test. The latter trend test is a robust non-parametric test utilized to identify statistically significant trends in timeseries. The significance level to accept a trend as statistically significant is chosen here as $p < 0.05$ (Hirsch et al., 1982; McLeod, 2011; Soltani et al., 2013).
- 2) The second stage of analysis entailed the visualization of spatially distributed yearly velocity plots for each method, year and orbit track. The yearly velocity is the timeseries trend for each pixel, each PS respectively, in mm/year. The focus is on the West orbit track as its data is the only one available for all years of the study period.
- 3) The snow free season of 2021 was emphasized as both methods deliver predominantly similar results, and all three orbit tracks are available. All orbits are merged into one timeseries with a single trend, with the statistical parameters mentioned above calculated accordingly. In addition, the differences between the upstream and downstream side are calculated and visualized.

- 4) Lastly, for the year 2021, the SBAS and PSI methods were plotted for a single orbit track displaying the data's statistical variance and quality presented through boxplot diagrams. This is specifically done on an example to demonstrate the range and behaviour of the mean values plotted in the other timeseries plots. This approach is not used throughout the whole timeseries analysis to maintain intuitive interpretation and visualization, since the graphs would be too overloaded to compare the methods and results effectively in an adequate way.

These analytical steps provide a robust approach to understanding the complex dynamics at play within the context of InSAR timeseries analysis. The statistical treatment of the data, combined with careful consideration of the relevant temporal and spatial parameters, provide insights that contribute to the overall understanding of the study's objectives.

3. Results

3.1 PSI and SBAS Timeseries Analysis

Figure 15 illustrates the PSI and SBAS timeseries analysis of LOS movements in millimetre. Positive values are defined as an uplift in the direction towards the sensor and negative values as an increase of distance in LOS. It is important to note that the main part of the road construction, the adding of the mineral filled layer, happened during the end of 2018 and the beginning of 2019. Consequently, the patterns observed in the years 2017 and 2018, prior to this substantial disruption, are described briefly. Detailed graphs can be found in the Appendix.

For the analysis of the timeseries, the mean values of each ecosite polygon are plotted over the snow free study period for each timestep. Each available orbit track is handled separately to compare the trends and measurements.

In 2017 and 2018, when the road has not yet been completed, only West and Middle orbit tracks are available. The differences in results between PSI and SBAS outweigh the differences between various ecosites and downstream and upstream side by far. The SBAS displacement amplitude is approximately higher by the factor 2-5, varying between ecosites and years. No substantial differences between upstream and downstream sides can be detected in both the bog and the fen using both methods, which is expected since the mineral material had not yet been placed for the road construction. However, a relatively strong positive signal is detected on August 7th, 2017, in the middle orbit track in both methods in the bog and in the SBAS fen results, but not in the PSI fen timeseries. When comparing the pattern relatively instead of the absolute values, some similarities between the methods are observed, with most trends in 2017 pointing in similar directions. In 2018, the PSI trends are mostly contrary to the SBAS ones. In the PSI method the trends of middle orbit track are in the fens statistically significant ($p\text{-value} < 0.05$). Also, the R^2 is quite high with 0.9 (north-side) and 0.86 respectively. All other trends in both methods in 2017 and 2018 are not statistically significant (Table 4, Table 5).

2019 is the first year with the completed road bisecting the peatlands. The amplitude remains approximately 3-4 times larger with SBAS compared to PSI. The trends in the bog ecosites are similar in both methods, and contrary in the fen. A peculiarity is the 21st of June as it represents a global maximum in the SBAS method whereas it is a minimum in

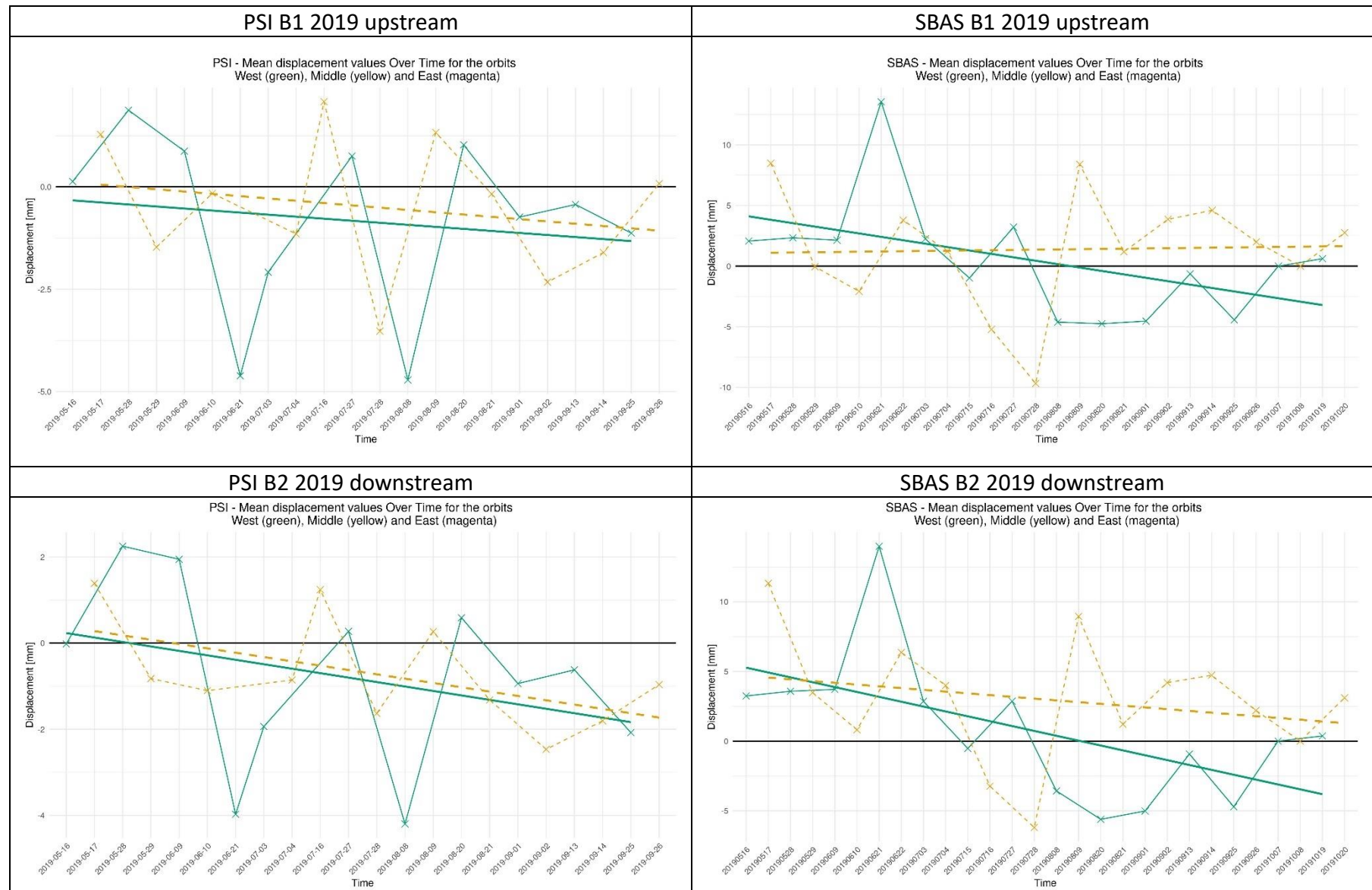
the PSI method, this is not simultaneously to a heavy rain event, but a total amount of 10 mm is measured between 19th and 21st of June. In the middle orbit track results on July 28th a minimum peak is detected in both methods for the bog, and for SBAS in the fen, where it is not detected by PSI. This minimum peak is followed by a strong uplift signal in the middle orbit for both PSI and SBAS. This coincides with a rain event in between this minimum and strong uplift signal. The PSI middle orbit trend in F1 ($R^2 = 0.78$, RMSE = 1.62) and SBAS west orbit track in B2 ($R^2 = 0.33$, RMSE = 3.99) are the only statistically significant trends (Table 4, Table 5).

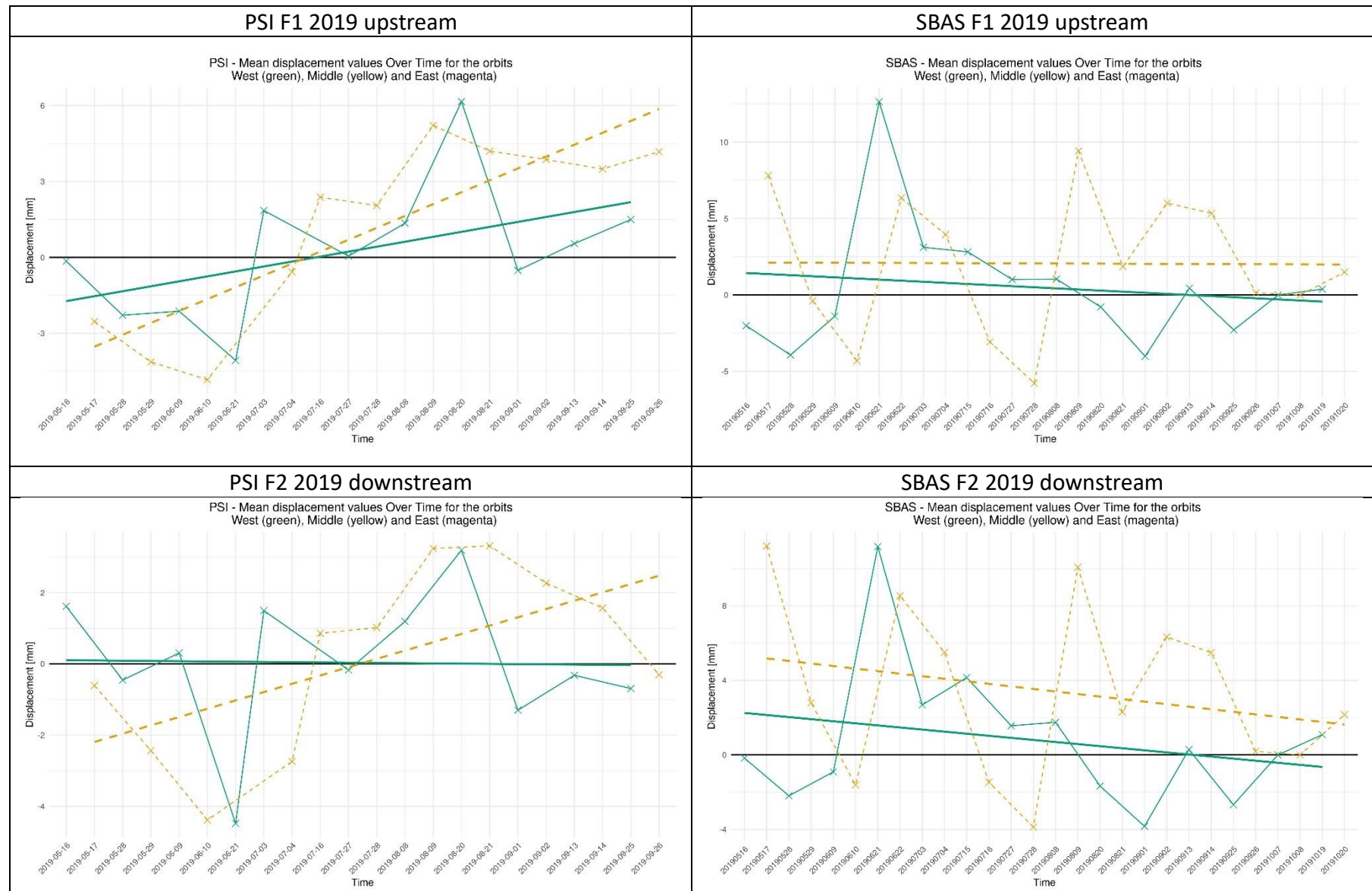
In 2020, the second year with the road effecting the hydrology, all three orbit tracks are available. The amplitude is 2-3 times larger with SBAS, but already closer as in the years before. Within each method, there are no obvious differences between upstream and downstream of the road. The SBAS trends are more neutral, closer to zero, in both bog and fen. PSI indicates an uplift in the bogs and a sinking tendency in west and middle orbits in the fen, whereas the east orbit indicates contrary an uplift in all four ecosites. The PSI East orbit tracks for B1, B2 and F2 are the statistically significant trends. East orbit track timeseries are quite similar in all the four ecosites and start later than the other tracks in June. Remarkable is July 17th as a peak to the surrounding data points in the timeseries is indicated in the fens and a minimum value in the bog. Around this date, there is a severe rain event which totals to over 70 mm in two days. After that date, both ecosites show smaller sinking data values and shift to a positive mean displacement during a constantly wet August until mid-September, where small and larger precipitation amounts occur. The end of September and the beginning of October are dry, and the uplift shown in the data decreases close to zero. The SBAS east orbit results show a similar pattern, but there are no significant trends. The 15th of June is a peculiar point in time, as it represents a global maximum in the PSI west orbit track and a minimum in the SBAS method. This is timewise a few days after a strong precipitation event amounting to approximately 60 mm (Figure 7).

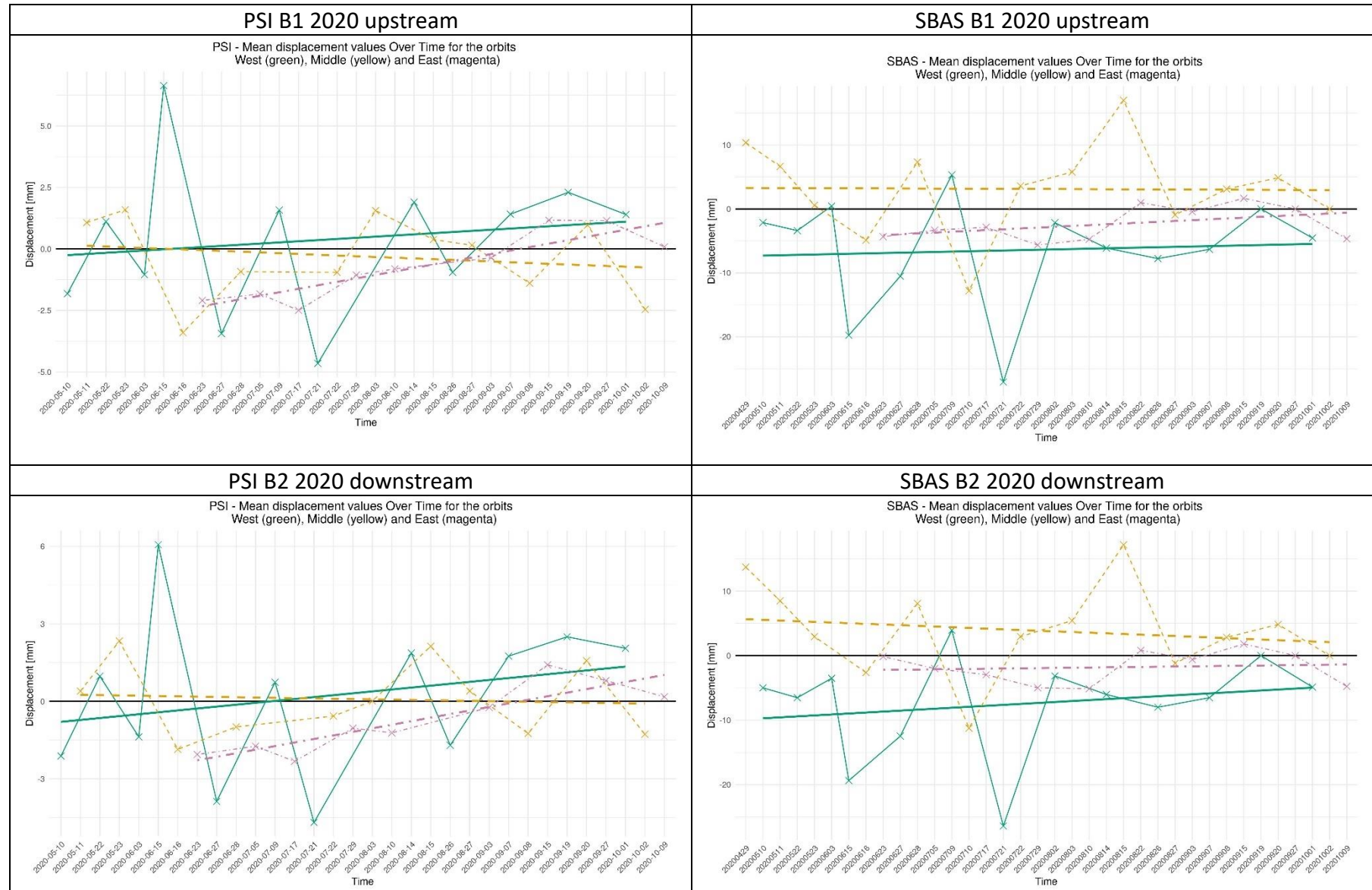
In 2021, with all three orbits available, amplitudes are similar, with SBAS being 1-2 times higher. The timeseries appears similar, especially when comparing the bog. Peaks are identical, but on the 29th of May in all ecosites, PSI shows an uplift maximum and SBAS a minimum. In the fen, PSI shows downward trends upstream and downstream, while SBAS

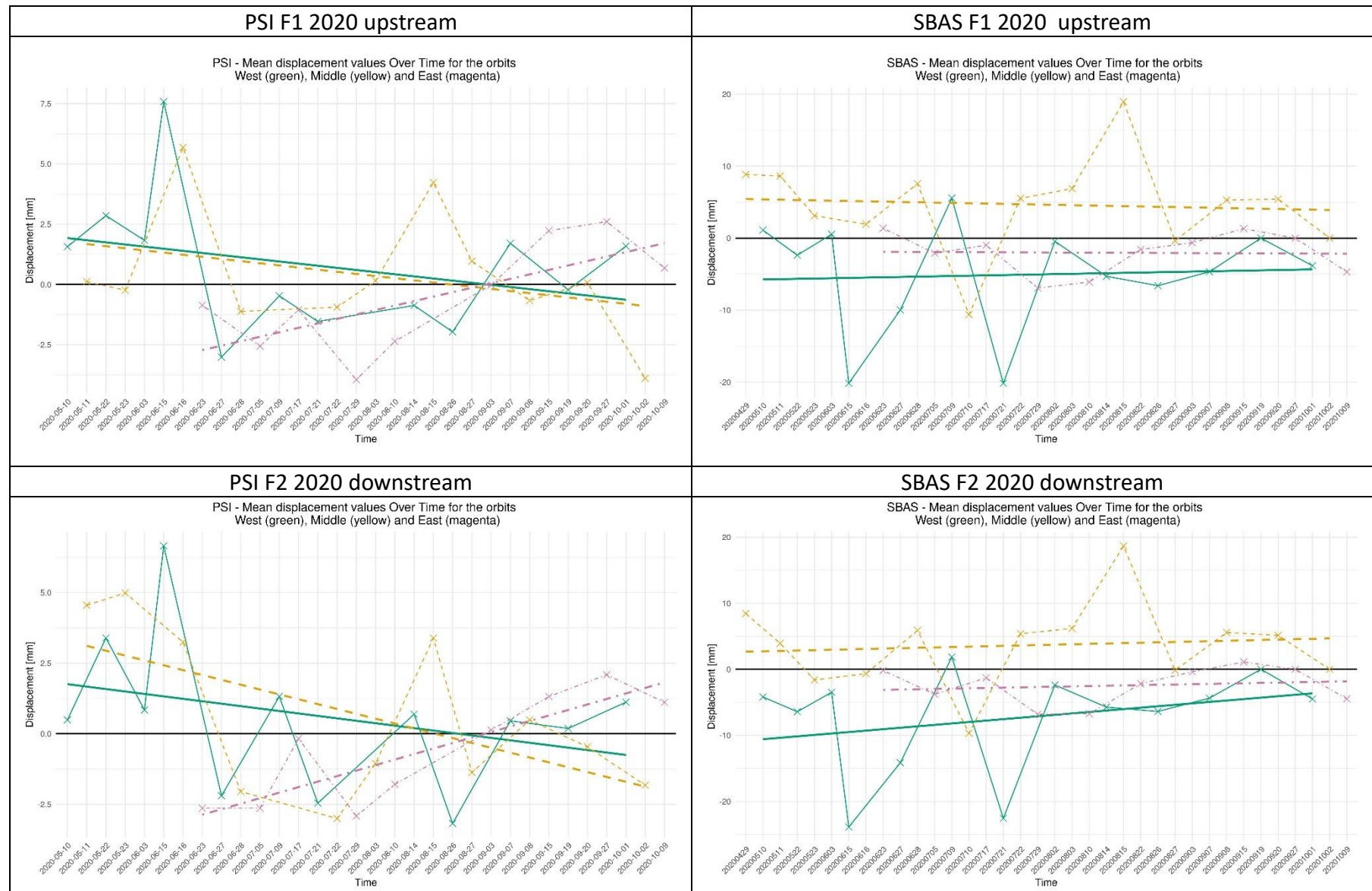
trends from various orbit tracks display contrary results. Statistically significant trends are PSI Middle and East track in the fens. No substantial differences are detected between upstream and downstream in either method.

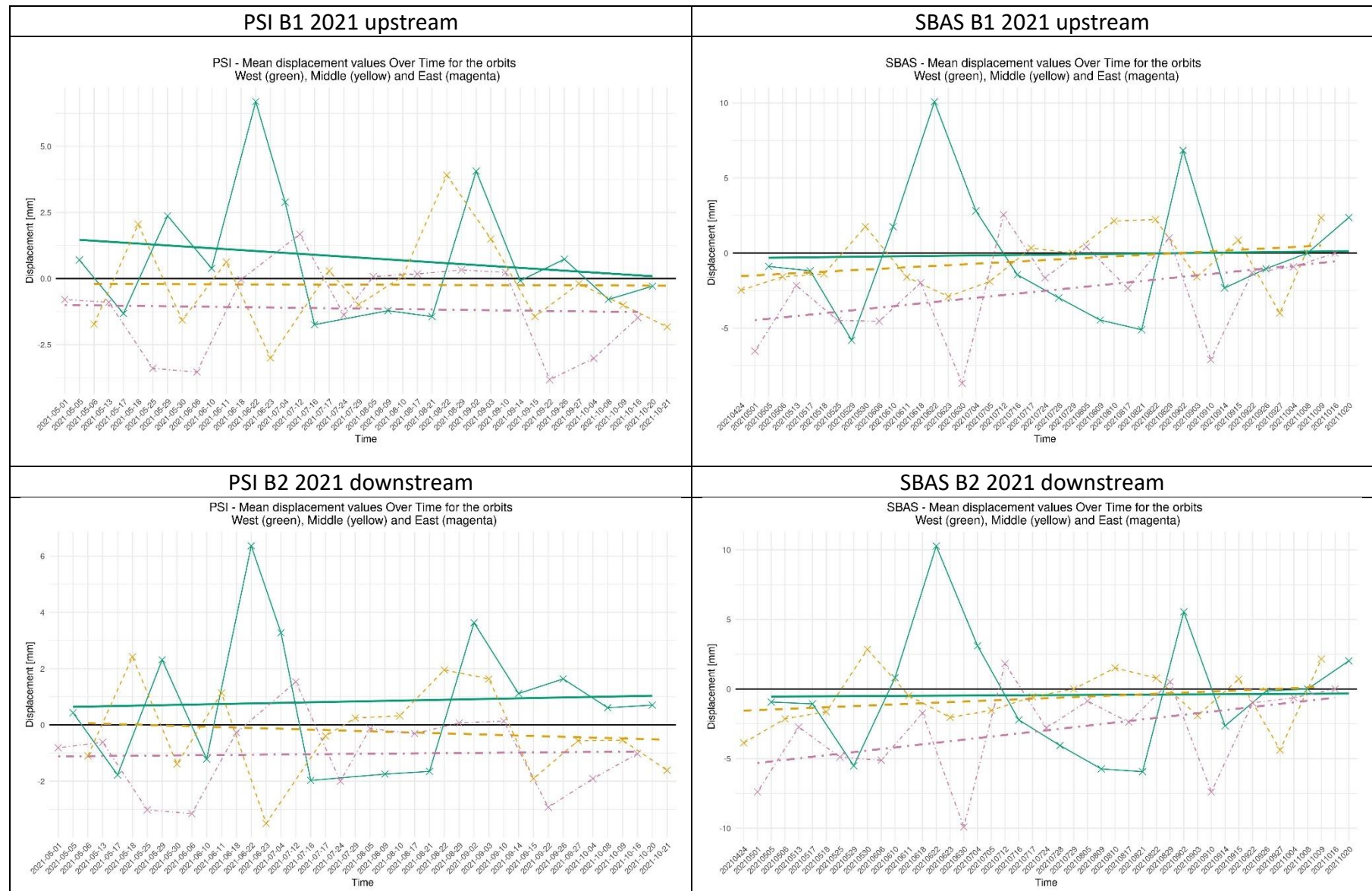
In 2022, with only West and East orbit track data available, the amplitudes disperse again to a factor of 5-8 times with SBAS being larger than PSI, but mainly in the West orbit. The East orbit track's range is similar in both methods. The trends are contrary comparing the two methods. PSI indicates an uplift in the bog and contrary trends in the fen. SBAS shows sinking tendencies in all ecosites and orbits. Statistically significant are the PSI trend in the West orbit, B2 and the SBAS East orbit, F2.

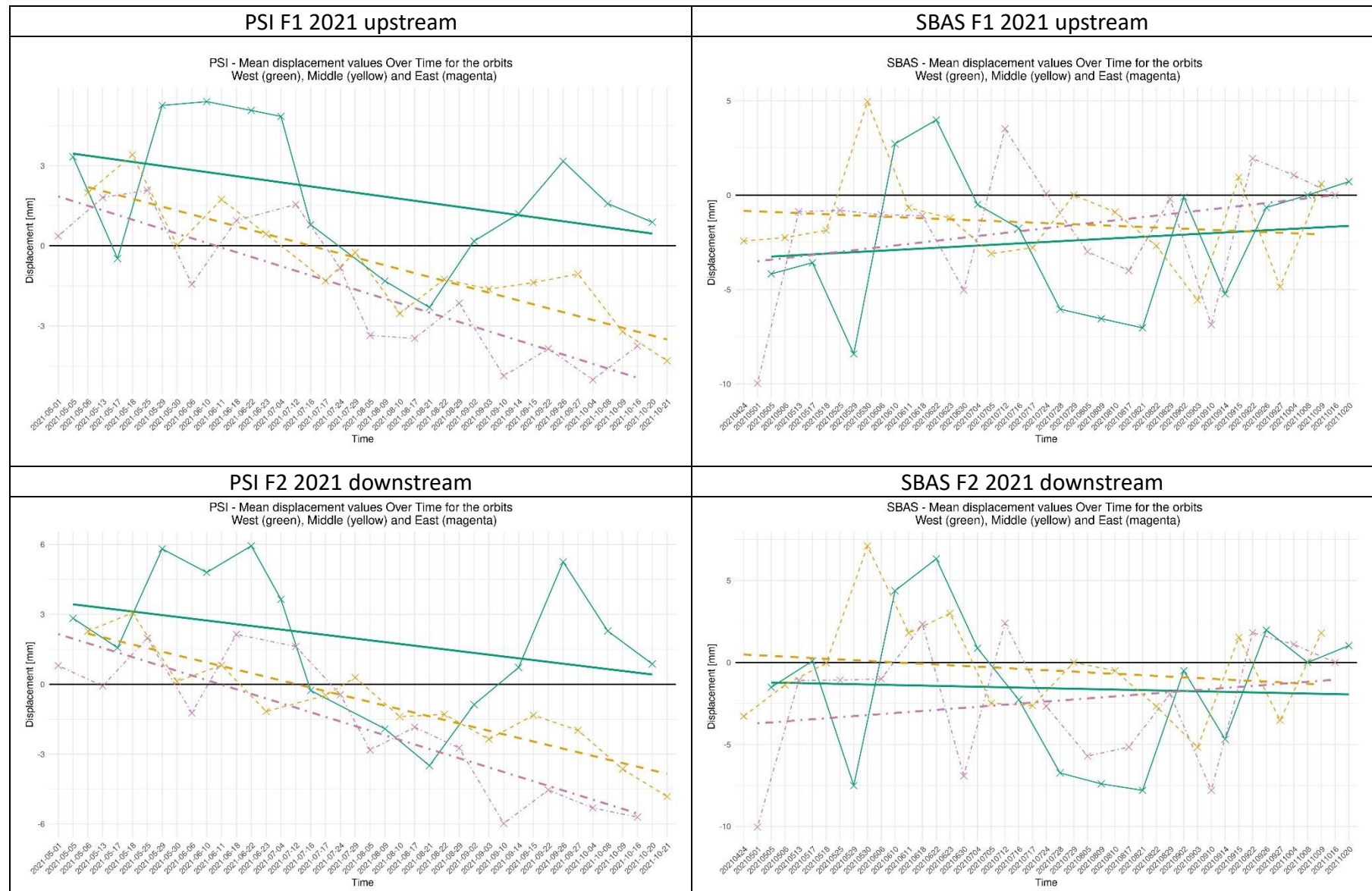


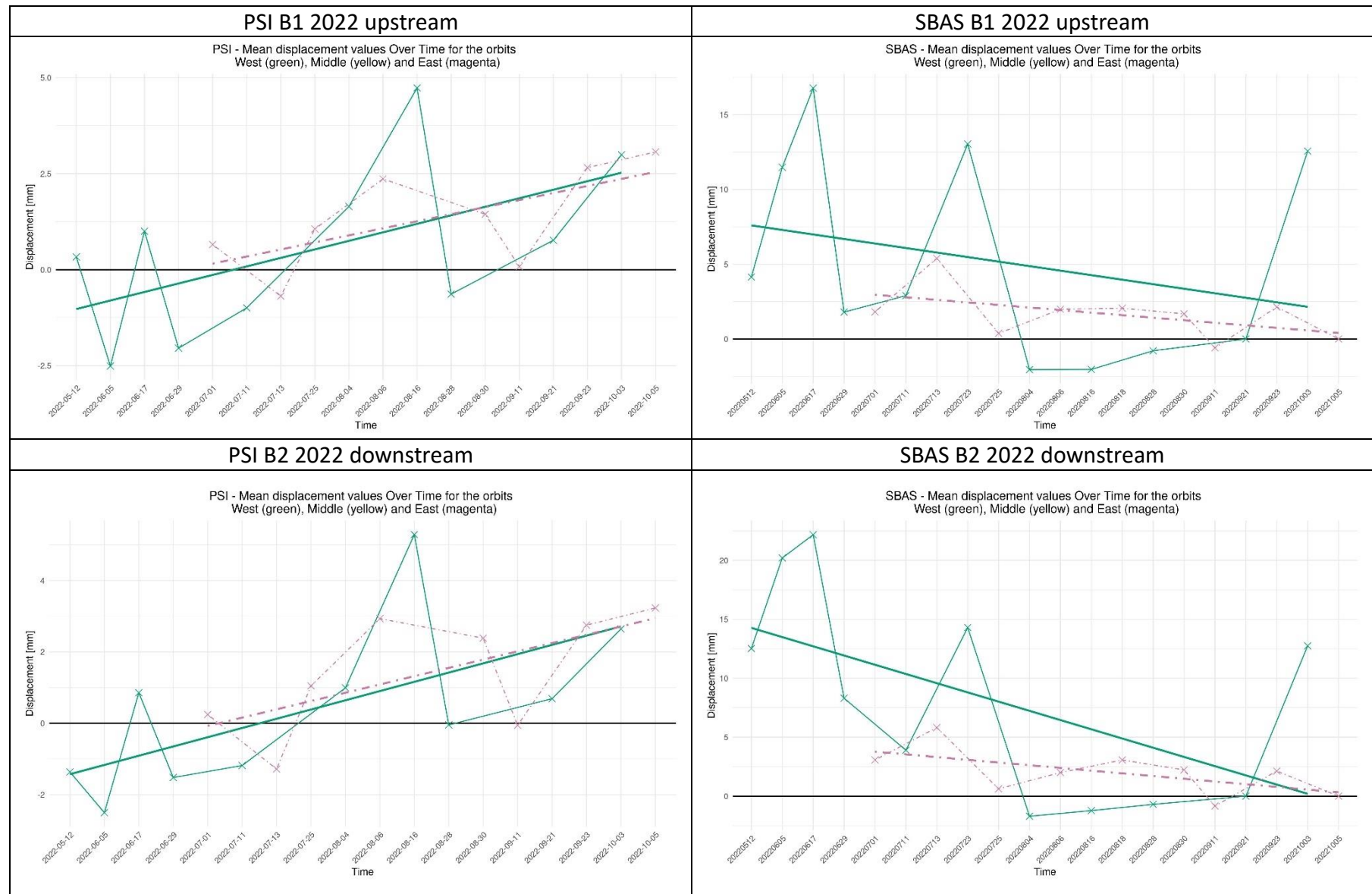












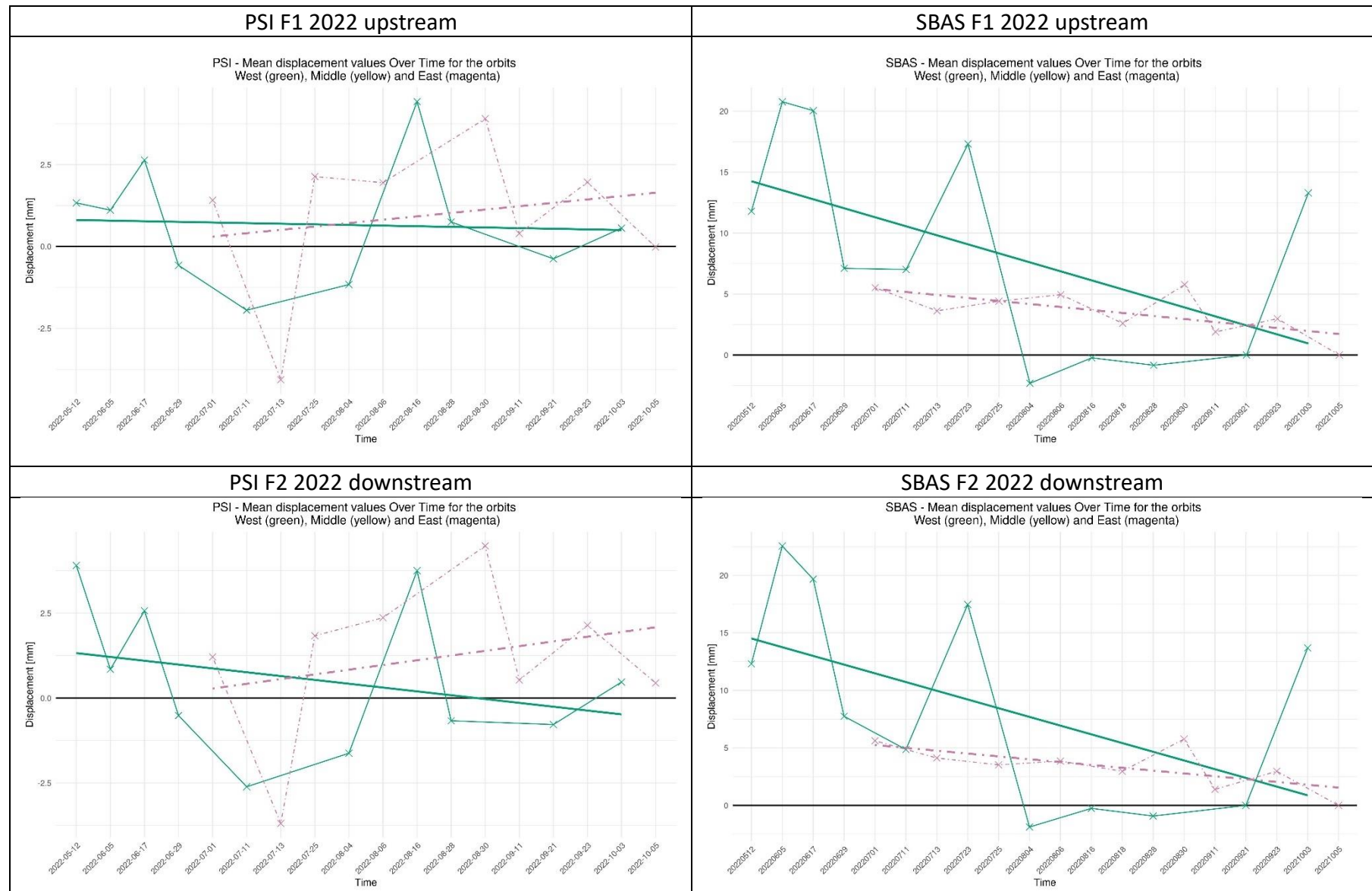


Figure 15: Timeseries plots for PSI and SBAS method results for the years 2019 – 2022. The plots are created for each Ecosite, respectively B1, B2 (for the Bog north and south of the road) and F1, F2 (for the Fen north and south of the road). The orbit tracks are represented by the colours green = West, yellow = Middle, and magenta = East, if the orbit track data is available in the specific year. On the x-axis the timeline is shown with explicit dates of the image acquisition. The y-axis shows the mean LOS displacement value of all valid pixels within a ecosite shapefile in mm.

Table 4: Statistical parameters of PSI timeseries analysis, namely R^2 , RMSE and retrieved from the Mann-Kendall timeseries trend test τ . If the τ result is statistically significant with p -value < 0.05 its cell is marked in light yellow.

PSI		B1 upstream				B2 downstream				F1 upstream				F2 downstream			
YEAR	ORBIT	R^2	RMSE	τ	p-value	R^2	RMSE	τ	p-value	R^2	RMSE	τ	p-value	R^2	RMSE	τ	p-value
2017	West	0.63	0.56	0.47	0.26	0.05	1.13	0.06	1.0	0.95	1.92	-0.60	0.13	0.91	2.72	-0.60	0.13
	Middle	0.38	1.39	0.47	0.07	0.01	1.33	0.16	0.60	0.90	1.88	-0.86	0.0006	0.86	2.18	-0.78	0.002
2018	West	0.16	1.27	0.22	0.46	0.35	0.75	0.39	0.17	0.00	2.44	0.05	0.9	0.08	2.81	0.28	0.35
	Middle	0.01	1.93	-0.11	0.72	0.01	2.38	-0.07	0.86	0.17	1.7	0.16	0.6	0.02	2.12	-0.24	0.37
2019	West	0.02	2.07	-0.20	0.44	0.1	1.92	-0.27	0.27	0.27	2.19	0.38	0.12	0.00	1.88	-0.16	0.53
	Middle	0.04	1.58	-0.13	0.64	0.27	1.00	-0.46	0.06	0.78	1.62	0.56	0.020	0.43	1.84	0.42	0.08
2020	West	0.02	2.81	0.21	0.37	0.05	2.8	0.27	0.24	0.09	2.55	-0.15	0.5	0.11	2.40	-0.24	0.30
	Middle	0.04	1.54	-0.24	0.35	0.01	1.36	-0.55	0.87	0.08	2.37	-0.16	0.5	0.37	2.18	-0.31	0.21
	East	0.79	0.57	0.72	0.010	0.79	0.57	0.67	0.016	0.50	1.46	0.50	0.07	0.73	0.93	0.67	0.016
2021	West	0.04	2.29	-0.08	0.75	0.01	2.38	0.10	0.66	0.16	2.25	-0.23	0.27	0.13	2.66	-0.21	0.32
	Middle	0.00	1.75	-0.08	0.74	0.01	1.58	-0.10	0.66	0.77	0.95	-0.67	0.0006	0.82	0.88	-0.78	0.0001
	East	0.00	1.65	0.03	0.91	0.01	1.33	0.12	0.58	0.73	1.27	-0.67	0.001	0.73	1.42	-0.67	0.001
2022	West	0.26	1.82	0.42	0.1	0.38	1.72	0.50	0.049	0.01	1.7	-0.15	0.6	0.13	1.97	-0.29	0.28
	East	0.39	0.95	0.57	0.063	0.4	1.21	0.50	0.10	0.05	2.14	0	1	0.08	2.10	0.07	0.90

Table 5: Statistical parameters of SBAS timeseries analysis, namely R^2 , RMSE and retrieved from the Mann-Kendall timeseries trend test τ . If the τ result is statistically significant with p -value < 0.05 its cell is marked in light yellow.

SBAS		B1 upstream				B2 downstream				F1 upstream				F2 downstream			
YEAR	ORBIT	R^2	RMSE	τ	p-value	R^2	RMSE	τ	p-value	R^2	RMSE	τ	p-value	R^2	RMSE	τ	p-value
2017	West	0.01	8.73	-0.14	0.76	0.09	8.55	0.14	0.76	0.04	7.22	-0.05	1	0.35	6.70	-0.24	0.55
	Middle	0.08	7.76	0.3	0.19	0.11	8.04	0.3	0.19	0.01	7.28	0.06	0.84	0.00	6.68	-0.03	0.95
2018	West	0.17	5.9	-0.15	0.54	0.15	5.39	-0.15	0.54	0.18	5.83	-0.12	0.63	0.16	5.97	-0.09	0.73
	Middle	0.09	5.74	-0.23	0.3	0.09	5.95	-0.23	0.3	0.14	5.4	-0.21	0.36	0.25	5.81	-0.23	0.30
2019	West	0.24	4	-0.25	0.23	0.33	3.99	-0.41	0.05	0.02	3.92	-0.1	0.66	0.06	3.44	-0.14	0.51
	Middle	0	4.67	0.03	0.91	0.05	4.21	-0.17	0.44	0.00	4.46	-0.08	0.74	0.06	4.30	-0.21	0.32
2020	West	0	8.31	-0.05	0.85	0.03	7.55	0.13	0.58	0.00	7.44	-0.05	0.85	0.06	7.41	0.15	0.50
	Middle	0	6.98	-0.15	0.5	0.04	6.81	-0.21	0.36	0.01	6.43	-0.26	0.25	0.01	6.31	0.03	0.95
	East	0.2	2.26	0.29	0.28	0.01	2.41	0.07	0.86	0.00	2.79	0.07	0.86	0.02	2.66	0.16	0.59
2021	West	0	4.2	0.05	0.84	0	4.3	0.03	0.92	0.02	3.57	0.14	0.49	0.00	4.27	0.01	1.00
	Middle	0.1	1.88	0.28	0.17	0.07	1.95	0.3	0.14	0.02	2.42	-0.01	1	0.03	2.98	-0.12	0.55
	East	0.15	2.82	0.33	0.09	0.2	2.88	0.37	0.06	0.1	3.21	0.2	0.32	0.05	3.68	0.14	0.49
2022	West	0.07	6.35	-0.2	0.44	0.3	6.98	-0.31	0.21	0.27	7.07	-0.38	0.12	0.27	7.30	-0.38	0.12
	East	0.26	1.4	-0.22	0.47	0.37	1.47	-0.44	0.12	0.47	1.28	-0.44	0.12	0.49	1.24	-0.56	0.05

3.2 Focus on 2021 Data

As in 2021 the two methods are peculiarly similar, it is chosen for a more detailed analysis. In addition, all three orbit tracks are available for examination. Furthermore, it is important to note that, 2021 had a particularly dry summer, despite the overall precipitation amount being close to average. The precipitation is distributed unequally though, with a relatively wet spring (May and June) and a dry summer (July, August, and September). This temporal pattern appears clearly in the variance and confidence intervals depicted in the 2021 timeseries boxplot graph (Figure 16). The three orbit tracks got merged in Figure 16 for ecosite B1 exemplarily (for B2, F1, F2 see Appendix). It becomes apparent, that in May and June the variability of the data is larger compared to the summer months. Mean (red crosses) and median (black horizontal line in IQ) values demonstrate a remarkable similarity across the entire dataset. The bottom and top border of the box in the plot corresponds to the 25th and 75th percentiles. The horizontal whiskers represent the mean \pm standard deviation, while the length of the straight whiskers visualize the median \pm 1.5 times the interquartile range (IQR). Any data points falling outside that value range are statistically classified as outliers. Noticeable is the peak on June 22nd coinciding with a four-day rain event with 5 mm to 10 mm precipitation per day. The next rain event with more than 5 mm precipitation per day occurs in the beginning of September, aligning with the next prominent peak in the data (observed on 2021-09-02). Following this event, the variability of the data increases once again.

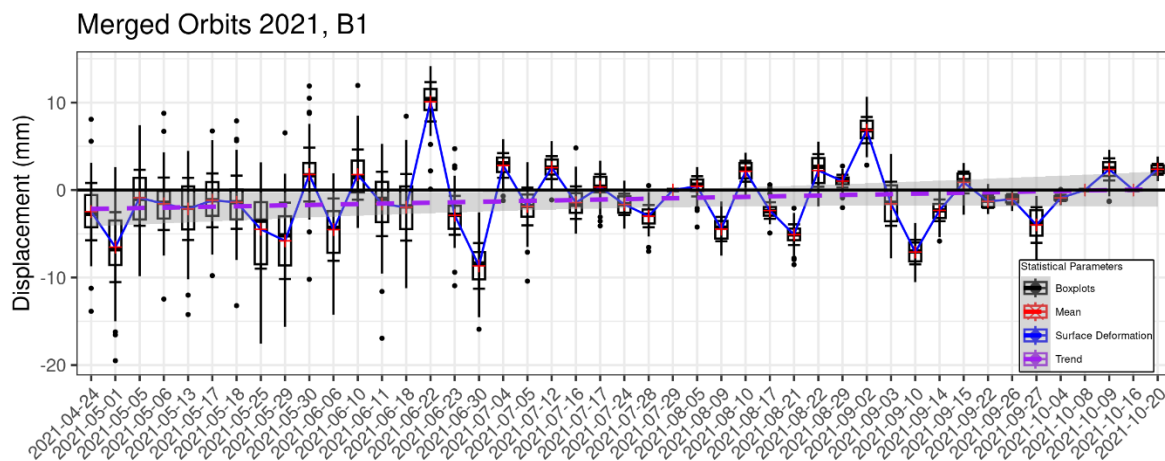


Figure 16: Timeseries 2021 focus on statistical parameters. West, Middle, East orbit track timeseries data of the SBAS method are merged and displayed with boxplot diagrams. Median = black horizontal line in box, mean = red cross, mean \pm standard deviation = horizontal whiskers, median \pm 1.5 IQR = length of vertical whiskers, extent box = IQR, outlier = black dots, trend of this merged timeline = purple dashed line with confidence interval.

Comparing the four ecosites in the merged timeseries plot for the SBAS method, a similar pattern can be detected. The minima and maxima are shown through all datasets but with different amplitudes. None of the trends are statistically significant, but the p-values for B1, B2 and F1 are lower here in the merged orbits as compared to the single orbit track data. The trend in B1, B2 and F1 is similar and all positive, whereas F2, the downstream fen, is close to zero (Table 6).

The intention behind generating the merged orbit data for all four ecosites is to facilitate a more comprehensive analysis of the disparities between the upstream and downstream side of both bog and fen. Consequently, the downstream side, represented by B2 and F2, is subtracted from the upstream side, B1 and F1. The resulting differences in displacements are visualized in Figure 17.

Upon closer examination of the differences between the two bogs, it becomes apparent that they are consistently around zero or tend to be slightly more positive. This implies that the north/upstream side experiences higher elevation or equal movement in the cases where the difference values are zero. On the contrary the differences observed in the fen during spring exhibit negative values, indicating that the downstream side experiences relatively to the upstream side more positive or less depression of the surface elevation. This pattern changes in the summer months when the difference values become positive. This suggests that F1, located on the upstream side of the road, is characterized with more uplift or less depression values than F2 (downstream) in terms of surface displacement over time, demonstrating the influence of the road on the surface elevation of the adjacent peatlands.

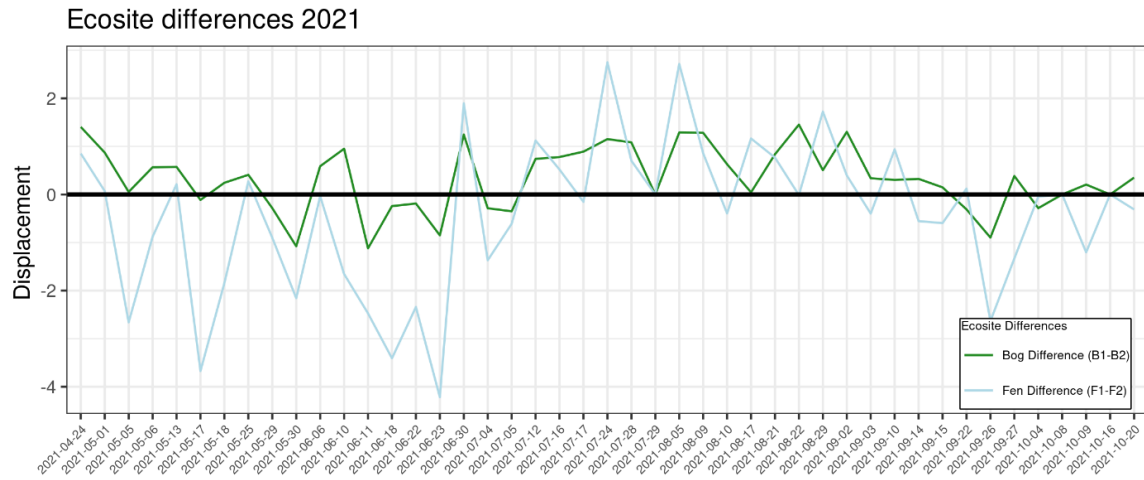


Figure 17: Displacement differences over time. In green is the difference between shapefile mean values of B1 – B2, in blue for F1-F2.

Table 6: Statistical parameters of the 2021 merged orbit track data timeseries, calculated with the SBAS method. τ and p -value are calculated with the Mann-Kendall test.

SBAS merged	R^2	RMSE	τ	p -value
B1	0.03	3.3	0.18	0.08
B2	0.04	3.4	0.17	0.09
F1	0.013	3.2	0.14	0.18
F2	0.0009	3.8	0.02	0.8

3.3 Spatial Distribution of Yearly Velocity Rates of West Orbit Track Data

Figure 18 illustrates the spatial distribution pattern of yearly LOS velocity rates in mm. It is important to note that, the main part of the road construction, the adding of the mineral filled layer, happened during the end of 2018 and the beginning of 2019. Consequently, the patterns observed in the years 2017 and 2018, prior to this substantial disruption, are described briefly. Detailed graphs can be found in the Appendix.

For the analysis of velocity rates, SBAS and PSI were applied. However, due to the limited availability of accepted PS in the PSI dataset, the results are not as informative and spatial patterns less suitable for interpretation. Therefore, only the velocity rates of 2019 obtained through the PSI method are presented to demonstrate the retrievable patterns. The differences between the patterns for all years are briefly discussed, focused on the west orbit track velocity as it is available through the whole study period. Additional graphs depicting the velocity rates from both methods over the whole study period can be found in the Appendix.

The SBAS velocity map of 2017 shows very pixelated patterns with contrary high values of uplift and sinking tendencies. PS are quite rare, so that no spatial patterns can be detected. In 2018 the SBAS velocity shows a large-scale sinking pattern with some hotspots and small contrary uplift pattern, e.g., east of the small east lake. The PS density is higher than in 2017, especially in the bogs. It is remarkable, that there are no patterns detectable, that are clearly disrupted or bisected along the road, which still is missing the mineral filled layer, but already has been vegetation cleared.

2019 SBAS velocity shows several patterns of interest, like the upwards movement around the two small lakes. The bog ecosystems are mostly characterized by a downwards movement. Especially high downwards movements, around -20 mm/year to -60 mm/year, can be detected at the transition from bog to fen, where on the contrary in the F1 an uplift around +20 mm/year is indicated. This uplift solely happens on the north side and stops at the road at the ineffective culvert EC12. At EC11 there are more uplift pixels on the south side vicinity, but exactly at the culvert there are a few sinking indicating pixels on the south and four upwards pointing pixels on the north side of the road. At EC8 the same pattern as EC12 can be spotted, even more definite. At EC 6 and EC7, east of the fen shapefiles, but still in fen landscape, there can be a more moderate downwards movement detected than on the south side. PSI has a higher PS density than in the years before. It allows to trace some of the large-scale patterns of the SBAS method, but no effects can be located at the culverts positions due to a lack of PS. In the bog, the density is high enough to portray a diverse image of velocities, dividing the bog shapefiles into half, with the east part showing a downwards and the west part showing an upwards movement for B1 and B2. In addition, the lifting pattern around the lakes is indicated.

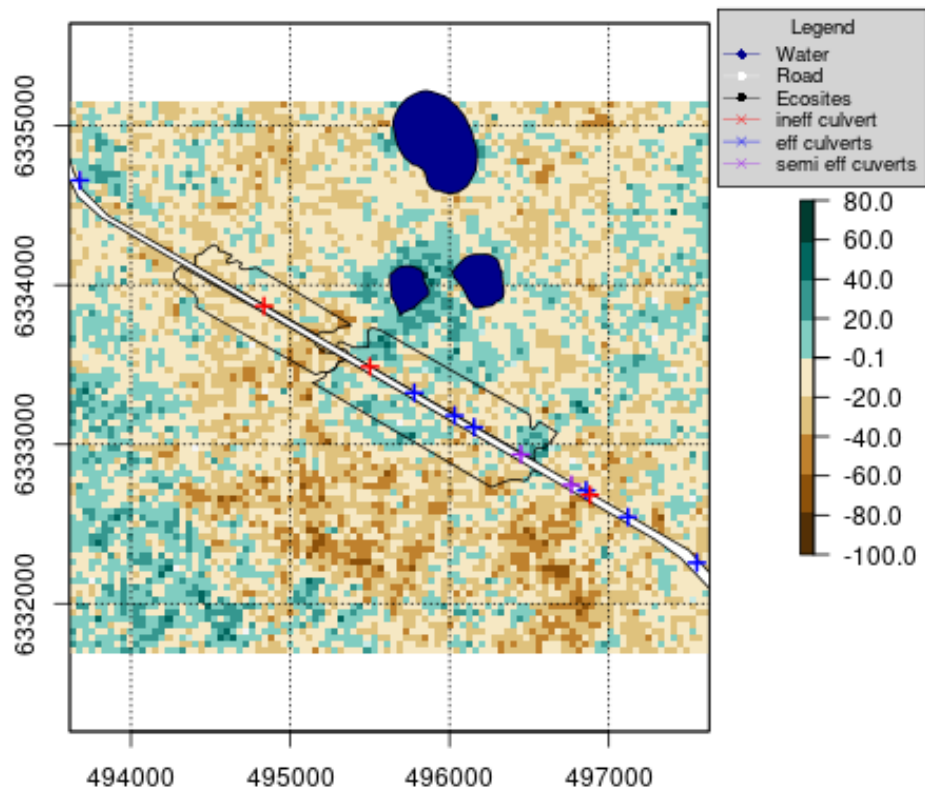
The measurements from 2020 are characterized by higher SBAS velocity values and more intense upwards movements as 2019. Again, the area around the lakes shows high upwards movements. Whereas the pattern at EC12 reverses compared to 2019, EC6 & 7 intensify their discrepancy between north and south side. EC11, an effective culvert shows no LOS velocity on the north side, but a strong upwards pattern on the south side, as well as EC12, which is a mostly ineffective culvert with big ponds on the north side, but it is flowing at high water levels. The PSI spatial pattern indicates no clear patterns in the vicinity of the road.

The measurements from 2021 indicate more moderate yearly velocity rates than the years before with values mostly between -20 mm/year to +20 mm/year. Around the lakes a small upwards tendency can be determined. The bogs show a mixed, but rather sinking tendency. F1 (upstream) shows rather an upwards pattern and F2 (downstream) a downward one. Peculiarly are the culverts EC12 and EC9. EC12 divides positive movement rates from negative ones on the south, as does EC9, which indicates a dysfunctionality. EC7 contrary shows a moderate sinking pattern on the north, and positive values on the south.

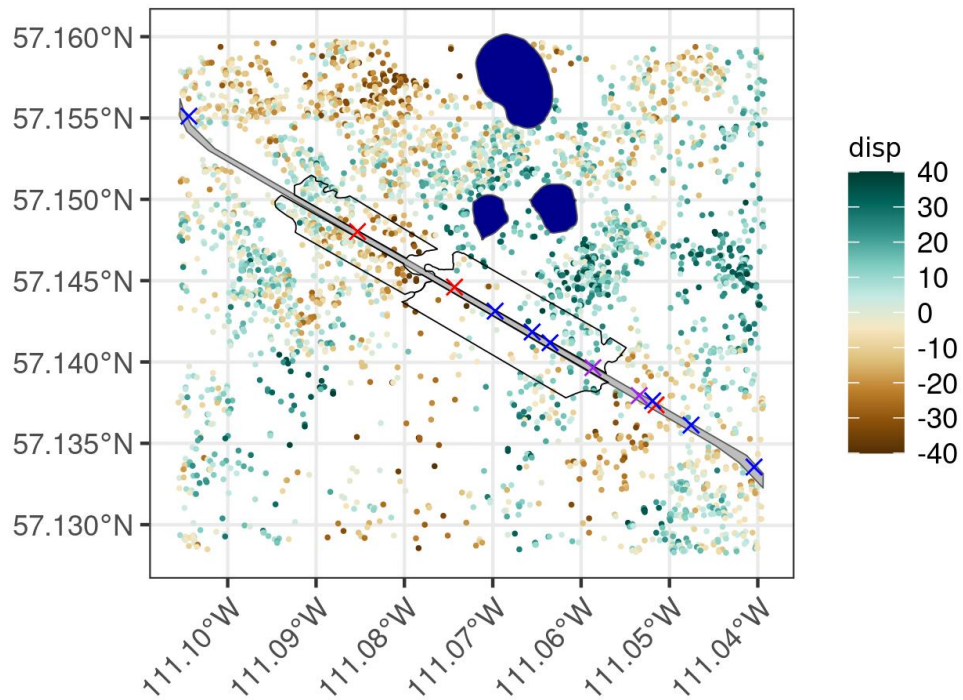
2022 is characterized by more extreme velocity rates and smaller scale patterns. Around the lakes a downward movement is detected. B1 shows a mix of slight downwards and upwards pointing velocities, whereas B2 shows severe downward ones around - 60 mm/year, particularly in the vicinity of EC13. EC12 & EC9 indicate a similar pattern, but with more moderate rates around ± 20 mm/year. EC8 in contrast shows negative rates in F1 and positive to more moderate negative ones in F2.

2019

SBAS Velocity (in mm/year) - 2019 West Orbit

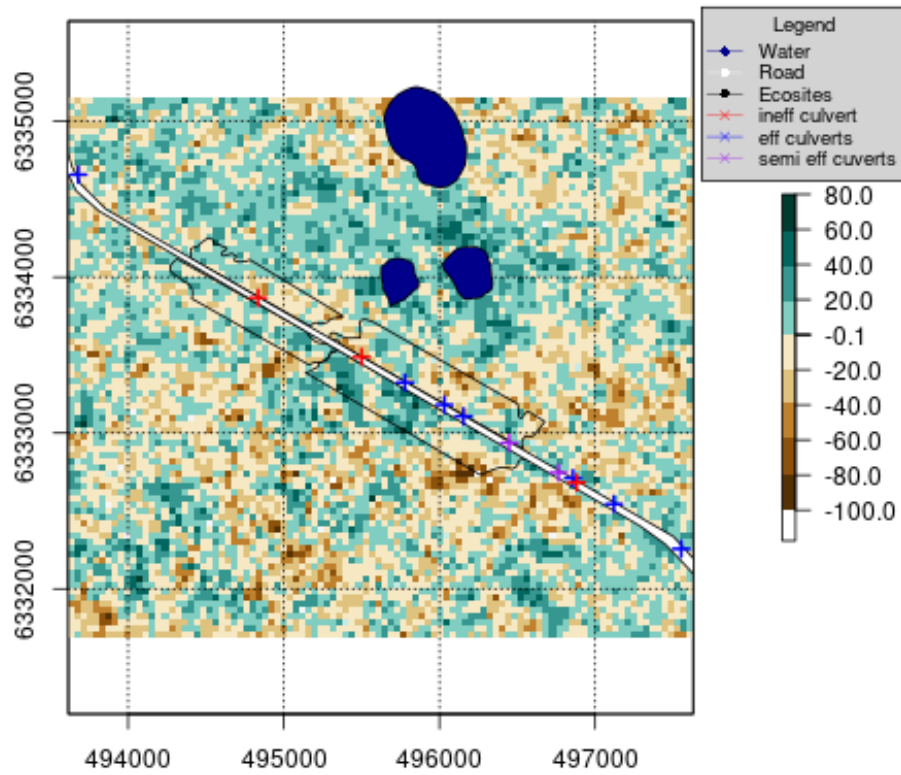


PSI velocity (mm/year) - 2019 West Orbit



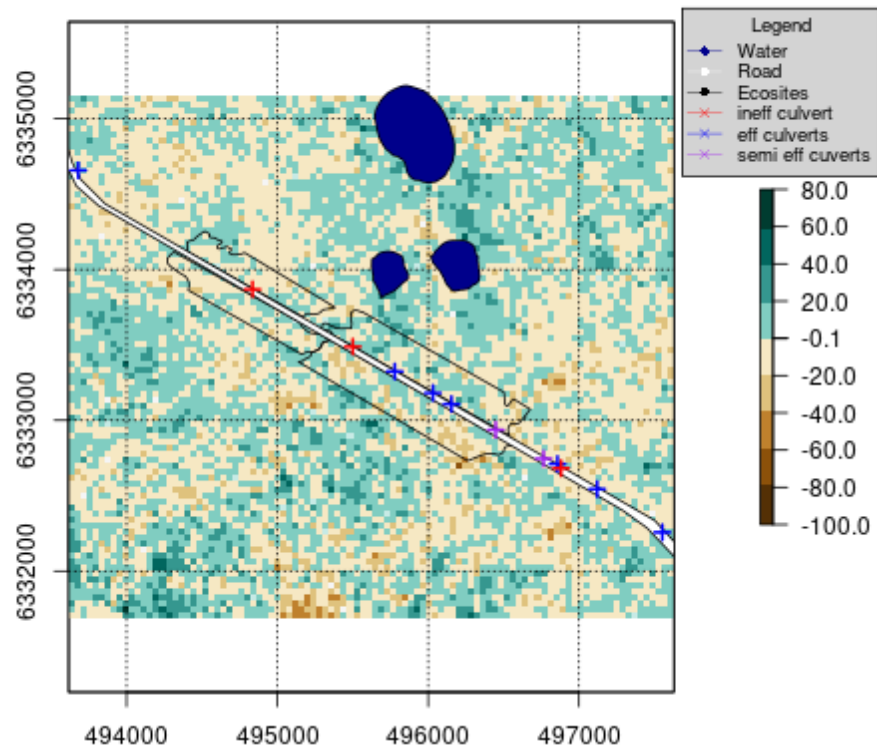
2020

SBAS Velocity (in mm/year) - 2020 West Orbit



2021

SBAS Velocity (in mm/year) - 2021 West Orbit



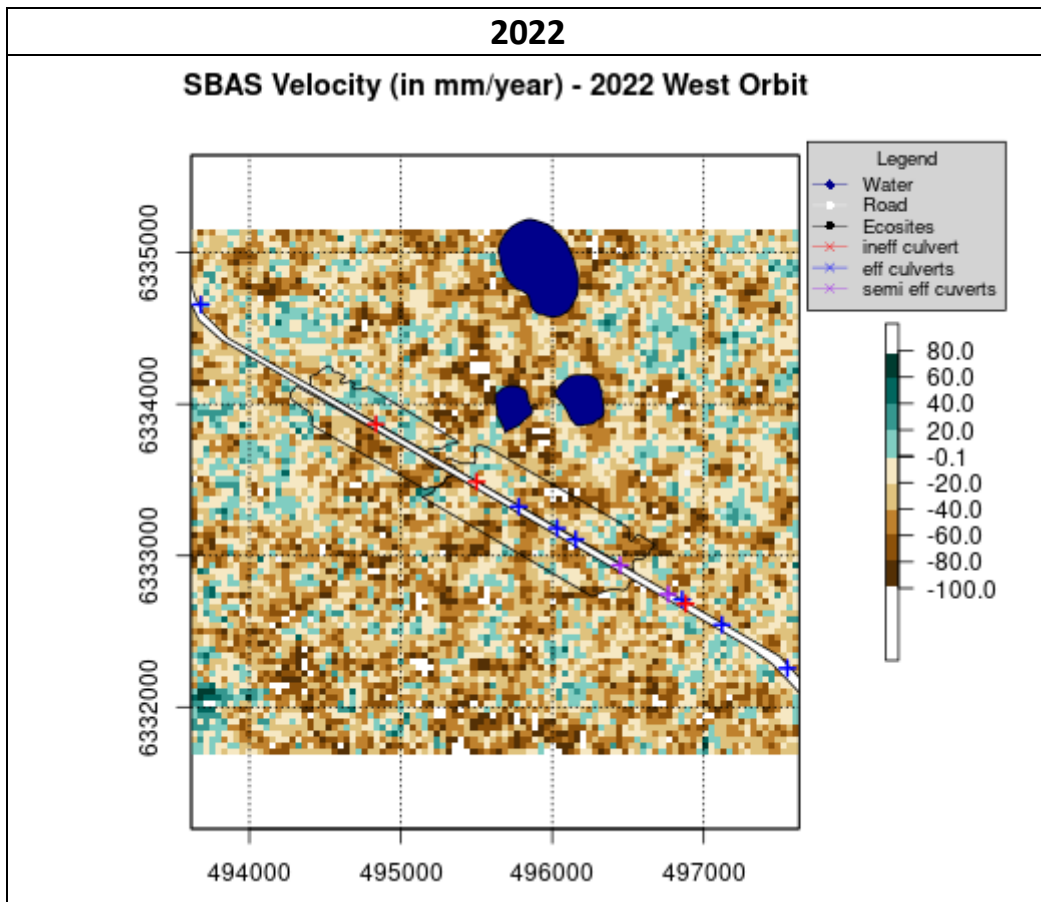


Figure 18: Spatial distribution of yearly LOS rates in mm generated from West Orbit track data. The SBAS results are illustrated from 2019 till 2022. The PSI only for 2019. The Figure shows velocity rates from -100 mm/year to +80 mm/year. The scale is on all graphs identical. Symbology: Blue = Water Mask, White shapefile = road, Ecosite Shapefile border = black, ineffective Culverts = red cross, effective culvert = blue cross. Spatial reference: NAD 1983 UTM Zone 12N.

4. Discussion

In the context of this study, which focuses on assessing edge effects of the resource access road in Aspen within boreal peatlands in Alberta, the goals are to apply and compare the PSI and SBAS method for analysing surface deformation. The interpretation of the results is not trivial nor straightforward due to the complex nature of data. Neither graphical visualization of the timeseries data for various ecosites over time, nor their statistical parameters provide a robust interpretation. However, the results suggest that InSAR techniques have the potential to detect surface motions caused from hydrological changes in the peatlands. Especially the velocity plots exhibit small-scale variations that offer valuable information for interpretation and for drawing conclusions. It is essential to account for possible errors and inaccuracies to obtain an accurate picture of the quality of the methods. Nonetheless, despite those limits, careful and sensitive analysis allows for some conclusions to be drawn as described in the following:

Timeseries Analysis:

The statistical robustness of the timeseries data is limited. Neither the trends nor the timeseries itself provide sufficient information for a detailed and specific interpretation. Several factors contribute to this limitation:

Firstly, the differences between the two methods mostly overshadow the distinctions among various ecosites and the downstream and upstream sides. Consequently, it becomes challenging to interpret patterns solely from one method, especially when it contradicts the other method. Those differences can be caused by methodological variations. For instance, the PSI method in this study has sparse but high-quality data in terms of coherence. On the other hand, the SBAS method accepts a lower coherence resulting in a larger dataset used for calculating the ecosites mean displacement. However, that takes low coherence pixels with unknown distributed scatter properties and a higher noise signal into account. Such noise can be caused by surface deformation or by errors or influences on the phase signal, like the atmospheric effects, artefacts, random noise, phase unwrapping errors, that have not been corrected during the processing. Those errors can still occur for high coherence pixels or PS, although the likelihood is reduced. The overall methodological goal is to extract the displacement from the phase information by separating it from those other influences (Crosetto et al., 2016). Furthermore, the

quality of a timeseries and its analysis results depend heavily on other factors. In this dataset relevant are:

- Poor Spacing: this issue arises from unevenly spaced time series data and can affect the reliability. In general, all the orbits have timesteps with regular spacing of 12 days, but sometimes data is missing, flawed or of poor quality and are not considered.
- Resolution of the data: this refers to the granularity of the time series data. A time series with a high time resolution can capture more fluctuations, whereas a lower resolution may only capture broader trends. This especially could contribute to the variations among the orbit track data within one method and heavily influences the trend directions (Hyndman and Athanasopoulos, 2018).

In essence, both of those factors are based on the number of data points, which is quite low with 7 to 15 for each orbit track. That is reflected in the statistical values and variability of the trends as well.

Secondly, the spatial mean of each shapefile is calculated, which smooths the individual datapoints. This approach, compared to median values, tends to account more for extreme values that can arise due to edge effects, but potentially causing the loss of important details (Cryer and Chan, 2008). The analysis of velocity maps reveals some small-scale differences, but in the timeseries analysis no substantial disparities are detected in ecosite characteristics upstream or downstream.

The third reason for divergent PSI and SBAS results can be attributed to signal attenuation through the presence of water during and after rainfall events. While the precise amount and moisture thresholds involve speculation, there are indications both in literature and the data that rain events introduce discrepancies and errors in the results (Danklmayer et al., 2009; Lu, 2007).

In addition to the loss of coherence mentioned earlier, the primary factor limiting the accuracy of differential interferometry is the presence of unaccounted phase propagation delays in the atmosphere. These delays occur as the electromagnetic radiation passes the ionosphere, stratosphere, and troposphere, starting from an altitude of approximately 700 km. The anomalies in delay arise from variations in the refractive index along the LOS.

These variations result from fluctuations in temperature, pressure, and water vapor content within the atmosphere between two radar acquisitions. Consequently, the phase information of the two signals is affected in distinct ways, leading to the generation of erroneous interferograms. Changes in the dielectric constant further modify the propagation velocity of radar energy, introducing a phase delay in the received signal (Danklmayer et al., 2009; Lu, 2007)

The effect of changed dielectric properties is described in the results, with the data points representing maximums in one and contrary minimums in the other method coinciding with rain events. This observation suggests a strong link between coherence, scatterer properties and the presence of water. It may even be a strong contributing factor to the differing amplitudes observed between the methods, especially considering 2021 experienced a particularly dry summer where the amplitudes are relatively similar. If this latter consideration is valid, even small amounts of moisture in the atmosphere and on the surface of scatterers could be sufficient to disperse the results of the methods. However, it is important to note, that the relationship between the influencing factors is complex, involving various interacting elements with undefined severity and unknown feedback mechanisms. As a result, making definitive statements about their precise impact is challenging.

To validate the results, three orbit tracks were utilized, which offered varying looking angles. The overall outcome of this validation approach was unsuccessful, as rarely trends are statistically robust or their tendency within one method is contrary. Another limitation is, that not all three tracks are available for every year, and even when they are, their image acquisitions happened at different time steps and started at different dates. The WT holds potential as a validation option, its availability though is restricted to a too short period for now. It may prove beneficial in future studies, but for this study and its results it is limited. The only possibility to draw parallels between WT and the timeseries is 2022, where the west orbit track of the SBAS method roughly portrays the WT trajectory with a rise in May and June and a sinking trend for the rest of the year. The timeseries of the east orbit starts too late to cover the rise in spring.

To address some of the statistical properties, the in-depth focus on the year 2021 is discussed. This serves mainly two purposes: first, to enhance and discuss the data variation and its causes, and second, to explore a longer time series through merging the orbit data and thereby providing a more comprehensive dataset.

Statistical Focus on 2021

In the context of the observed dry conditions, particularly during the summer months of 2021, it is conjectured that the results and amplitudes obtained from both methods showing great similarity. This arises from the discussed influence of moisture, encompassing changes in propagation and reflecting properties. Another supporting indication can be found in the PSI velocity map showing a higher overall coherence, as it contains more PS. Further evidence in favour of this thesis is derived from the in-depth focus on 2021 statistical analysis, which reveals compelling arguments. The rainfall events can be tracked through an increase in data variability. Specifically, the spring season exhibited a relatively wet period with high variability, whereas the subsequent dry summer showed reduced variability. Notably, a prominent peak in data variability and surface uplift coincided with a substantial rain event on June 22nd. Following this event, a period of low variability and surface stability persisted throughout the dry summer until early September, when variability and surface responses increased in conjunction with another rain event. It is important to note, that these observations were made in a bog, indicating that during dry and warm summers, a significant sinking tendency would not be expected due to the minimal influence of groundwater.

The statistical analysis of the merged orbit timeseries indicates a higher level of robustness compared to individual orbits, although the observed differences are not statistically significant. The validity of merging data from three different orbit tracks needs consideration. On the positive side, the merged dataset demonstrates more robust statistical parameters, and the similarity in amplitude and trends among the orbits in 2021 provides further support. It is important to acknowledge that each orbit is derived from distinct observations taken at different times and from varying looking angles, posing challenges in terms of validation for this approach. The differing looking angles introduce longer atmospheric transition paths, potentially influencing the properties of scatterers (Danklmayer et al., 2009). Nevertheless, all orbits observe the same in-situ phenomenon.

A detailed examination of the data reveals no substantial differences between the median and mean values, which indicate, that the choice on which one to use does not significantly impact the results. However, the IQR intervals and range of outlier values remain considerable, particularly during the spring season. This likely contributes to the varying trends and non-robust nature of the statistical analysis.

The observed differences between the ecosites show a pattern that aligns with the ecological and physical properties of peatlands. The data quality and informative value already has been discussed, yet the physics-based logical conclusion here is so prominent that it must be emphasized. As bogs are ombrogenous systems, the influence of WT for the surface deformation is limited, especially compared to the groundwater connected fens. Consequently, the dry period in the summer months coinciding with sinking WT is expected to be less pronounced in the bogs compared to the fens. Taking this one step further, this implies that a hydrological barrier, such as the road, would induce fewer differences in a bisected bog than in a disrupted fen. This is primarily due to the hydrological properties of fens, which rely on the influence of groundwater, subsurface and surface flows. These dynamics can be observed in the patterns of the difference graph (Figure 17, Government of Alberta, 2015).

Spatial Distribution of Yearly Velocity Rates of West Orbit Track

The annual velocity spatial pattern of the west orbit track offers insights into small-scale surface movements. The visualizations provide a comprehensive depiction of variations along the road. A key indication, that these differences are attributed to the road intersecting the peatlands, rather than to randomness or road independent ecosystem parameters, is the inability to detect such patterns in the figures for 2017 and 2018. During those years, the road consisted only in the form of a vegetation cleared line and some peat compression caused by heavy machinery, without significant impact to disrupt horizontal hydrological flows. Another supporting factor is the correlation between the observed patterns and the position of semi-effective and ineffective culverts. In the immediate vicinity of several pixels around the culverts, clear effects and signals can be detected.

A limitation is, that prior knowledge of culvert locations is required to ensure the proper detection of these patterns. Vice versa, once the culvert locations are known, rough monitoring can be designed to provide a general overview of their functionality. Especially

considering the road's relatively young age of only three years, it is expected that these effects will increase in size and magnitude over time (Willier et al., 2022). Additionally, the long-term efficiency of culverts tends to decrease due to blockages or shifting surfaces, making them less effective. While qualitative detection of increasing edge effects and the functionality of semi-effective culverts is possible, quantitative statements remain difficult to obtain. The resolution coverage is too broad to robustly assess these factors. The different levels of functionality are clearly demonstrated among the three culverts (EC11, EC7, EC6) shown in section 2.2.3. EC11 serves as an example of a well-working culvert, as indicated by its performance. Conversely, EC6 exhibits signs of improper functioning, which is demonstrated by both, the velocity plots, and the image. It is functioning at very high WT levels, but ultimately classified as a malfunctioning one. An interesting feature to note is the presence of a parallel culvert connecting the ponds of EC6 with the semi effective EC7 culvert. The parallel culvert is fully functional. In 2020 the discrepancy between upstream and downstream is increased in their vicinity, but in 2021 a contrasting pattern emerges, indicating a certain degree of water exchange. These estimates are based on the data but are consistent with the in-situ observations. This suggests that the employed method is capable of tracking in-situ surface deformations to a certain extent. The pattern in 2021 reveals a none to slightly sinking tendency in the bogs and contrary velocity trends in the fen with F1 experiencing an uplift and F2 a sinking movement. That aligns with the expected physical behaviour, as the bog is relatively isolated from groundwater influence, whereas it drives the fens surface movement dynamics. This observation highlights the impacts of a hydrological barriers. The effects are in the rough extend of the chosen shapefiles.

In 2022, fewer timesteps are available and the precipitation effects through summer are more pronounced.

It can be observed that the bog exhibits a higher number of PS throughout the study period, compared to the fen. The greater abundance of PS indicates a higher coherence over time and a variation of scatterers in that area. This disparity may be attributed to vegetation differences, like a higher tree density. Shrub scatterers are more susceptible to wind, than tree stems and are characterized by lower coherence values. Consequently, the SBAS method is more suitable for the spatial velocity plots of this study area in the

northern peatlands of Alberta. The PSI is preferred in areas with infrastructure or strong scatterers (Bradley et al., 2021). The timeseries approach where the spatial pattern of the ecosite shapefile is calculated to a mean value is still a valid approach, as the fewer PS have a higher quality. As it is hard to validate InSAR methods in general, a comparison between two approaches increases the robustness of statements and puts them in an appropriate context (Crosetto et al., 2016).

Possible Errors of InSAR Analysis

Several factors can introduce errors and affect the quality of results in the context of InSAR analysis. The impact of rain events and subsequent changes in moisture levels, as well as atmospheric variations on wave propagation have already been addressed. However, it is important to consider additional potential sources of errors that can influence the reliability of the outcomes.

One crucial aspect, that determines the quality of InSAR results, is coherence. Coherence refers to the level of correlation or similarity between radar images acquired at different times. Various factors can affect coherence, including temporal, spatial, and volumetric decorrelation, ground changes, and the above-mentioned soil, surface & vegetation moisture. These factors have been identified in studies such as De Zan et al. (2015), Tampuu et al. (2020), and their influences on coherence should be taken into account when interpreting InSAR results. Temporal decorrelation refers to the decrease in coherence over time between image acquisitions at different points in time. It occurs due to environmental changes and is particularly prominent when there is a significant time gap between acquisitions. The spatial decorrelation is a result of viewing the targets from different positions. The volumetric decorrelation is related to loss of coherence caused by a structure change or volumetric properties. This addresses changes in the distribution of scatterers or reflective surfaces causing variations in the radar wave interactions. By considering these potential error sources, researchers can enhance the accuracy and credibility of their analyses (Crosetto et al., 2016; ESA, 2007; Liu et al., 2015; Tampuu et al., 2020).

The short snow-free period is another obstacle in obtaining surface deformation in northern peatlands. Although snow-free doesn't mean, that under snow cover no hydrological parameter changes are happening in the soil, but as long snow is present

surface movements are not traceable due to the different scattering characteristics of snow and ice.

Additionally, there are methodological choices, that influence the results. The choice of the shapefiles' extents is based on the ecosite distribution and aligned with the groundwater well placement. The quality of the timeseries results, compared to the small-scale velocity map analysis, can prompt to question this choice, or at least initiate a discussion on whether a different approach based on data patterns, or an AI clustering would yield better outcomes. On the other hand, the velocity map results show that the observed effects do not extent beyond the current boundaries of the polygons. This ensures that the timeseries adequately includes the phenomena.

5. Conclusion and Outlook

The overarching aim of this research study is to characterize surface deformation within boreal peatlands through the InSAR techniques PSI and SBAS on the Aspen road. The complex nature of data presents a formidable challenge in terms of interpretation. Timeseries analysis, while promising, exhibits limited statistical robustness, with differences between the two methodologies outweighing distinctions among diverse ecosites and between the upstream and downstream sides. Factors such as inadequate spacing and data resolution contribute to this limitation.

Despite these challenges, the in-depth examination of 2021, notably the disparities amongst ecosites and the velocity plots, provided valuable information for interpretation and drawing conclusions. This demonstrates the feasibility of extracting information about edge effects of energy development infrastructure, especially concerning mineral-filled access roads, using InSAR. Following the careful assessment of the outcomes, a prudent qualitative evaluation can be undertaken. However, for quantification of edge effects data's statistical robustness falls short and too large amount of the results are contradicting each other.

In the future, the forthcoming Sentinel 1C mission holds promise to restore superior time resolution, as it has been lacking since the breakdown of Sentinel 1B in December 2021. Other SAR systems and algorithms also show potential. One enduring issue of PSI algorithms remain that identical data processed via various methods produces different errors and therefore different results. This, coupled with the complexity of PSI results, makes a ground validation a complex task. It is crucial to comprehensively discuss the uncertainties of both approaches to effectively assess the results and their significance. Moreover, considering future InSAR applications, like a large-scale monitoring, there is potential in augmenting automation, accelerating quality control, and improving data processing capabilities, especially given the dimension of the AOS. This could prove valuable for monitoring not only the edge effects of access roads, but also wells, and extensive WT movements (Crosetto et al., 2016).

The most value of information in this study add the SBAS velocity map. A key element is the capability of the approach to provide space-time characteristics with extended special coverage allowing to identify peculiar features (Lanari et al., 2007). The SBAS method is

designed to improve density and spatial distribution of survey points to return better measurements in vegetated areas, where the PS methods habitually struggle due to incoherence (Bradley et al., 2021).

The Aspen area offers considerable opportunities for further exploration, given the relative recent establishing of the road in 2019 and the likely intensification of hydrological changes over time. Supplemental GW measurements and the precise weather station data, which are available recently, can provide important insights and support validation. On top, for this area a validation approach of the InSAR techniques and its results could be possible, as there are large-scale LiDAR mission data available. With a mission executed in 2017 and another in 2022, this could provide a high degree of precision for InSAR result validation, especially if multi-year trends in an ecosite can be detected.

In summary, the methodological approach and pattern clusters observed in this study suggest a greater success in detecting large-area movements. Yet, continued monitoring of the road and temporal changes could yield promising results, especially in relation to the detection of culvert patterns. Despite the current ambiguity and absence of clear and concrete conclusions, the study's findings remain valuable. They could serve to detect large-scale patterns more effectively and monitor the functional status of culverts, thereby developing into a potential source of information. These gained insights need to be utilized to guide planning and decision-making process, particularly in the design of new roads, positioning of culverts, and evaluation of their efficiency.

Additional research topics to explore might include:

- Conducting comparative studies of other access roads with already more pronounced edge effects.
- Assessing large-scale WT movements and patterns.
- Implementing AI or machine learning techniques for automated, large-scale data processing and pattern detection.
- Building models to predict future changes based on existing data and trends, especially regarding a potential meteorological pattern change caused by climate change.
- Assessing restoration of peatlands in terms of monitoring restoration of natural peat conditions, removing old roads, rewetting dry areas.

References

- Alaska Satellite Facility, 2023a. InSAR on Demand. URL <https://storymaps.arcgis.com/stories/68a8a3253900411185ae9eb6bb5283d3> (accessed 5.23.23).
- Alaska Satellite Facility, 2023b. HyP3 Sentinel 1 InSAR Product Guide. URL https://hyp3-docs.asf.alaska.edu/guides/insar_product_guide/#processing-options (accessed 5.23.23).
- Alberta Parks, 2015. Natural regions & subregions of Alberta: a framework for Alberta's parks. Alberta Tourism, Parks and Recreation, Edmonton, Alberta.
- Alshammari, L., Boyd, D.S., Sowter, A., Marshall, C., Andersen, R., Gilbert, P., Marsh, S., Large, D.J., 2020. Use of Surface Motion Characteristics Determined by InSAR to Assess Peatland Condition. *J. Geophys. Res. Biogeosciences* 125. <https://doi.org/10.1029/2018JG004953>
- Alshammari, L., Large, D., Boyd, D., Sowter, A., Anderson, R., Andersen, R., Marsh, S., 2018. Long-Term Peatland Condition Assessment via Surface Motion Monitoring Using the ISBAS DInSAR Technique over the Flow Country, Scotland. *Remote Sens.* 10, 1103. <https://doi.org/10.3390/rs10071103>
- Aslan, G., Cakir, Z., Lasserre, C., Renard, F., 2019. Investigating Subsidence in the Bursa Plain, Turkey, Using Ascending and Descending Sentinel-1 Satellite Data. *Remote Sens.* 11, 85. <https://doi.org/10.3390/rs11010085>
- Atzberger, C., 2013. Advances in Remote Sensing of Agriculture: Context Description, Existing Operational Monitoring Systems and Major Information Needs. *Remote Sens.* 5, 949–981. <https://doi.org/10.3390/rs5020949>
- Bamler, R., Hartl, P., 1998. Synthetic aperture radar interferometry.
- Bartels, S.F., Chen, H.Y.H., Wulder, M.A., White, J.C., 2016. Trends in post-disturbance recovery rates of Canada's forests following wildfire and harvest. *For. Ecol. Manag.* 361, 194–207. <https://doi.org/10.1016/j.foreco.2015.11.015>
- Berardino, P., Fornaro, G., Lanari, R., Sansosti, E., 2002. A new algorithm for surface deformation monitoring based on small baseline differential SAR interferograms. *IEEE Trans. Geosci. Remote Sens.* 40, 2375–2383. <https://doi.org/10.1109/TGRS.2002.803792>
- Blasco, J.M.D., Fomelis, M., Desnos, Y.L., Engdahl, M., Fernandez, D., Veci, L., Lu, J., Wong, C., 2018. SNAP - StaMPS Integrated processing for Sentinel-1 Persistent Scatterer Interferometry.
- Bocking, E., Cooper, D.J., Price, J., 2017. Using tree ring analysis to determine impacts of a road on a boreal peatland. *For. Ecol. Manag.* 404, 24–30. <https://doi.org/10.1016/j.foreco.2017.08.007>

- Boreal Ecosystem and Recovery Assessment, 2023. URL www.beraproject.org.
- Bradley, A.V., Andersen, R., Marshall, C., Sowter, A., Large, D.J., 2021. Identification of typical eco-hydrological behaviours using InSAR allows landscape-scale mapping of peatland condition (preprint). *Biological: Eco-Hydrology*. <https://doi.org/10.5194/esurf-2021-58>
- Canadian Association of Petroleum producers, 2022. What and where are the Oil Sands.
- Crosetto, M., Monserrat, O., Cuevas-González, M., Devanathéry, N., Crippa, B., 2016. Persistent Scatterer Interferometry: A review. *ISPRS J. Photogramm. Remote Sens.* 115, 78–89. <https://doi.org/10.1016/j.isprsjprs.2015.10.011>
- Cryer, J.D., Chan, K., 2008. Time series analysis: with applications in R, 2nd ed. ed, Springer texts in statistics. Springer, New York.
- Danklmayer, A., Doring, B.J., Schwerdt, M., Chandra, M., 2009. Assessment of Atmospheric Propagation Effects in SAR Images. *IEEE Trans. Geosci. Remote Sens.* 47, 3507–3518. <https://doi.org/10.1109/TGRS.2009.2022271>
- De Zan, F., Zonno, M., Lopez-Dekker, P., 2015. Phase Inconsistencies and Multiple Scattering in SAR Interferometry. *IEEE Trans. Geosci. Remote Sens.* 53, 6608–6616. <https://doi.org/10.1109/TGRS.2015.2444431>
- Delgado Blasco, J., Fomelis, M., Stewart, C., Hooper, A., 2019. Measuring Urban Subsidence in the Rome Metropolitan Area (Italy) with Sentinel-1 SNAP-StaMPS Persistent Scatterer Interferometry. *Remote Sens.* 11, 129. <https://doi.org/10.3390/rs11020129>
- Ducks Unlimited Canada, 2016. Resource Roads and Wetlands.
- Elmes, M.C., Kessel, E., Wells, C.M., Sutherland, G., Price, J.S., Macrae, M.L., Petrone, R.M., 2021. Evaluating the hydrological response of a boreal fen following the removal of a temporary access road. *J. Hydrol.* 594, 125928. <https://doi.org/10.1016/j.jhydrol.2020.125928>
- ESA, 2023. Sentinel 1. URL <https://sentinel.esa.int/web/sentinel/user-guides/sentinel-1-sar>
- ESA, 2021. About Copernicus Sentinel 1: Info Graph.
- ESA, 2015. Sentinel-1: Data Access and Products: Fact Sheet.
- ESA, 2012. Sentinel-1. ESA's Radar Observatory Mission for GMES operational service.
- ESA, 2007. InSAR Principles - Guidelines for SAR Interferometry Processing and Interpretation.
- Filicetti, A., Cody, M., Nielsen, S., 2019. Caribou Conservation: Restoring Trees on Seismic Lines in Alberta, Canada. *Forests* 10, 185. <https://doi.org/10.3390/f10020185>

- Government of Alberta, 2015. Alberta wetland classification system. Alberta Environment and Sustainable Resource Development, Edmonton, Alberta.
- Hanssen, R.F., Van Leijen, F.J., 2008. Monitoring water defense structures using radar interferometry, in: 2008 IEEE Radar Conference. Presented at the 2008 IEEE Radar Conference (RADAR), IEEE, Rome, Italy, pp. 1–4. <https://doi.org/10.1109/RADAR.2008.4720874>
- Hirsch, R.M., Slack, J.R., Smith, R.A., 1982. Techniques of Trend Analysis for Monthly Water Quality Data.
- Hooper, A., Bekaert, D., Hussain, E., Spaans, K., 2018. StaMPS/MTI Manual.
- Howie, S.A., Hebda, R.J., 2018. Bog surface oscillation (mire breathing): A useful measure in raised bog restoration. *Hydrol. Process.* 32, 1518–1530. <https://doi.org/10.1002/hyp.11622>
- Hoyt, A.M., Chaussard, E., Seppäläinen, S.S., Harvey, C.F., 2020. Widespread subsidence and carbon emissions across Southeast Asian peatlands. *Nat. Geosci.* 13, 435–440. <https://doi.org/10.1038/s41561-020-0575-4>
- Hyndman, R.J., Athanasopoulos, G., 2018. *Forecasting: Principles and Practice*.
- Imperial, 2022. Kearl Weather Station Data.
- Imperial, 2018. Imperial Investment in Aspen Project to Proceed.
- Izumi, Y., Takeuchi, W., Widodo, J., Sulaiman, A., Awaluddin, A., Aditiya, A., Razi, P., Anggono, T., Sumantyo, J.T.S., 2022. Temporal Subset SBAS InSAR Approach for Tropical Peatland Surface Deformation Monitoring Using Sentinel-1 Data. *Remote Sens.* 14, 5825. <https://doi.org/10.3390/rs14225825>
- Jansing, E.D., 2021. *Introduction to Synthetic Aperture Radar: Concepts and Practice*.
- Khodaei, B., Hashemi, H., Salimi, S., Berndtsson, R., 2023. Substantial carbon sequestration by peatlands in temperate areas revealed by InSAR. *Environ. Res. Lett.* 18, 044012. <https://doi.org/10.1088/1748-9326/acc194>
- King, K.S., Yetter, J., 2011. Groundwater and Alberta's Oil Sands Mines. *Ground Water* 49.
- Lanari, R., Casu, F., Manzo, M., Zeni, G., Berardino, P., Manunta, M., Pepe, A., 2007. An Overview of the Small BAseline SubSet Algorithm: a DInSAR Technique for Surface Deformation Analysis. *Pure Appl. Geophys.* 164, 637–661. <https://doi.org/10.1007/s00024-007-0192-9>
- Li, S., Xu, W., Li, Z., 2022. Review of the SBAS InSAR Time-series algorithms, applications, and challenges. *Geod. Geodyn.* 13, 114–126. <https://doi.org/10.1016/j.geog.2021.09.007>

- Liu, L., Schaefer, K.M., Chen, A.C., Gusmeroli, A., Zebker, H.A., Zhang, T., 2015. Remote sensing measurements of thermokarst subsidence using InSAR: Insar Thermokarst. *J. Geophys. Res. Earth Surf.* 120, 1935–1948. <https://doi.org/10.1002/2015JF003599>
- Lu, Z., 2007. InSAR Imaging of Volcanic Deformation over Cloud-prone Areas – Aleutian Islands. *Photogramm. Eng. Remote Sens.* 73, 245–257. <https://doi.org/10.14358/PERS.73.3.245>
- Ma, S., Xu, C., Shao, X., Xu, X., Liu, A., 2021. A Large Old Landslide in Sichuan Province, China: Surface Dsiplacement Monitoring and Potential Instability Assessment. *Remote Sens.* 13. <https://doi.org/10.3390/rs13132552>
- Malberg, H., 2002. Meteorologie und Klimatologie: eine Einführung ; mit 56 Tabellen, 4., aktualisierte und erw. Aufl. ed. Springer, Berlin Heidelberg.
- Mancini, F., Grassi, F., Cenni, N., 2021. A Workflow Based on SNAP–StaMPS Open-Source Tools and GNSS Data for PSI-Based Ground Deformation Using Dual-Orbit Sentinel-1 Data: Accuracy Assessment with Error Propagation Analysis. *Remote Sens.* 13, 753. <https://doi.org/10.3390/rs13040753>
- Marshall, C., Sterk, H.P., Gilbert, P.J., Andersen, R., Bradley, A.V., Sowter, A., Marsh, S., Large, D.J., 2022. Multiscale Variability and the Comparison of Ground and Satellite Radar Based Measures of Peatland Surface Motion for Peatland Monitoring. *Remote Sens.* 14, 336. <https://doi.org/10.3390/rs14020336>
- McLeod, A.J., 2011. R-package “Kendall” Documentation.
- Mohammadimanesh, F., Salehi, B., Mahdianpari, M., Brisco, B., Motagh, M., 2018. Wetland Water Level Monitoring Using Interferometric Synthetic Aperture Radar (InSAR): A Review. *Can. J. Remote Sens.* 44, 247–262. <https://doi.org/10.1080/07038992.2018.1477680>
- Park, S.-W., Hong, S.H., 2020. Nonlinear Modeling of Subsidence From a Decade of InSAR Time Series. *Geophysical Research Letters* 48.
- Plach, J., M., Wood, M., E., Macrae, M., L., Osko, T., J., Petrone, Richard, M., 2017. Effect of a semi-permanent road on N,P, and CO₂ dynamics in a poor fen on the Western Boreal Plain, Canada. *eco, Ecohydrology* 15. <https://doi.org/DOI:10.1002/eco.1874>
- Price, J.S., 2003. Role and character of seasonal peat soil deformation on the hydrology of undisturbed and cutover peatlands. *Water Resour. Res., Water Resources Research* 39. <https://doi.org/doi:10.1029/2002WR001302>
- Roberts, D.R., Bayne, E.M., Beausoleil, D., Dennett, J., Fisher, J.T., Hazewinkel, R.O., Sayanda, D., Wyatt, F., Dubé, M.G., 2022. A synthetic review of terrestrial biological research from the Alberta oil sands region: 10 years of published literature. *Integr. Environ. Assess. Manag.* 18, 388–406. <https://doi.org/10.1002/ieam.4519>

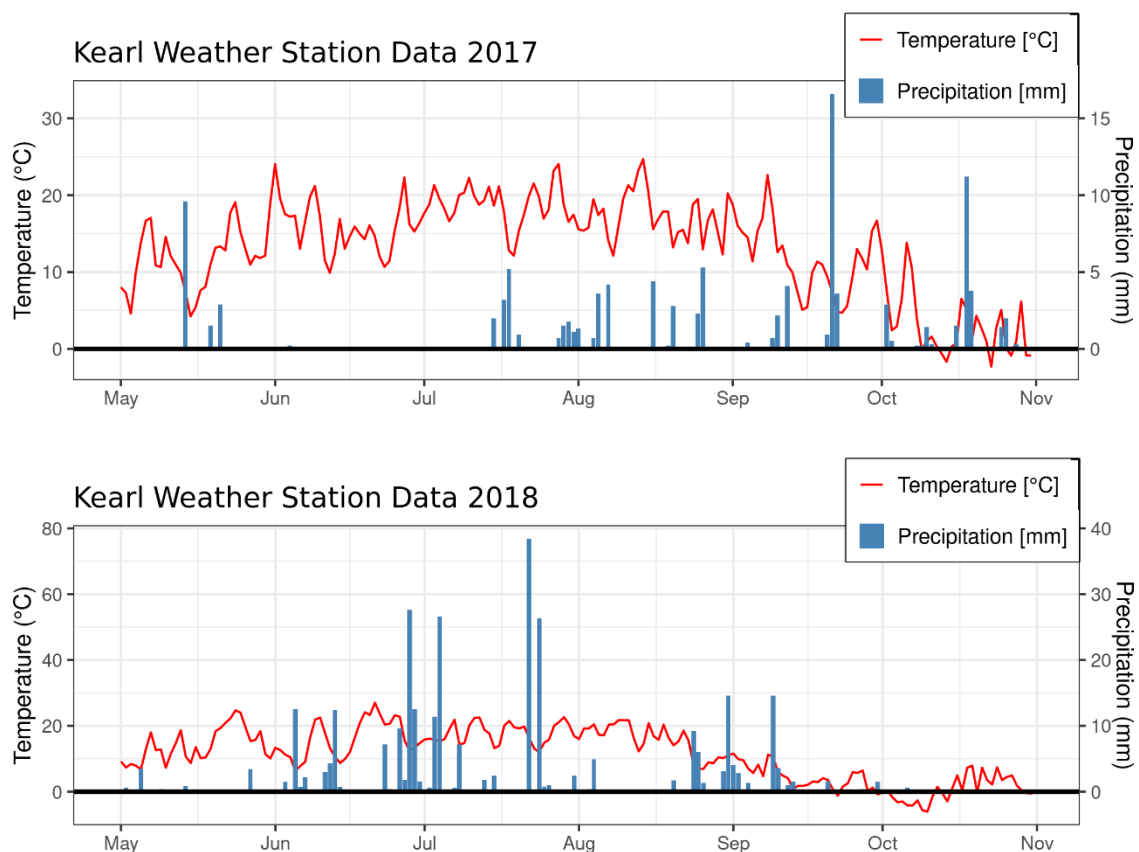
- Rosen, P.A., Hensley, S., Joughin, I.R., Li, F.K., Madsen, S.N., Rodríguez, E., Goldstein, R.M., 2000. Synthetic Aperture Radar Interferometry. *Proc. IEEE* 88.
- Saraswati, S., Bhusal, Y., Trant, A.J., Strack, M., 2020a. Roads Impact Tree and Shrub Productivity in Adjacent Boreal Peatlands. *Forests* 11, 594. <https://doi.org/10.3390/f11050594>
- Saraswati, S., Petrone, R.M., Rahman, M.M., McDermid, G.J., Xu, B., Strack, M., 2020b. Hydrological effects of resource-access road crossings on boreal forested peatlands. *J. Hydrol.* 584, 124748. <https://doi.org/10.1016/j.jhydrol.2020.124748>
- Saraswati, S., Strack, M., 2019. Road Crossings Increase Methane Emissions From Adjacent Peatland. *J. Geophys. Res. Biogeosciences* 124, 3588–3599. <https://doi.org/10.1029/2019JG005246>
- Serco Italia SPA, 2020. SNAP2StaMPS: Data preparation for StaMPS PSI processing with SNAP - Mexico City 2020.
- Soltani, M., Rousta, I., Taheri, S.S.M., 2013. Using Mann-Kendall and Time Series Techniques for Statistical Analysis of Long-Term Precipitation in Gorgan Weather Station.
- Tampuu, T., Praks, J., Uiboupin, R., Kull, A., 2020. Long Term Interferometric Temporal Coherence and DInSAR Phase in Northern Peatlands. *Remote Sens.* 12, 1566. <https://doi.org/10.3390/rs12101566>
- Vitt, D.H., Halsey, L.A., Bauer, I.E., Campbell, C., 2000. Spatial and temporal trends in carbon storage of peatlands of continental western Canada through the Holocene 37.
- Willier, C.N., Dennett, J.M., Devito, K.J., Bater, C.W., Nielsen, S.E., 2022. The extent and magnitude of edge effects on woody vegetation in road-bisected treed peatlands in boreal Alberta, Canada. *Ecohydrology* 15. <https://doi.org/10.1002/eco.2455>
- Yunjun, Z., Fattahib, H., Amelung, F., 2019. Small baseline InSAR time series analysis: Unwrapping error correction and noise reduction.
- Zhou, Z., Li, Z., Waldron, S., Tanaka, A., 2019. InSAR Time Series Analysis of L-Band Data for Understanding Tropical Peatland Degradation and Restoration. *Remote Sens.* 11, 2592. <https://doi.org/10.3390/rs11212592>

Appendix

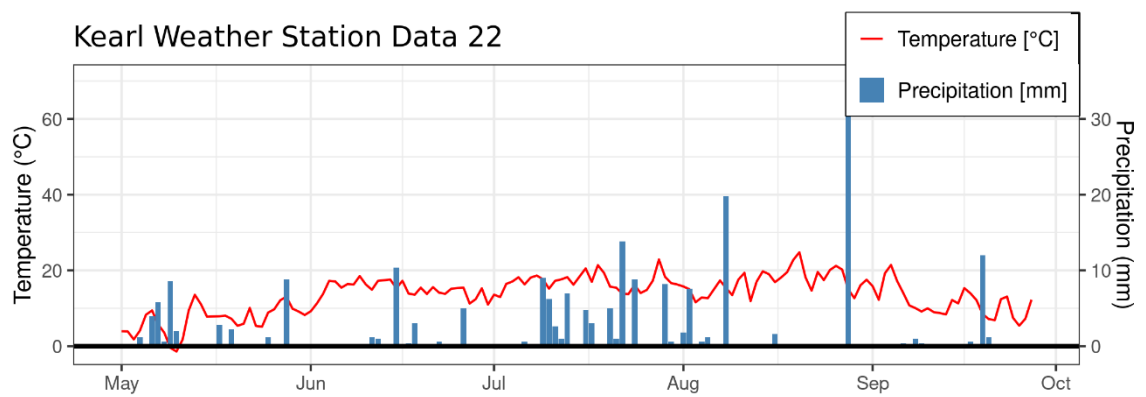
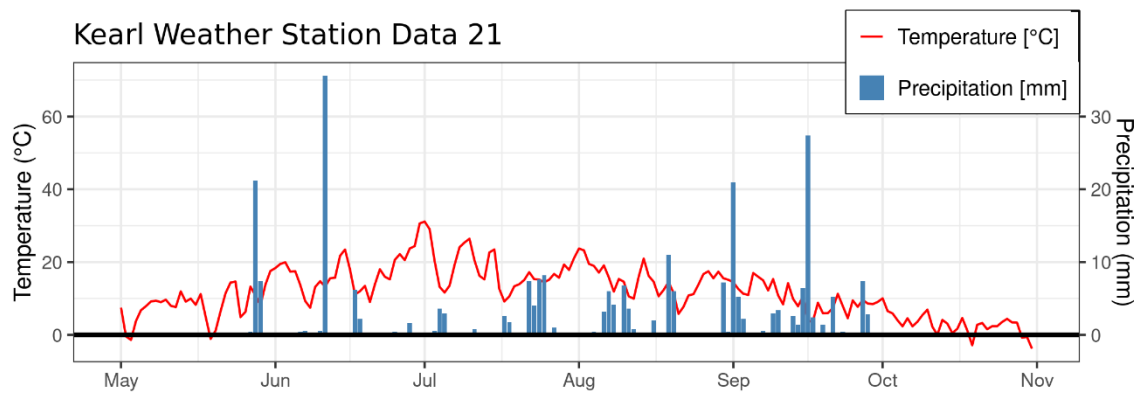
The Appendix A.1 to A.4 includes supplementary graphs and figures that provide visual support for the thesis, although they do not introduce significant additional information. A.5 contains the scripts in RStudio, Python and MATLAB, that have been used to plot the figures and calculate the results and statistical parameters. They are only included in the supplementary material added on the CD-ROM. They are excluded in the printed version due to sustainability reasons.

A.1. Weather Station data

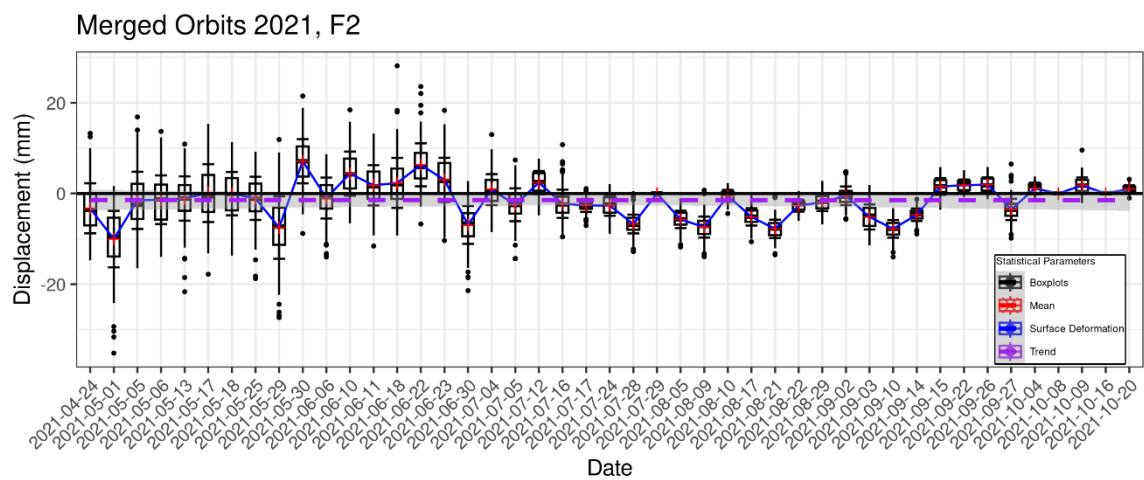
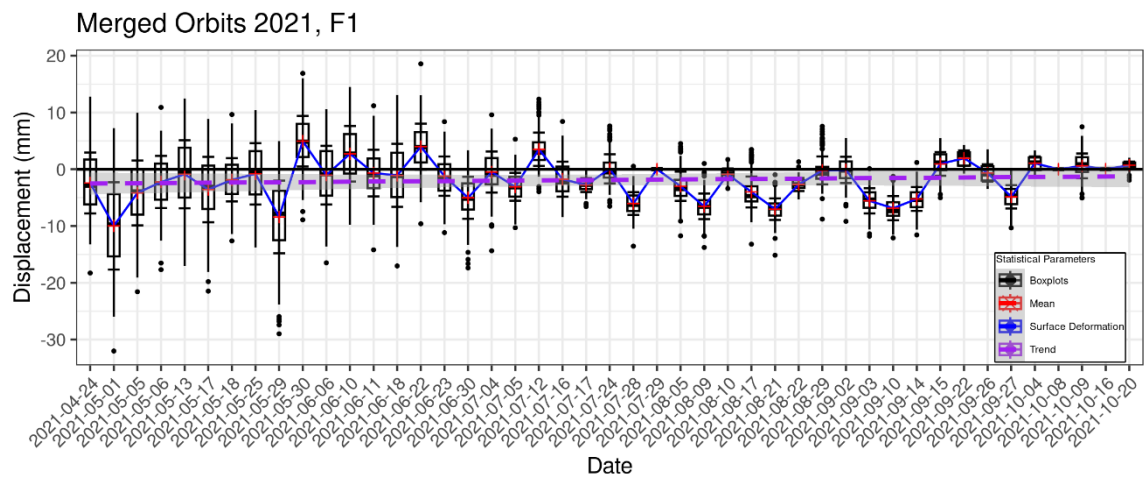
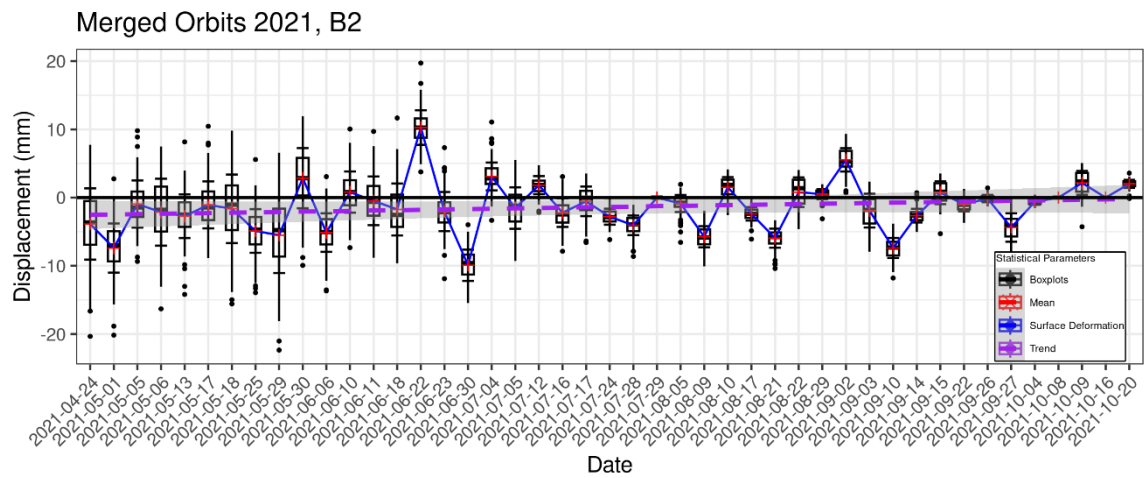
The Kearl weather station data from 2017 and 2018:



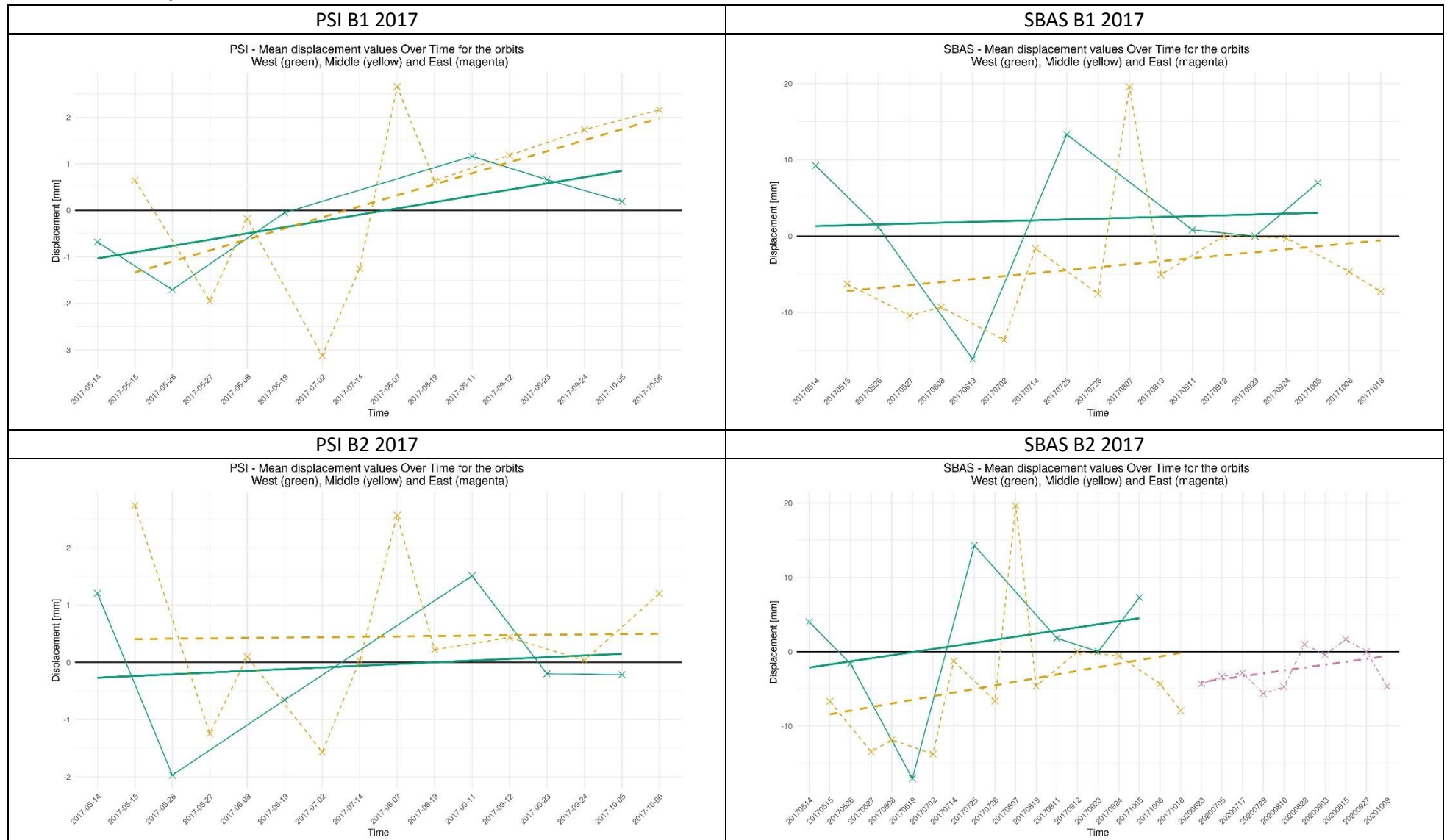
The Aspen weather station data:

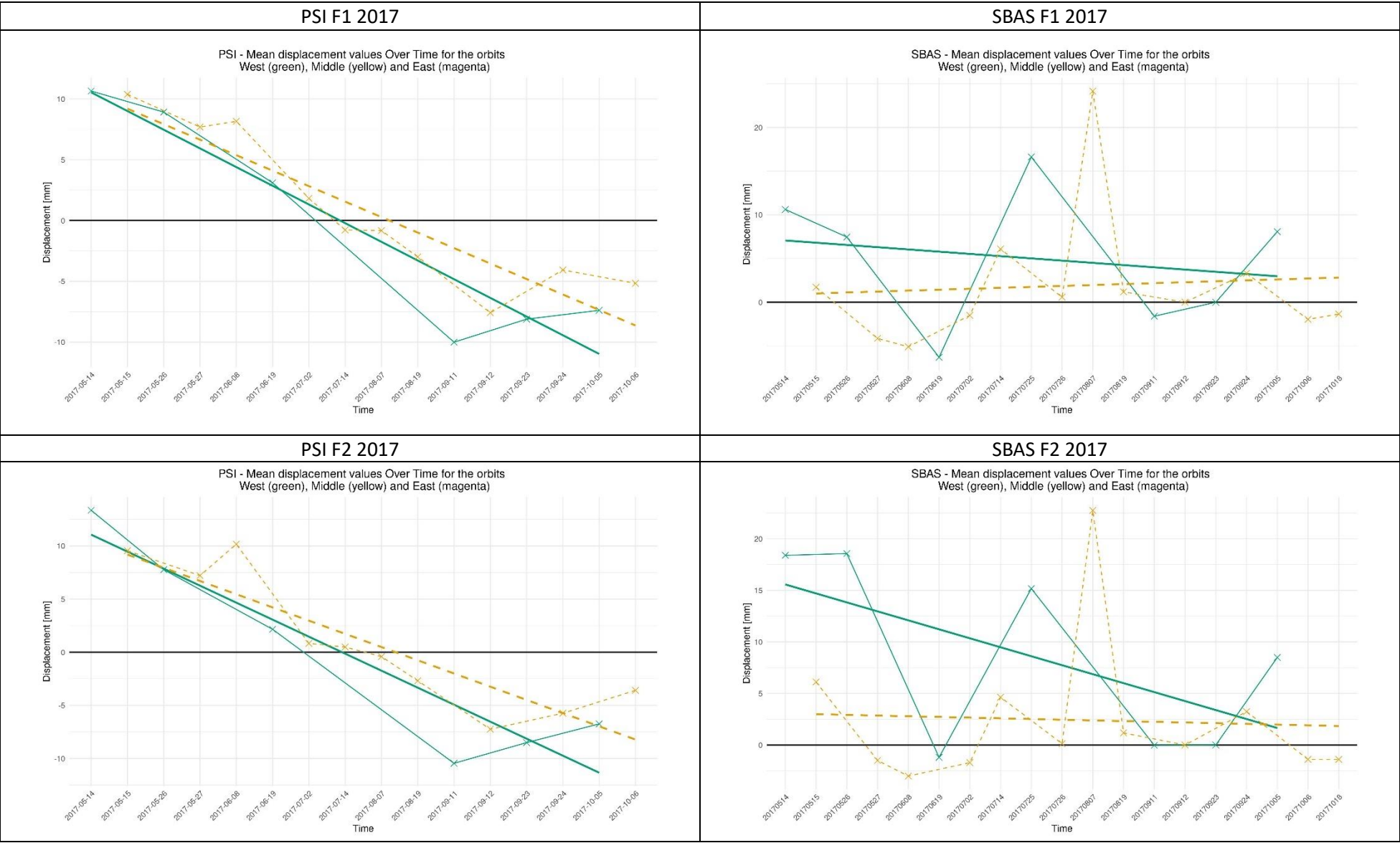


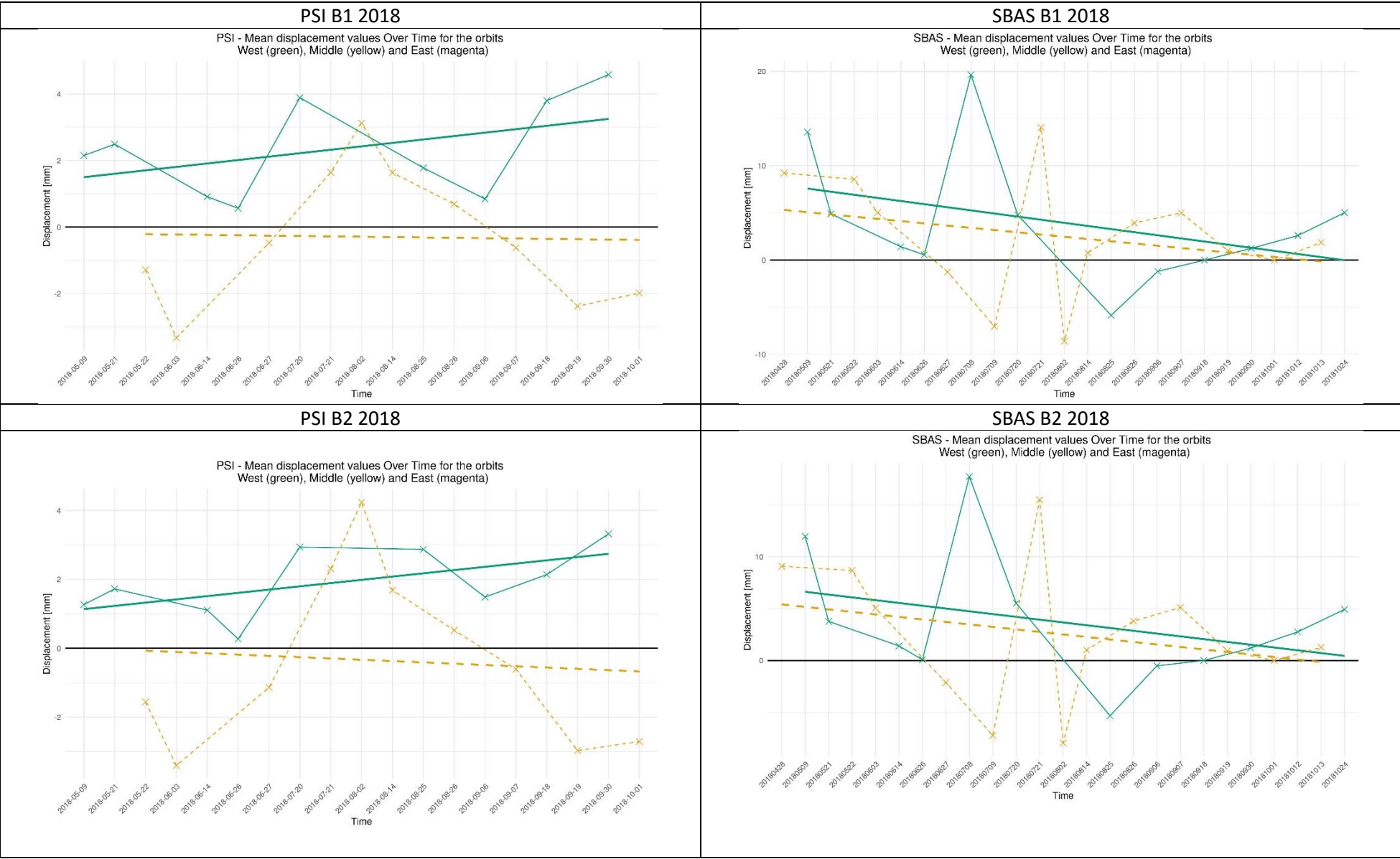
A.2 Statistical focus on 2021

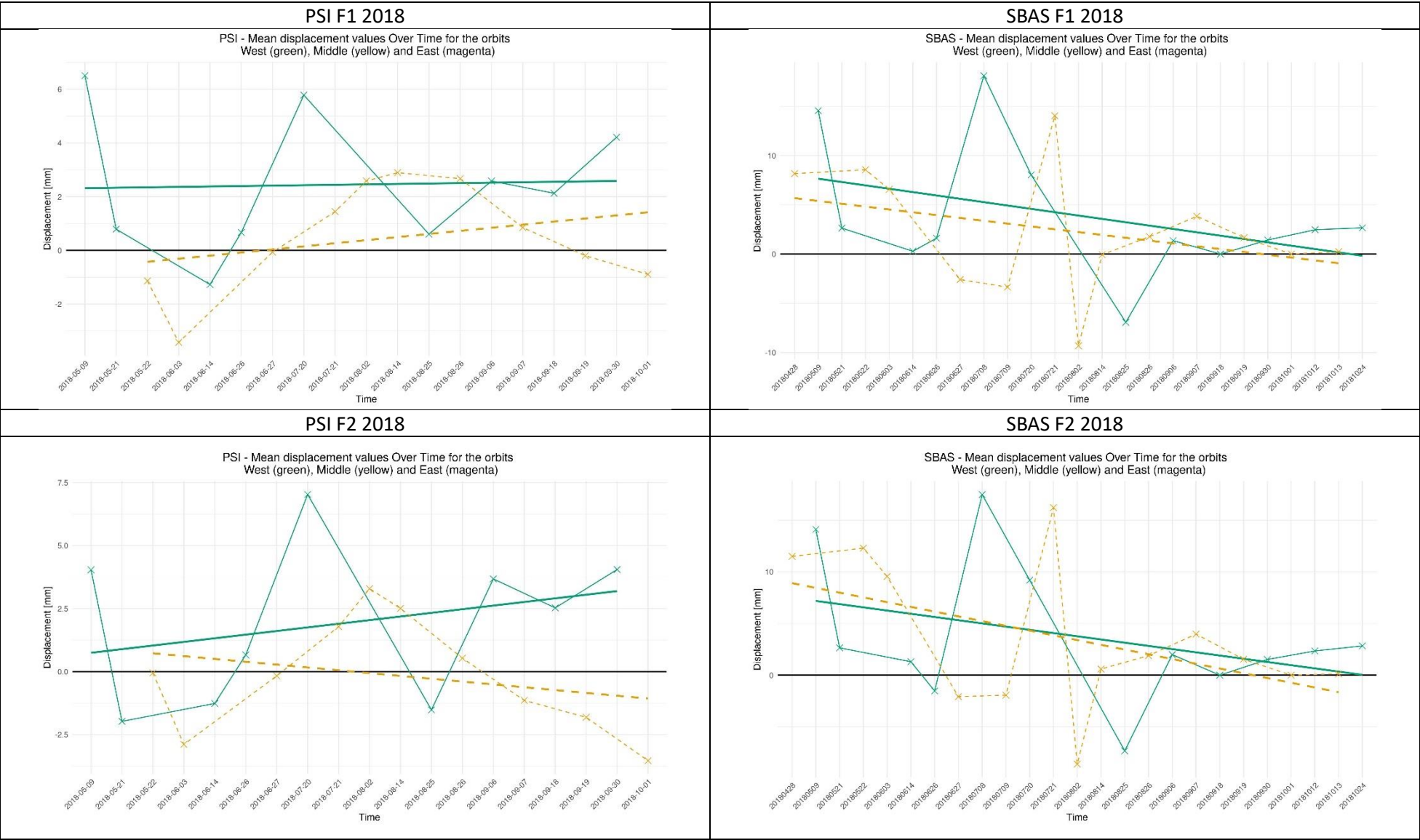


A.3 Timeseries plots SBAS and PSI 2017 and 2018

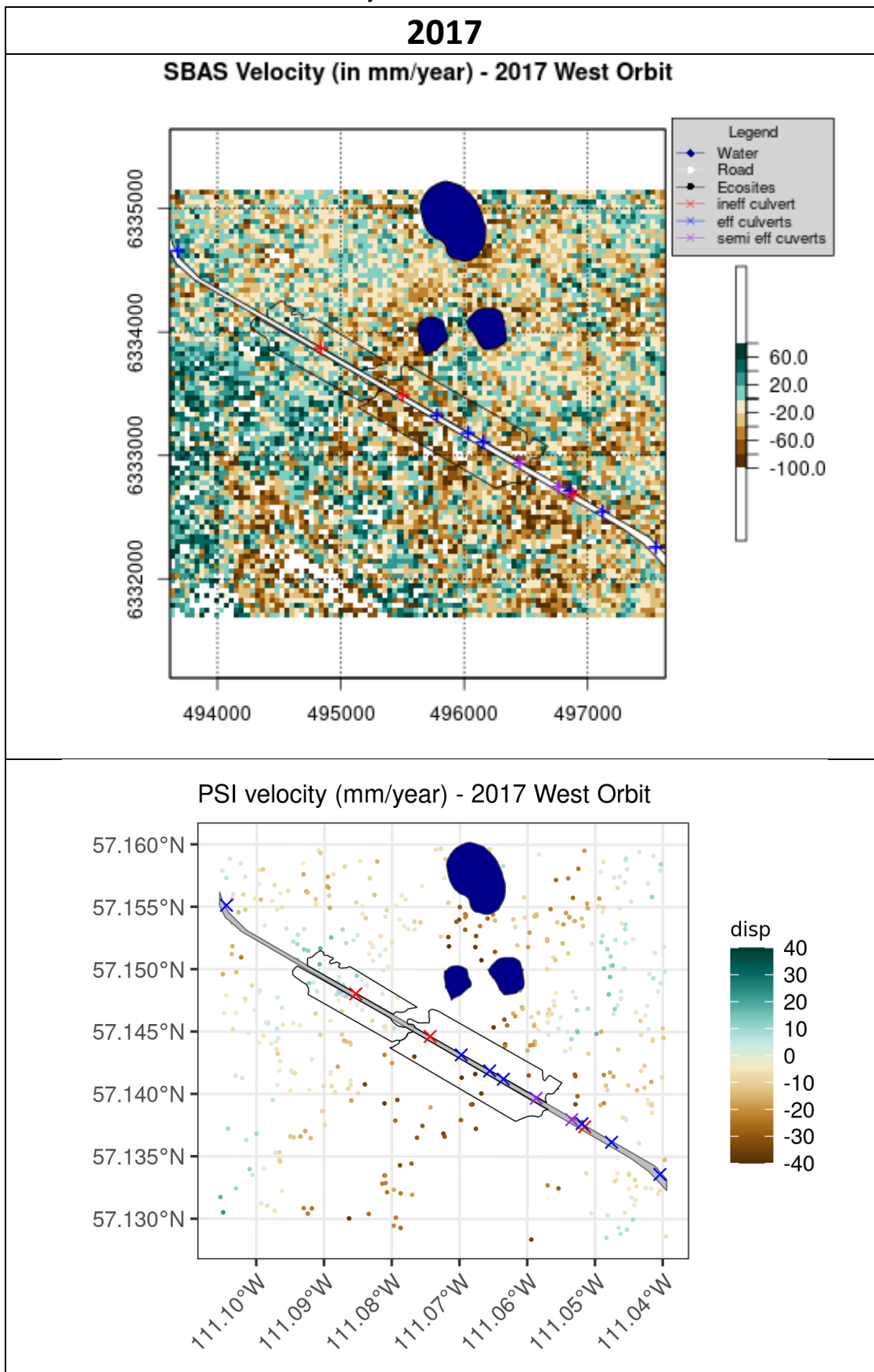






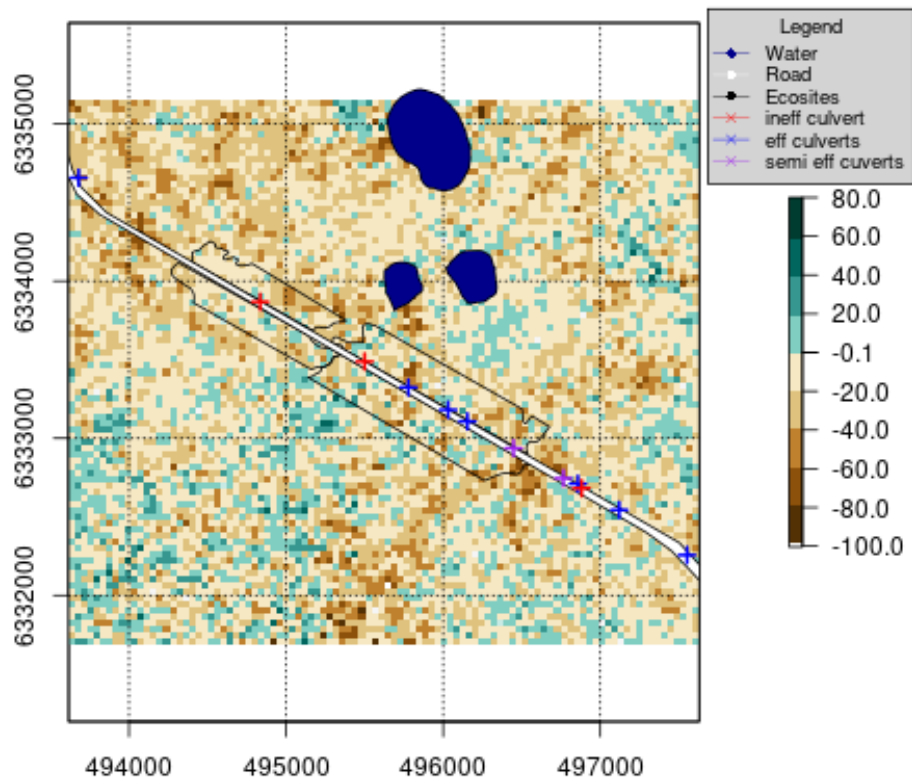


A.4 SBAS and PSI additional Velocity Plots

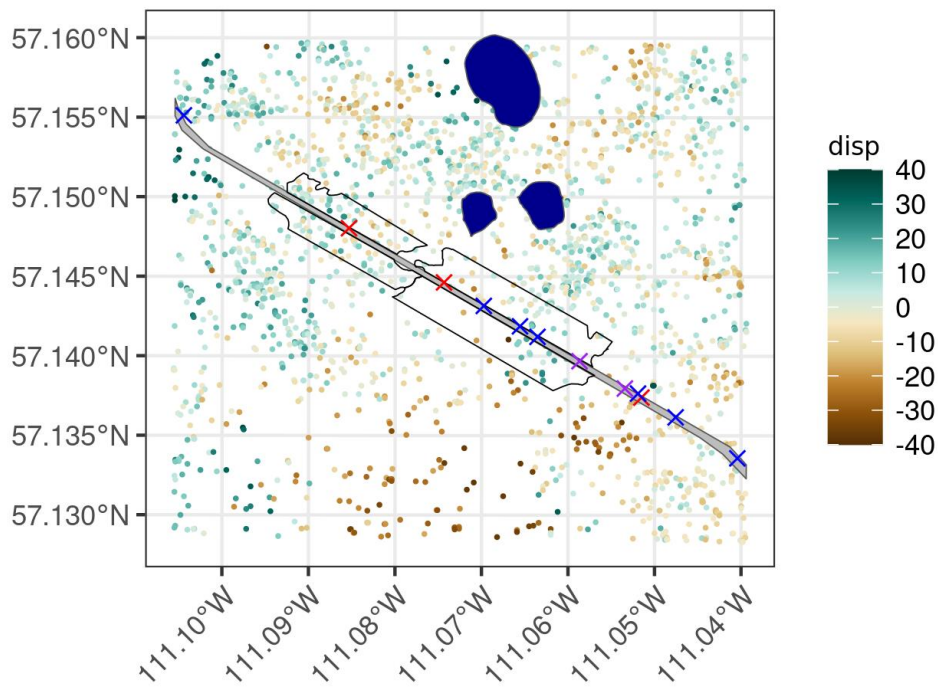


2018

SBAS Velocity (in mm/year) - 2018 West Orbit

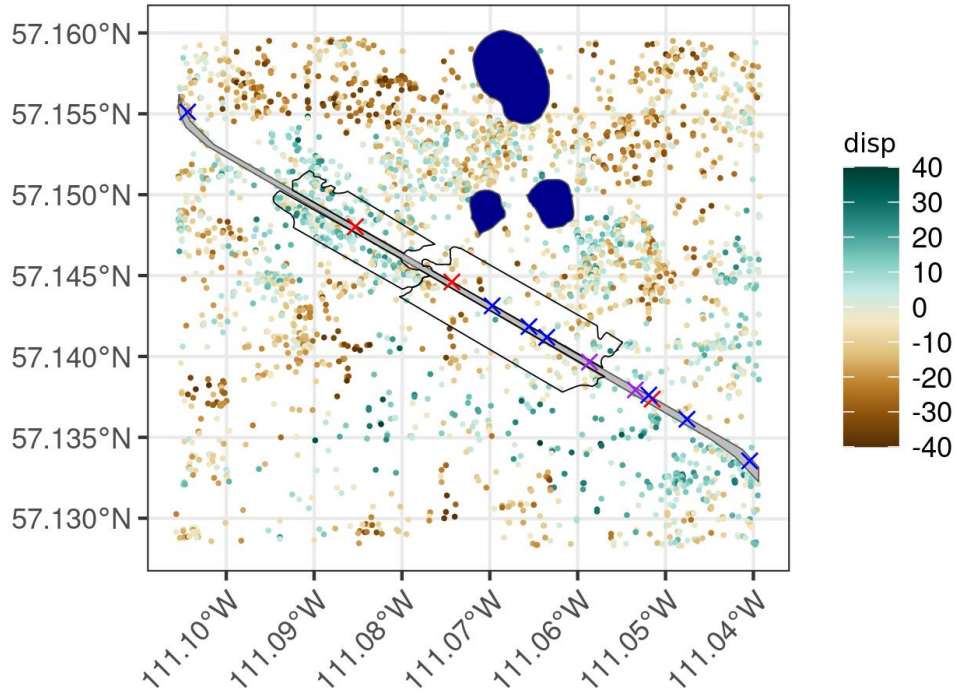


PSI velocity (mm/year) - 2018 West Orbit



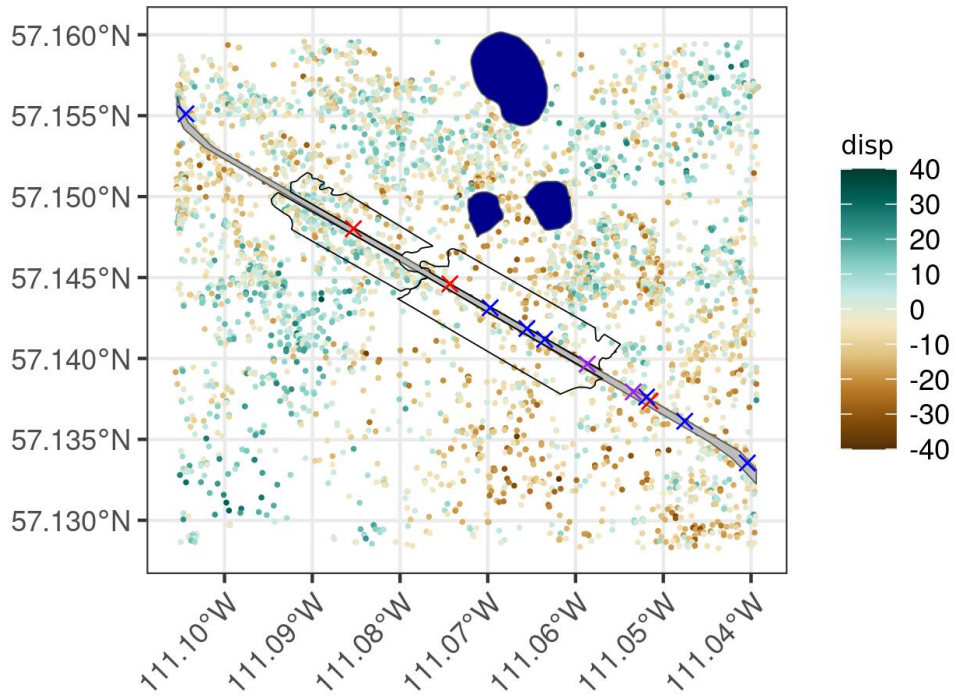
2020

PSI velocity (mm/year) - 2020 West Orbit

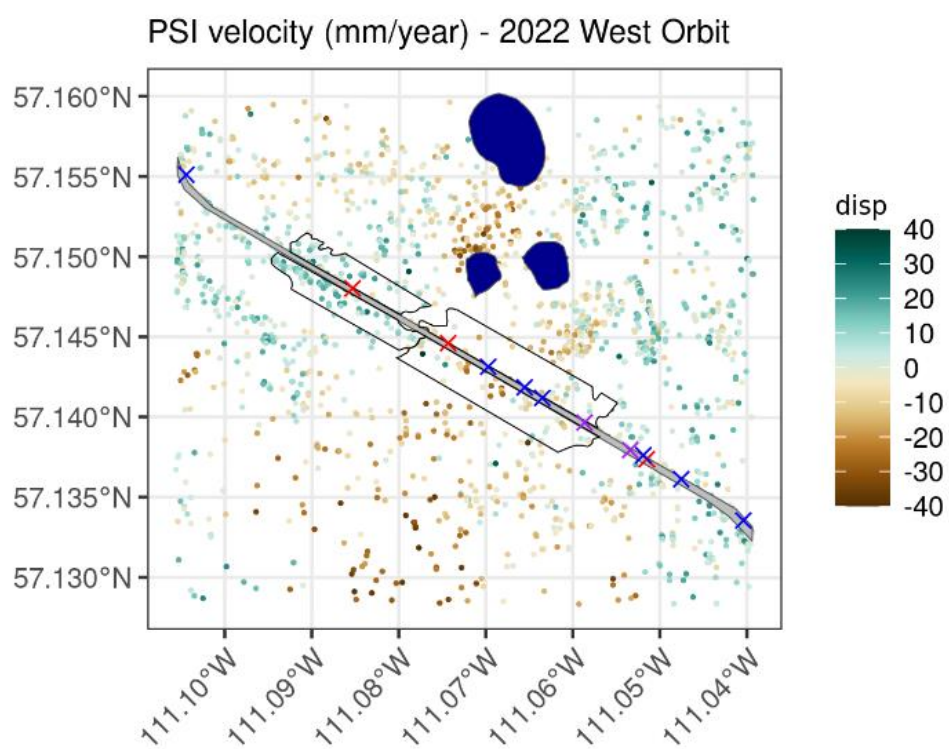


2021

PSI velocity (mm/year) - 2021 West Orbit



2022



A.5 Scripts of data analysis and visualization

PSI Timeseries

The statistical analysis is marked out with '#', as you have to use the Date as.Date() instead of as.character() as it is used for plotting to show the timesteps completely. The parameter "v-do_" defines to use the dataset with estimated DEM and Orbit errors removed. Use "v" to use the product without removal of that error estimation.

```
library(sf)
library(dplyr)
library(ggplot2)
library(tidyr)
library(Kendall)
library(stats)
library(forecast)

setwd("../Documents/PSI/results")

#Define Functions

#Loads csv file and returns sf_dataset, georeferenced in latlon
load.stamps <- function(x){
  dat <- read.csv(paste0(getwd(), "/", x))
  dates.days <- as.vector(t(dat[1, 4:ncol(dat)]))
  dates.date <- as.Date(dates.days, origin = "0000-01-01")
  ref.points <- as.vector(t(dat[1, 1:2]))
  dat <- dat[-1, ]
  rownames(dat) <- seq_len(nrow(dat))
  ps.loc <- cbind(
    uid = seq_len(nrow(dat)),
    lon = dat[, 1],
    lat = dat[, 2],
    disp = dat[, 3],
    dat[, 4:ncol(dat)]
  )

  return(list(dates.days = dates.days,
             dates.date=dates.date,
             ref.points=ref.points,
             ps.loc=ps.loc))
}

clip_sf_data <- function(dataset, shapefile, crs_shapefile = "+init=epsg:26912"){
  shfile <- st_read(shapefile) %>%
    st_zm(drop= TRUE, what="ZM") %>%
    transform(crs = crs_shapefile)

  dataset_sf <- dataset %>%
    st_as_sf(coords = c("lon", "lat"), crs = "+proj=latlon +datum=WGS84") %>%
    st_transform(crs=crs_shapefile)

  st_intersection(dataset_sf, shfile)

  return(dataset_sf)
}

#Execute Loop with functions
years <- 2017:2022
file_list <- list.files(pattern = "*.csv")
```



```

shapefiles <- c("A1small.shp", "A2small.shp", "B1_FS_Fwc.shp", "B2_FS_Fwc.shp")
shfile <- shapefiles[4]
ecosite <- strsplit(shfile, "\\.")[[1]][1]

typ = "v-do_"

for (year_to_filter in years){
  filtered_files_1year <- file_list[grep(paste0(typ, year_to_filter), file_list)]

  for (csv_file in filtered_files_1year) {
    file_name <- strsplit(csv_file, "_")[[1]]
    orbit_name <- strsplit(file_name[3], "\\.")[[1]]
    year_orbit <- paste(file_name[length(file_name)-1], orbit_name[1], sep="_")
    df_name <- paste0("df", year_orbit)

    ds <- load.stamps(csv_file)
    ds_variable <- ds$ps.loc
    colnames(ds_variable) <- c("uid", "lon", "lat", "disp", as.character(ds$dates.date))

    ds_clipped <- clip_sf_data(ds_variable, shapefile = shfile)
    df <- ds_clipped[, -(1:2)]

    df_means <- df %>%
      st_drop_geometry() %>%
      as.data.frame() %>%
      select_if(is.numeric) %>%
      summarise_all(mean, na.rm = TRUE) %>%
      .[, -c(ncol(.)-1, ncol(.))]

    df_means_long <- df_means %>%
      gather(key = "Date", value = "Mean") %>%
      df_means_long$Date <- as.character(as.Date(substr(df_means_long$Date, 2,
nchar(df_means_long$Date)), format("%Y.%m.%d")))

    #colnames(df_means_long) <- sub("X", "", colnames(df_means_long)) not working

    assign(df_name, df_means_long, envir = .GlobalEnv)
    print(df_name)
  }
}

#####
#Plot the results

df_names <- ls()[sapply(ls(), function(x) is.data.frame(get(x)))]
statistic_results <- list()

i = 0
for (year_to_filter in years){

  i = i+1
  df_filtered <- df_names[grep(year_to_filter, df_names)]

  #new version of creating df1, df2, df3 ain regards of the orbit name
  orbit <- substr(df_filtered, start = nchar("df") + 6, stop = nchar(df_filtered))
  data_frame_list_statistic <- list()
  if("WestOrbit" %in% orbit){
    df1 <- get(df_filtered[grepl("WestOrbit", orbit)])
    data_frame_list_statistic[[1]] <- df1
  }
  if("MiddleOrbit" %in% orbit){

```

```

df2 <- get(df_filtered[grepl("MiddleOrbit", orbit)])
if(exists("df2")){
  data_frame_list_statistic[[2]] <- df2
}
}
if("EastOrbit"%in% orbit){
  df3 <- get(df_filtered[grepl("EastOrbit", orbit)])
  if(length(data_frame_list_statistic)==2){
    data_frame_list_statistic[[3]] <- df3
  }else{
    data_frame_list_statistic[[2]] <- df3
  }
}
#calculate statistics
#iteration_results <- list()

#for (j in 1:length(data_frame_list_statistic)){
#  df_statistic <- data_frame_list_statistic[[j]]
#  lm_model <- lm(Mean ~ Date, data = df_statistic)

#  r_squared <- summary(lm_model)$r.squared

#  rmse <- sqrt(mean(lm_model$residuals^2))

#  mann_kendall <- Kendall(df_statistic$Mean, as.numeric(df_statistic$Date))

#  results <- list(R_squared = r_squared, RMSE = rmse, Mann_Kendall = mann_kendall,
ecosite)

#  iteration_results[[j]] <- results
# }
#statistic_results[[i]] <- iteration_results

#Create base plot
p <- ggplot() +
  #labs(title = "PSI - Mean displacement values Over Time for the orbits \n West <span
style='color:#009E73;'>(green)</span>, Middle <span style='color:#E69F00;'>(yellow)
</span> and East <span style='color:#CC79A7;'>(magenta) </span>",
  # x = "Time", y = "Mean displacement Value (in mm)") +
  labs(title = "PSI - Mean displacement values Over Time for the orbits \n West (green),
Middle (yellow) and East (magenta)",
  x = "Time", y = "Displacement [mm]") +
  theme_minimal() +
  theme(plot.title = element_text(hjust = 0.5),
        axis.text.x = element_text(angle = 45, hjust = 1))+
  geom_hline(yintercept = 0, color = "black", linewidth = 0.7)

if (exists("df1")){ #check if df1 exists
  #Add mean values and connecting lines for dataframe 1
  p <- p +
    geom_point(data = df1, aes(x=Date, y = Mean), shape = 4, size = 3, color = "#009E73")
+ #alternative colorcode = "#009E73" "black"
    geom_line(data = df1, aes(x = Date, y = Mean, group = 1), linetype = "solid", color =
"#009E73")

  # Add trendline for dataframe 1
  p <- p +
    geom_smooth(data= df1, aes(x = Date, y = Mean, group = 1), method = "lm", se= FALSE,
linetype = "solid", color = "#009E73" )
}

```

```

if (exists("df2")){ #check if df2 exists
  #add mean values and connecting lines for dataframe 2
  p <- p +
    geom_point(data = df2, aes(x=Date, y = Mean), shape = 4, size = 3, color = "#E69F00")
+ # alternative colorcode = "#E69F00" "#0072B2"
    geom_line(data = df2, aes(x = Date, y = Mean, group = 1), linetype = "dashed", color
= "#E69F00")

  # Add trendline for dataframe 1
  p <- p +
    geom_smooth(data= df2, aes(x = Date, y = Mean, group = 1), method = "lm", se= FALSE,
linetype = "dashed", color = "#E69F00" )
}
if (exists("df3")){ #check if df3 exists
  #add mean values and connecting lines for dataframe 3
  p <- p +
    geom_point(data = df3, aes(x=Date, y = Mean), shape = 4, size = 3, color = "#CC79A7")
+ # alternative colorcode = "CC79A7" "#56B4E9"
    geom_line(data = df3, aes(x = Date, y = Mean, group = 1), linetype = "dotdash", color
= "#CC79A7")

  # Add trendline for dataframe 3
  p <- p +
    geom_smooth(data= df3, aes(x = Date, y = Mean, group = 1), method = "lm", se= FALSE,
linetype = "dotdash", color = "#CC79A7" )

}

print(p + theme(plot.title = ggtext::element_markdown())) #this is to render the HTML
formatted title text (colored)
p

#save file
plot_filename <- paste("PSI_DOA_DisplacmentValues", year_to_filter, ecosite, ".jpeg", sep
= "_")
if (file.exists(plot_filename)){
  file.remove(plot_filename)
}
ggsave(filename = plot_filename, plot = p, width = 10, height = 6, bg= "white")

#Open image
#viewer(plot_filename)

#print out a message
cat("Plot for year", year_to_filter, "saved as", plot_filename, "\n")

#Reset dataframes at the end of each iteration
rm(df1,df2,df3)
}

#print statistic
for (i in 1:length(statistic_results)){
  for (j in 1:length(statistic_results[[i]])) {
    print(paste("Iteration", i, "Calculation", j , "results:"))
    print(statistic_results[[i]][[j]])
  }
}
}

```

SBAS Timeseries

The code is easy adjustable to plot the Median instead of the Mean.

```
# Import Libraries
library(raster)
library(rgdal)
library(rhdf5)
library(sf)
library(ggplot2)
library(htmltools)
library(ggtext)

# Set parameters
parent_dir <- "Mintpy"
years <- seq(2017,2022)
shapefiles <- c("Mintpy/Mask_shapefiles/A1small.shp","Mintpy/Mask_shapefiles/A2small.shp",
               "Mintpy/Mask_shapefiles/B1_FS_Fwc.shp","Mintpy/Mask_shapefiles/B2_FS_Fwc.shp")

# Prepare the shapefile of the ecosite
shfile <- st_read(shapefiles[4])
ecosite <- shfile$Name

# Function for reading hdf5 file and returning a dataframe
reading_clipping_exporting_hdf5 <- function(filepath, shapefile, xmin = 488720, xmax =
500800,
                                           ymin =6310080 , ymax= 6336000, crs
="+init=epsg:26912") {

  h5_file <- H5Fopen(file_path,"H5F_ACC_RDONLY")
  timeseries <- h5read(h5_file, "timeseries")
  timeseries <- aperm(timeseries, c(2,1,3))

  date <- h5read(h5_file, "date")

  rasters <- lapply(1:dim(timeseries)[3], function(i){ raster(timeseries[ , ,i]) })
  raster_stack <- stack(rasters)

  extent(raster_stack) <- c(xmin, xmax, ymin , ymax)
  projection(raster_stack) <- CRS(crs)

  H5Fclose(h5_file)

  shfile <- st_transform(shapefile, crs = crs(raster_stack))
  shfile <- st_zm(shfile, drop = TRUE, what = "ZM")

  raster_cropped <- crop(raster_stack, extent(shfile))
  rstack_clipped <- mask(raster_cropped, shfile)

  rstack_mean <- cellStats(rstack_clipped, mean) * 1000
  rstack_median <- cellStats(rstack_clipped, median) * 1000
  s_values <- cellStats(rstack_clipped, sd) * 1000

  df <- data.frame(Date = date, Mean = rstack_mean, Median = rstack_median,
Standarddeviation = s_values)

  return(df)
}
```

```
#####
#prepare the shapefile of the ecosite

shapefiles <-
c("Mintpy/Mask_shapefiles/A1small.shp", "Mintpy/Mask_shapefiles/A2small.shp", "Mintpy/Mask_shapefiles/B1_FS_Fwc.shp", "Mintpy/Mask_shapefiles/B2_FS_Fwc.shp")
shfile <- st_read(shapefiles[4])
ecosite <- shfile$Name
#shfile$geometry
#plot(shfile["MaskID"])

#####
#Create Loop for graphs

#Loop through each folder
for (year_to_filter in years){
  #filter for all folders containing the searched year in the name, Loop it from 2017 till 2022
  filtered_dirs_1year <-
  filtered_dirs[grepl(paste0("Mintpy_", year_to_filter), filtered_dirs)]

  for (folder in filtered_dirs_1year) {
    #construct the full path to the timeseries.h5 hdf5 file
    file_path <- file.path(folder, "timeseries.h5")

    #Check if the first file exists
    folder_name <- strsplit(folder, "_")[1][[1]]
    year_orbit <- paste(folder_name[length(folder_name)-1],
    folder_name[length(folder_name)], sep="_")
    df_name <- paste0("df", year_orbit, collapse= "_") #collapse is like sep, but only
inbetween and not in the end
    df_variable <- reading_clipping_exporting_hdf5(filepath= file_path, shapefile= shfile)
    df_variable_frame <- as.data.frame(df_variable)
    #df_variable_frame$Date <- as.Date(df_variable_frame$Date, format = "%Y%m%d")
    assign(df_name, df_variable_frame, envir = .GlobalEnv)
    print(df_name)
  }
}

#####
#Plotting the results

#get all the dataframes
df_names <- ls()[sapply(ls(), function(x) is.data.frame(get(x)))])

for (year_to_filter in years){
  df_filtered <- df_names[grepl(year_to_filter, df_names)]
  #old version of creating df1, df2 ,df3
  # for (i in seq_along(df_filtered)){#anderes Criteria benötigt
  #   assign(paste0("df", i), get(df_filtered[i]))
  # }

  #new version of creating df1, df2, df3 ain regards of the orbit name
  orbit <- substr(df_filtered, start = nchar("df") +6, stop = nchar(df_filtered))
  if("WestOrbit" %in% orbit){
    df1 <- get(df_filtered[grepl("WestOrbit", orbit)])
  }
}
```

```

if("MiddleOrbit"%in% orbit){
  df2 <- get(df_filtered[grepl("MiddleOrbit", orbit)])
}
if("EastOrbit"%in% orbit){
  df3 <- get(df_filtered[grepl("EastOrbit", orbit)])
}

#Create base plot
p <- ggplot() +
  labs(title = "SBAS - Mean displacement values Over Time for the orbits \n West (green),
Middle (yellow) and East (magenta)",
       x = "Time", y = "Displacement [mm]") +
  theme_minimal() +
  theme(plot.title = element_text(hjust = 0.5),
        axis.text.x = element_text(angle = 45, hjust = 1))+
  geom_hline(yintercept = 0, linewidth = 0.7, color = "black")

if (exists("df1")){ #check if df1 exists
  #Add mean values and connecting lines for dataframe 1
  p <- p +
    geom_point(data = df1, aes(x=Date, y = Mean), shape = 4, size = 3, color = "#009E73")
+ #alternative colorcode = "#009E73" "black"
    geom_line(data = df1, aes(x = Date, y = Mean, group = 1), linetype = "solid", color =
"#009E73")

  # Add trendline for dataframe 1
  p <- p +
    geom_smooth(data= df1, aes(x = Date, y = Mean, group = 1), method = "lm", se= FALSE,
linetype = "solid", color = "#009E73" )
}

if (exists("df2")){ #check if df2 exists
  #add mean values and connecting lines for dataframe 2
  p <- p +
    geom_point(data = df2, aes(x=Date, y = Mean), shape = 4, size = 3, color = "#E69F00")
+ # alternative colorcode = "#E69F00" "#0072B2"
    geom_line(data = df2, aes(x = Date, y = Mean, group = 1), linetype = "dashed", color =
"#E69F00")

  # Add trendline for dataframe 1
  p <- p +
    geom_smooth(data= df2, aes(x = Date, y = Mean, group = 1), method = "lm", se= FALSE,
linetype = "dashed", color = "#E69F00" )
}

if (exists("df3")){ #check if df3 exists
  #add mean values and connecting lines for dataframe 3
  p <- p +
    geom_point(data = df3, aes(x=Date, y = Mean), shape = 4, size = 3, color = "#CC79A7")
+ # alternative colorcode = "CC79A7" "#56B4E9"
    geom_line(data = df3, aes(x = Date, y = Mean, group = 1), linetype = "dotdash", color =
"#CC79A7")

  # Add trendline for dataframe 3
  p <- p +
    geom_smooth(data= df3, aes(x = Date, y = Mean, group = 1), method = "lm", se= FALSE,
linetype = "dotdash", color = "#CC79A7" )

  print(p + theme(plot.title = ggtext::element_markdown())) #this is to render the HTML
formatted title text (colored)
p

```

```

#save file
plot_filename <- paste("SBAS_DisplacementValues", year_to_filter, ecosite, ".jpeg", sep =
"-")
if (file.exists(plot_filename)){
  file.remove(plot_filename)
}
ggsave(filename = plot_filename, plot = p, width = 10, height = 6, bg= "white")

#print out a message
cat("Plot for year", year_to_filter, "saved as", plot_filename, "\n")

#Reset dataframes at the end of each iteration
rm(df1,df2,df3)
}
}

```

PSI Velocity

```
library(sf)
library(sp)
library(raster)
library(rgdal)
library(viridis)
library(scales)

#setwd
setwd("../")
setwd("Documents")
setwd("PSI/results")
wd<- getwd()

load.stamps <- function(x){
  dat <- read.csv(paste(wd,"/", x, sep = ""))
  dates.days <- as.vector(t(dat[1, 4:ncol(dat)]))
  dates.date <- as.Date(dates.days, origin = "0000-01-01")
  ref.points <- as.vector(t(dat[1, 1:2]))
  dat <- dat[c(2:nrow(dat)), ]
  rownames(dat) <- seq(length = nrow(dat))
  ps.loc <- cbind(uid = 1:nrow(dat),
                  lon = dat[, 1],
                  lat = dat[, 2],
                  disp = dat[, 3],
                  dat[, 4:ncol(dat)])

  #return(dat)
  return(list(dates.days = dates.days,
              dates.date=dates.date,
              ref.points=ref.points,
              ps.loc=ps.loc))
}

clip_sf_data <- function(dataset,shapefile, crs_shapefile = "+init=epsg:26912"){
  #Load shapefile
  #shfile <- st_read(shapefile)
  shfile = shapefile
  crs <- crs_shapefile
  #crs <- CRS("+proj=utm +zone=12 +datum=WGS84")

  #Drop Z and transform shapefile
  shfile= st_zm(shfile, drop= TRUE, what="ZM")
  shfile <-transform(shfile, crs = crs)

  dataset_sf <-st_as_sf(dataset, coords = c("lon", "lat"), crs = "+proj=latlon
+datum=WGS84")
  dataset_sf_utm <- st_transform(dataset_sf, crs=crs)

  #extract points within polygon

  dataset_sf_utm_clipped <- st_intersection(dataset_sf_utm, shfile)

  return(dataset_sf_utm_clipped)
}

#####
AoI = st_read("AoI_ASPEN_small.shp")
shfileB1 <- st_read("A1small.shp")
shfileB2 <- st_read("A2small.shp")
```



```

shfileF1 <- st_read("B1_FS_Fwc.shp")
shfileF2 <- st_read("B2_FS_Fwc.shp")
roadmask <- st_read("RoadMask.shp")
watermask1 <- st_read("WaterMask1.shp")
watermask2 <- st_read("WaterMask2.shp")
watermask3 <- st_read("WaterMask3.shp")
AoI= st_zm(AoI, drop= TRUE, what="ZM")

#clip roadmask
roadmask <- st_intersection(roadmask,AoI)
ineff_description = c("ineffective")
eff_description <-c("effective")
semi_description <- c("semi-effective")
cul_new <- st_read("effective Cul.shp")
cul_new <- st_transform(cul_new, crs = 26912)

ineff_cul_new <- subset(cul_new, cul_new$Descript %in% ineff_description)
eff_cul_new <- subset(cul_new, cul_new$Descript %in% eff_description)
eff_cul_new <- subset(eff_cul_new, (!eff_cul_new$Name %in% c("EC2","EC3","EC1")))
semi_eff <- subset(cul_new, cul_new$Descript %in% semi_description)
#####

#automated run

file_list <- list.files(pattern = "*.csv")
years <- seq(2017,2022)

#typ = "v_"
typ = "v-do_"

color_min <- -80
color_max <- 60

for (year_to_filter in years){
  #filter for all folders containing the searched year in the name, loop it from 2017 till 2022
  filtered_files_1year <- file_list[grep(paste0(typ,year_to_filter),file_list)]

  for (csv_file in filtered_files_1year) {
    #Create uniform df names based on year and orbit (extracted from csv_file name)
    file_name <- strsplit(csv_file, "_")[[1]]
    orbit_name <- strsplit(file_name[3], "\\.")[[1]]
    year_orbit <-paste(file_name[length(file_name)-1], orbit_name[1], sep="_")
    df_name <- paste0("df",year_orbit, collapse= "_") #collapse is like sep, but only
inbetween and not in the end

    ds <- load.stamps(csv_file)
    ds_variable <- ds$ps.loc
    colnames(ds_variable)<- c("uid", "lon", "lat", "disp", as.character(ds$dates.date))

    #extract relevant variables
    ds_relevant <- ds_variable[c("disp", "lat", "lon")]

    # perform clipping by AoI
    clipped_data <- clip_sf_data(ds_relevant, AoI)
    h <- ggplot(data= clipped_data)+
      geom_histogram(aes(x = disp), bins = 80, fill = "lightblue", color = "black")+
      scale_x_continuous(breaks = seq(-80,50, by =10))+
      labs(x= "Displacement", y = "Frequency", title = " Histogramm of Displacement")+
      theme_bw()

    filenamehisto <- paste0("PSI_hist_",year_orbit,".png")
    ggsave(filename = filenamehisto, plot = h, width = 21, height = 10, units = "cm", dpi =

```

```

300)

#colors <- RColorBrewer::brewer.pal(10, "BrBG")
#scale <- scales::rescale(c(-80,0,20,40))
p <- ggplot(data = clipped_data)+
  geom_sf(data= clipped_data, aes(color=disp), size = 0.2)+
  #scale_color_viridis_c(name = "Displacement", option = "D", limits = c(color_min,
color_max))+ Alternative
  scale_color_gradientn(colors= RColorBrewer::brewer.pal(10,"BrBG"), limits=c(-40,40),
breaks = seq(-40,40,by = 10), na.value = "transparent")+
  geom_sf(data= roadmask, fill = "gray")+
  geom_sf(data= watermask1, fill= "darkblue")+
  geom_sf(data= watermask2, fill= "darkblue")+
  geom_sf(data= watermask3, fill= "darkblue")+
  geom_sf(data= shfileB1, fill= "transparent", color = "black")+
  geom_sf(data= shfileB2, fill= "transparent", color = "black")+
  geom_sf(data= shfileF1, fill= "transparent", color = "black")+
  geom_sf(data= shfileF2, fill= "transparent", color = "black")+
  geom_sf(data= ineff_cul_new, shape = 4, color= "red", size = 2)+
  geom_sf(data= eff_cul_new, shape =4, color = "blue", size = 2)+
  geom_sf(data= semi_eff, shape = 4, color = "purple", size = 2)+

  labs(fill = "Displacment", title = paste0("PSI velocity (mm/year) - ", gsub("_", " ",
gsub("([a-z])([A-Z])", "\\1 \\2",year_orbit))))+

  theme_bw() +
  theme(plot.title = element_text(size = 10),legend.position = "right", legend.title =
element_text("Displacement", size = 8, vjust = 0.2) ,plot.margin = margin(35,20,20,20),
axis.text.x = element_text(angle = 45, hjust =1))

  filenamevelo <- paste0("PSI_velo_",year_orbit,".png")
  ggsave(filename=filenamevelo, plot = p, width = 21, height = 10, units = "cm", dpi =
300)
}
}

```

SBAS Velocity

###import Libraries

```
library(raster)
library(rgdal)
library(rhdf5)
library(sf)
library(ggplot2)
library(reshape2)
library(data.table)
library(scales)
library(RColorBrewer)
```

#####

#set wkdir

```
wkdir <- getwd()
wkdir
#setwd("Documents")
```

#specify the parent direcorey containing the folders

```
parent_dir <- "Mintpy"
```

#Get a List of all directories within the parent directory

```
all_dirs <- list.dirs(parent_dir, recursive = FALSE) #recursive = FALSE, to not go into
subdirectories
```

#Filter the list of expressions based on the criteria using regular expressions

```
filtered_dirs <- all_dirs[grepl("^Mintpy/Mintpy", all_dirs)]
```

#####

```
years <- seq(2017,2022)
```

```
AoI_filepath = "Mintpy/Mask_shapefiles/AoI_ASPEN_small.shp"
```

```
shfileB1 <- st_read("Mintpy/Mask_shapefiles/A1small.shp")
shfileB2 <- st_read("Mintpy/Mask_shapefiles/A2small.shp")
shfileF1 <- st_read("Mintpy/Mask_shapefiles/B1_FS_Fwc.shp")
shfileF2 <- st_read("Mintpy/Mask_shapefiles/B2_FS_Fwc.shp")
roadmask <- st_read("Mintpy/Mask_shapefiles/RoadMask.shp")
watermask1 <- st_read("Mintpy/Mask_shapefiles/WaterMask1.shp")
watermask2 <- st_read("Mintpy/Mask_shapefiles/WaterMask2.shp")
watermask3 <- st_read("Mintpy/Mask_shapefiles/WaterMask3.shp")
```

#read Well GPS points

```
ineff_description = c("ineffective")
eff_description <- c("effective")
semi_description <- c("semi-effective")
cul_new <- st_read("effective Cul.shp")
cul_new <- st_transform(cul_new, crs = 32612)
```

```
ineff_cul_new <- subset(cul_new, cul_new$Descript %in% ineff_description)
eff_cul_new <- subset(cul_new, cul_new$Descript %in% eff_description)
semi_eff <- subset(cul_new, cul_new$Descript %in% semi_description)
```

#Create Loop for graphs

```
read_aperm_converttoraster_georeference_clippAoI_hdf5 <- function(filepath, xmin = 488720,
xmax = 500800, ymin = 6310080, ymax = 6336000, crs = "+init=epsg:32612",
AoI_filepath="Mintpy/Mask_shapefiles/AoI_ASPEN_small.shp", Velocity = TRUE){
  h5_file <- H5Fopen(filepath, "H5F_ACC_RDONLY")
  #Read the velocity dataset and permuate
  velocity <- h5read(h5_file, "velocity")
  velocity <- aperm(velocity, c(2,1))
```

```

velocityStd <- h5read(h5_file, "velocityStd")
velocityStd <- aperm(velocityStd,c(2,1))

# close HDF5 file
H5Fclose(h5_file)

#####
#convert matrix to a raster
velocity_ra <- raster(velocity)
velocityStd_ra <- raster(velocityStd)

#####
#georeference raster
extent(velocity_ra) <- c(xmin = xmin, xmax = xmax, ymin =ymin, ymax= ymax)
extent(velocityStd_ra) <- c(xmin = xmin, xmax = xmax, ymin = ymin , ymax= ymax)
projection(velocity_ra) <- CRS(crs)
projection(velocityStd_ra) <- CRS(crs)

AoI<- st_read(AoI_filepath)
AoI= st_zm(AoI, drop= TRUE, what="ZM")

#Crop Raster
velocity_ra_aoi <- crop(velocity_ra, AoI)
velocity_ra_aoi <- mask(velocity_ra_aoi, AoI)

velocityStd_ra_aoi <- crop(velocityStd_ra, AoI)
velocityStd_ra_aoi <- mask(velocityStd_ra_aoi, AoI)

#chanfe unit to millimeters instead of meters
velocity_ra_aoi <- velocity_ra_aoi * 1000
velocityStd_ra_aoi <- velocityStd_ra_aoi * 1000

#return results
# if (velocity){
#   return(velocity_ra_aoi)
#} else{
#   return(velocityStd_ra_aoi)}
return(velocity_ra_aoi)
}

#set colorrange
breaks <- c(-100, -80, -60, -40, -20, -0.1, 0, 0.1, 20, 40, 60, 80)
num_col <- 11
palette <-brewer.pal(num_col, "BrBG")
#palette <- viridis(num_col, option = "D", begin = 0, end = 1)

#Loop through each folder
for (year_to_filter in years){
  #filter for all folders containing the searched year in the name, Loop it from 2017 till
  2022
  filtered_dirs_1year <-
  filtered_dirs[grepl(paste0("Mintpy_",year_to_filter),filtered_dirs)]

  for (folder in filtered_dirs_1year) {
    #construct the full path to the velocity.h5 hdf5 file
    file_path <- file.path(folder, "velocity.h5")

```

```

#Check if the first file exists
folder_name <- strsplit(folder, "_")[1][1]
year_orbit <- paste(folder_name[length(folder_name)-1],
folder_name[length(folder_name)], sep="_")
ra_name <- paste0("ra",year_orbit, collapse= "_") #collapse is like sep, but only
inbetween and not in the end
ra_velo <- read_aperm_converttoraster_georeference_clippAoI_hdf5(filepath= file_path)
assign(ra_name, ra_velo, envir =.GlobalEnv)
print(ra_name)

main= paste("SBAS Velocity (in mm/year) -", gsub("_", " ", gsub("([a-z])([A-Z])", "\\1
\\2",year_orbit)))

filename <- paste0("velocity_Plot_", ra_name, ".png")
storage_path <- paste0(wkdir, "/", filename)
png(storage_path)

#Plot
par(mar=c(5,5,5,4),xpd= TRUE) # set the plot margins (in inches) to 5 an all sides #xpd
= boolean, clipping to plot or clipping to figure region
#plot

plot(ra_velo, legend = T, main =main, legend, breaks = breaks, col = palette)
grid(nx= NULL, ny = NULL, col= "black",lty="dotted") #nx and ny control the number of
gridlines, NULL sets to default value which depends on plot size
plot(shfileB1$geometry, add=TRUE) #, border= "red")
plot(shfileB2$geometry, add=TRUE) #, border= "red")
plot(shfileF1$geometry, add=TRUE) #, border= "red")
plot(shfileF2$geometry, add=TRUE) #, border= "red")
plot(roadmask$geometry, add=TRUE, col = "white")
plot(watermask1$geometry, add= TRUE, col = "darkblue", density=10, fill = TRUE) #col =
"darkblue",
plot(watermask2$geometry, add= TRUE, col = "darkblue", density = 0.5)
plot(watermask3$geometry, add= TRUE, col = "darkblue", density = 0.3)

plot(ineff_cul_new$geometry, pch =3, col = "blue", lwd =2,add=TRUE)
plot(ineff_cul_new$geometry, pch = 3, col ="red", lwd=2,add=TRUE)
plot(semi_eff$geometry, pch = 3, col ="purple",lwd = 2, add=TRUE)
#plot(impound$geometry, pch ="+", col ="purple", add=TRUE)
#points(effective_cul$Longitude,effective_cul$Latitude, pch = 3, cex =2, col = "red")

#first Legend
legend_text <-c("Water", "Road", "Ecosites", "ineff culvert", "eff culverts", "semi eff
cuverts")
legend_colors <- c("darkblue", "white", "black", "red", "blue", "purple")
#Legend_symbols <- c(16,16,16,4,4)

legend("topright",inset=c(-0.34,-0.02),xpd= TRUE,legend = legend_text, title="Legend",
col = legend_colors, pch= rep(c(16,4), times= c(3,3)), lwd = 0.5, bty="o", bg="lightgray",
x.intersp =0.9, y.intersp = 0.9, cex = 0.8 )

dev.off()
}
}

```

Focus 2021

###import Libraries

```
library(raster)
library(rgdal)
library(rhdf5)
library(sf)
library(ggplot2)
library(htmltools)
library(ggtext)
library(dplyr)
library(tidyr)

#####
#set wkdir
getwd()
#make sure wd = "/Documents", otherwise use setwd("Documents"), or remove one level with
setwd("../")
#specify the parent direcorey containing the folders
parent_dir <- "Mintpy"

#Get a List of all directories within the parent directory
all_dirs <- list.dirs(parent_dir, recursive = FALSE) #recursive = FALSE, to not go into
subdirectories

#Filter the list of expressions based on the criteria using regular expressions
filtered_dirs <- all_dirs[grepl("^Mintpy/Mintpy", all_dirs)]

#filter for the year in the name
#years <- seq(2017,2022)
years = 2021
df_list <- list()
#####
# create a function for the processes between reading hdf5 file and returning a dataframe
(Date,Mean Values, Median Values) #changed epsg to 26912 from 32612(asia)
reading_clipping_exporting_hdf5 <- function(filepath, shapefile, xmin = 488720, xmax =
500800, ymin =6310080 , ymax= 6336000, crs ="+init=epsg:26912" ){
  "this function reads a hdf5 file
  take the timeseries data and stack it to a new raster layer
  clips it by a shapefile (which has to be georeferenced first)
  and returns a dataframe containing the date as variablenames and the non NA values as
observables"

  #Load the raster to clip
  #Data is in hdf5 files, need to create rasters from it and stack them

  #Read the HDF5 file
  h5_file <- H5Fopen(file_path, "H5F_ACC_RDONLY")

  #Read the timeseries dataset
  timeseries <- h5read(h5_file, "timeseries")

  #change dimensions of array
  timeseries_permuted <- aperm(timeseries,c(2,1,3))
  timeseries <- timeseries_permuted

  date <- h5read(h5_file, "date")

  #convert the timeseries data to a List of rasters
  rasters <- lapply(1:dim(timeseries)[3],function(i){
    raster(timeseries[ , ,i])
  })
```

```

#convert the list to a rasterstack object
raster_stack <- stack(rasters)

#set the extent and projection of the rasterstack object
extent(raster_stack) <- c(xmin, xmax, ymin , ymax)
projection(raster_stack) <- CRS(crs)
plot(raster_stack[[1]])
# close HDF5 file
H5Fclose(h5_file)

#georeference shapefile
shfile <- st_transform(shapefile, crs = crs(raster_stack))
#Make xy shape, drop Z and M
shfile= st_zm(shfile, drop= TRUE, what="ZM")

#crop the raster to the extent of the shapefile
raster_cropped <- crop(raster_stack, extent(shfile))

#clipp the raster stack with the shapefile raster
rstack_clipped <- mask(raster_cropped, shfile)

date <- as.Date(date, format= "%Y%m%d")
#values_df <- data.frame(matrix(ncol = nlayers(rstack_clipped), nrow =
prod(dim(rstack_clipped[[1]]))))
values_df <- list()
for (element in 1:nlayers(rstack_clipped)){

  layer_values <- as.data.frame(rstack_clipped[[element]])

  layer_values <- na.omit(layer_values, drop = FALSE)

  #name the column with corresponding date
  #date <- format(date, "%Y-%m-%d")
  colnames(layer_values) <- date[element]

  #add the values to the dataframe as a new column
  values_df[[element]] <- layer_values

}
#merge data.frames in one data.frame
merged_df <- do.call(cbind, values_df)

return(merged_df)
}

#####
#prepare the shapefile of the ecosite

shapefiles <-
c("Mintpy/Mask_shapefiles/A1small.shp", "Mintpy/Mask_shapefiles/A2small.shp", "Mintpy/Mask_shapefiles/B1_FS_Fwc.shp", "Mintpy/Mask_shapefiles/B2_FS_Fwc.shp")
xx <- 1
shname <- c("B1", "B2", "F1", "F2")
shfile <- st_read(shapefiles[xx])
ecosite <- shfile$Name
#shfile$geometry

```

```

#plot(shfile["MaskID"])

#####
#Create Loop for graphs

#Loop through each folder
for (year_to_filter in years){
  #filter for all folders containing the searched year in the name, Loop it from 2017 till
  2022
  filtered_dirs_1year <-
  filtered_dirs[grepl(paste0("Mintpy_",year_to_filter),filtered_dirs)]

  for (folder in filtered_dirs_1year) {
    #construct the full path to the timeseries.h5 hdf5 file
    file_path <- file.path(folder, "timeseries.h5")

    #Check if the first file exists
    folder_name <- strsplit(folder, "_")[1][1]
    year_orbit <-paste(folder_name[length(folder_name)-1],
    folder_name[length(folder_name)], sep="_")
    df_name <- paste0("df",year_orbit, collapse= "_") #collapse is like sep, but only
    inbetween and not in the end
    df_variable <-reading_clipping_exporting_hdf5(filepath= file_path,shapefile=
    shfile)*1000 #change unit to mm instead of meters
    assign(df_name, df_variable, envir =.GlobalEnv)
    print(df_name)
  }
}

df_long1 <- df2021_EastOrbit %>%
  pivot_longer(cols = everything(), names_to = "Date", values_to="Value")
df_long2 <- df2021_MiddleOrbit %>%
  pivot_longer(cols = everything(), names_to = "Date", values_to="Value")
df_long3 <- df2021_WestOrbit %>%
  pivot_longer(cols = everything(), names_to = "Date", values_to="Value")

df_long <- rbind(df_long1, df_long2, df_long3)

summary_df <- df_long %>%
  group_by(Date) %>%
  summarise(mean = mean(Value),
            sd = sd(Value),
            n = n())
df_list[[xx]]<- as.data.frame(summary_df)

g <- ggplot(df_long, aes(x = Date, y = Value, group = Date)) +
  #stat_boxplot(geom ="errorbar", width = 5)+
  geom_boxplot(width = 0.5, coef = 1.5, notch = FALSE, outlier.shape = 19, aes(color =
  "Boxplots"), outlier.size = 0.5) + #, outlier.shape = NA

  geom_errorbar(data = summary_df, aes(y = mean, ymin = mean - sd, ymax = mean + sd),
    width = 0.5) + #, color = "blue", linewidth = 0.6
  geom_line(data = summary_df, aes(x = Date, y = mean, group =1, color = "Surface
  Deformation")) +
  geom_point(data= summary_df, aes(x = Date, y = mean, color = "Mean"), pch = 3)+
  geom_smooth(data= summary_df, method = "lm", aes(x=Date,y=mean, group = 1, color
  ="Trend"), linetype ="dashed" )+
  geom_hline(yintercept = 0, linewidth = 0.7)+

  labs(x = "Date", y = "Displacement (mm)") +

```



```

ggtitle(paste0("Merged Orbits 2021, ", shname[xx]))

g <- g +
  labs(colour = "Statistical Parameters")+
  scale_color_manual(values = c("black", "red", "blue", "purple"),
    guide = guide_legend(override.aes = list(shape = c(20, 4,18,18), size
= 3)))+
  theme_bw()+
  theme(plot.margin = margin(35,20,20,20),axis.text.x = element_text(angle = 45, hjust=1),
    legend.key = element_rect(colour = NA, fill = NA),
    legend.key.size = unit(0.4,"cm"),
    legend.key.height = unit(0.4, "cm"),
    legend.key.width = unit(0.5, "cm"),
    legend.title = element_text(size = 5),
    legend.text = element_text(size = 5),
    legend.justification = c(0.98,0.02), legend.position = c(0.98,0.02),
    legend.box.background = element_rect(linewidth = 0.7),
    legend.margin = margin(0.1,0.1,0.1,0.1)) #,
    #legend.key.size = unit(0.15, "cm")) #, legend.key.size = unit(1, "lines")

g
ggsave(paste0("2021_merged_orbits_", shname[xx], ".png"), plot = g, width = 21, height = 10,
units = "cm")

#####
summary_df1 <- df_long1 %>%
  group_by(Date) %>%
  summarise(mean = mean(Value),
    sd = sd(Value),
    n = n())

g <- ggplot(df_long1, aes(x = Date, y = Value, group = Date)) +
  #stat_boxplot(geom = "errorbar", width = 5)+
  geom_boxplot(width = 0.5, coef = 1.5, notch = FALSE, outlier.shape = 19, outlier.colour =
"black", outlier.size = 0.5) + #, outlier.shape = NA

  geom_errorbar(data = summary_df1, aes(y = mean, ymin = mean - sd, ymax = mean + sd),
    width = 0.5) + #, color = "blue", linewidth = 0.6
  geom_line(data = summary_df1, aes(x = Date, y = mean, group = 1), color = "blue") +
  geom_point(data = summary_df1, aes(x = Date, y = mean), color = "red", pch = 3)+
  geom_smooth(data = summary_df1, method = "lm", aes(x = Date, y = mean, group = 1), color
= "blue", linetype = "dotted" )+
  geom_hline(yintercept = 0, linewidth = 1)+

  labs(x = "Date", y = "Displacement (mm)") +
  ggtitle("Focus on statistics 2021 East orbit, B1")+
  theme(plot.margin = margin(35,20,20,20),axis.text.x = element_text(angle = 45, hjust=1))
#, vjust = 0.5

g
ggsave("2021_EastOrbit_Focus.png", plot = g, width = 15, height = 10, units = "cm")

#####
#plot differneces

b1 <- df_list[[1]]
b2 <- df_list[[2]]
f1 <- df_list[[3]]
f2 <- df_list[[4]]

df_b_diff <- data.frame(Date = b1$Date, Difference = b1$mean - b2$mean)
#df_b_diff$Date <- as.Date(df_b_diff$Date)

```

```

df_f_diff <- data.frame(Date = f1$Date, Difference = f1$mean - f2$mean)

g6 <- ggplot(df_b_diff, aes(x = Date, y = Difference, color = "Bog Difference (B1-B2)"))+
  geom_line(aes(group = 1))+
  geom_line(data= df_f_diff, aes(x = Date, y = Difference, color = "Fen Difference (F1-
F2)", group = 1))+
  scale_color_manual(values = c("forestgreen", "lightblue"))+
  geom_hline(yintercept = 0, linewidth = 1)+
  # scale_x_date(labels = function(x) format(x, "%b %y"), date_breaks = "1 month")+
  labs(x = NULL, y= "Displacement ", title = "Ecosite differences 2021", color = "Ecosite
Differences")+
  theme_bw()+
  theme(plot.margin = margin(35,20,20,20), axis.text.x = element_text(angle = 45, hjust =1,
size = 6),
        legend.title = element_text(size = 6),
        legend.text = element_text(size = 6),
        legend.justification = c(0.98,0.02), legend.position = c(0.98,0.02),
        legend.box.background = element_rect(linewidth = 0.7),
        legend.margin = margin(0.1,0.1,0.1,0.1))

g6
ggsave("Ecosite_Diff_2021.png", plot = g6, width = 21, height = 10, units = "cm")

```

Meteo Station Plots

```
library(ggplot2)
library(lubridate)
library(scales)
library(gridExtra)

#setwd
#setwd("..")
#setwd("Documents/data/MetStation/Kearl")
getwd()

#import data
data<- read.csv("Kearl_daily_cleared.csv", header=TRUE, sep=",")

data$season <- ifelse(month(data$date) >=3 & month(data$date) <= 10, "summer", "winter")

data$month <- month(data$date, label = TRUE)
data$date <- as.Date(data$date)

dfs_by_year <- split(data, format(data$date, "%Y"))

#calculate prec sum and temp mean of Jan and July
sum_precp_yearly <- list()
mean_temp_jan <- list()
mean_temp_jul <- list()
for (year in seq(2017,2022)){
  year_df <- dfs_by_year[[as.character(year)]]
  sum_precp_yearly[year-2016] <- sum(year_df$precipitation)
  mean_temp_jan[year-2016] <- mean(year_df$temperature[format(year_df$date, "%m") == "01"])
  mean_temp_jul[year-2016] <- mean(year_df$temperature[format(year_df$date, "%m") == "07"])
}

#combine plots for all years underneath
plot_list <- list()

#Loop
for (year in seq(2017,2022)){
  year_df <- dfs_by_year[[as.character(year)]]
  year_df <- subset(year_df, format(date, "%m") %in% c("05", "06", "07", "08", "09", "10"))

  p <- ggplot(year_df, aes(x = date)) +
    geom_line(aes(y = temperature, color = "Temperature [°C]")) +
    geom_bar(data = year_df, aes(y = precipitation * 2, fill = "Precipitation [mm]"), stat
="identity") +
    scale_y_continuous(sec.axis = sec_axis(trans=~.*0.5, name = "Precipitation (mm)", name
= "Temperature (°C)") +
    scale_x_date(date_labels = "%b", date_breaks = "1 month") +
    labs(x = NULL, title = paste("Kearl Weather Station Data", year)) +
    geom_hline(yintercept = 0, linewidth = 1) +
    theme_bw()

  p <- p +
    scale_color_manual(values = c("Temperature [°C]" = "red", "Precipitation [mm]" =
"steelblue")) +
    scale_fill_manual(values = c("Precipitation [mm]" = "steelblue")) +
    theme(plot.margin = margin(35,20,20,20),
    plot.title = element_text(paste("Kearl Weather Station Data", year)),
    legend.position = c(0.8835, 1.05),
    legend.text = element_text(size = 10), # I changed this to 12, assuming you want
it to be visible
    legend.key.size = unit(0.9, "line" ),
    legend.spacing.y = unit(0, "cm"),
    legend.box.background = element_rect(color = "black", size = 0.5)) +
```

```

guides(fill = guide_legend(title = NULL), color = guide_legend(title = NULL))

#add plot to plot list
plot_list[[as.character(year)]] <- p
p
ggsave(paste0("Kearl_seasonal",year,".png"),p, width = 20, height =8, units = "cm")
}

```

Groundwater Wells

```

library(ggplot2)
library(lubridate)
library(scales)
library(gridExtra)
library(dplyr)

#setwd
#setwd("../")
#setwd("Documents/data/gw_wells")
getwd()

#import data

data<- read.csv("gw_checked_surfacdepth.csv", header=TRUE, sep=",")
#####
data$Date.and.Time <- as.POSIXct(data$Date.and.Time, format = "%d-%m-%Y %H:%M")

variable_names <- names(data)
variable_names1 <- variable_names[c(8,13,15,16,19)]

result_list <- list()
for (var_name in variable_names1){
  data_daily <-mutate(data,date = as.Date(data$Date.and.Time))
  data_daily <- data_daily %>%
    group_by(date) %>%
    summarize(!var_name := mean(!as.name(var_name),na.rm =TRUE))
  result_list[[var_name]] <-data_daily
}

#write.csv(result_list, "selected_wells_daily.csv", row.names = FALSE)

#data_daily<- read.csv("selected_wells_daily.csv", header=TRUE, sep=",")
#####
#plot wells T2-2, T4-NC-2 for south and T3-EC-3, T1-5 for north side
#change to T2_5
#t2_2 <-
data.frame(result_list$MAR.T2.2.checked.$date,result_list$MAR.T2.2.checked.$MAR.T2.2.checked.$date)
#colnames(t2_2)[1]<- "Date"
#colnames(t2_2)[2]<- "T2_2"
t2_5 <-
data.frame(result_list$MAR.T2.5.checked.$date,result_list$MAR.T2.5.checked.$MAR.T2.5.checked.$date)
colnames(t2_5)[1]<- "Date"
colnames(t2_5)[2]<- "T2_5"
t4_2 <-
data.frame(result_list$MAR.T4.NC.2.checked.$date,result_list$MAR.T4.NC.2.checked.$MAR.T4.NC.2.checked.$date)
colnames(t4_2)[1]<- "Date"

```

```

colnames(t4_2)[2]<- "T4_2"
t3_3 <-
data.frame(result_list$MAR.T3.EC.3.checked.$date,result_list$MAR.T3.EC.3.checked.$MAR.T3.EC
.3.checked.*-1)
colnames(t3_3)[1]<- "Date"
colnames(t3_3)[2]<- "T3_3"
t1_5 <-
data.frame(result_list$MAR.T1.5.checked.$date,result_list$MAR.T1.5.checked.$MAR.T1.5.checked
.*-1)
colnames(t1_5)[1]<- "Date"
colnames(t1_5)[2]<- "T1_5"
t3_4 <-
data.frame(result_list$MAR.T3.EC.4.checked.$date,result_list$MAR.T3.EC.4.checked.$MAR.T3.EC
.4.checked.*-1)
colnames(t3_4)[1]<- "Date"
colnames(t3_4)[2]<- "T3_4"

p <- ggplot(data= t2_5, aes(x= Date, y= T2_5))+
  geom_smooth(aes(color = "T2_5 Fen South"), span = 0.07, se= FALSE)

p <- p +
  geom_smooth(data = t4_2, aes(x= Date, y= T4_2, color = "T4_2 Fen South"), span = 0.07)+
  geom_line(data = t4_2, aes(x = Date, y = T4_2, color = "T4_2 Fen South"))

p <- p +
  geom_smooth(data= t3_3, aes(x= Date, y= T3_3, color = "T3_3 Fen North"), span= 0.07, se =
FALSE)

p <- p +
  geom_smooth(data= t1_5, aes(x= Date, y= T1_5, color = "T1_5 Fen North"), span = 0.07, se
= FALSE)

'p<- p+
  geom_line(data = t3_4, aes(x = Date, y = T3_4, color = "T3_4"), linewidth = 0.2, alpha =
0.3)'

p <- p +
  scale_x_date(labels = function(x) format(x, "%b %y"), date_breaks = "1 month")+
  labs(x = NULL,y= "WT depth to surface", title = "Selected GW Wells")+
  theme_bw()+
  theme(plot.margin = margin(35,20,20,20), axis.text.x = element_text(angle = 45, hjust
=1))

p <- p +
  geom_hline(yintercept = 0, linewidth = 1)

p <- p +
  labs(colour = "Groundwater Wells")+
  scale_color_manual(values = c( "limegreen","steelblue", "forestgreen", "lightblue"))

p

ggsave("gw_well3.png", plot = p, width = 21, height = 10, units = "cm", dpi = 300)

# plot only May-Oct

#automatic way:

names_list = c("t1_5","t2_2","t3_3", "t3_4","t4_2")
dataframelist <- list(t1_5 = t1_5,t2_2=t2_2, t3_3=t3_3, t3_4=t3_4, t4_2=t4_2)
new_datasets <-list()

```

```

for (name in names_list){
  new_datasets[[paste0(name, "_", 21)]]<-
dataframelist[[name]][substr(dataframelist[[name]]$Date, 1,4) == "2021",]
  new_datasets[[paste0(name, "_", 22)]]<-
dataframelist[[name]][substr(dataframelist[[name]]$Date, 1,4) == "2022",]
}

element_names <- names(new_datasets)
for (element in element_names){
  new_datasets[[element]] <- subset(new_datasets[[element]], format(Date, "%m") %in%
c("05", "06", "07", "08", "09", "10"))
}
#Extract all elements as a separat data frame
for (i in seq_along(new_datasets)){
  assign(element_names[i], new_datasets[[i]])
}

#plot 21 season

g21 <- ggplot(data= t2_2_21, aes(x= Date, y= T2_2))+
  geom_smooth(color = "steelblue", span = 0.07, se= FALSE)
  #geom_Line(color = "steelblue")

g21 <- g21 +
  geom_smooth(data = t4_2_21, aes(x= Date, y= T4_2), color = "lightblue", span = 0.07)
  #geom_Line(data = t4_2_21, aes(x = Date, y = T4_2), color = "lightblue")

g21 <- g21 +
  geom_smooth(data= t3_3_21, aes(x= Date, y= T3_3),color = "limegreen", span= 0.07, se =
FALSE)
  #geom_Line(data= t3_3_21, aes(x = Date, y = T3_3), color = "limegreen")

g21 <- g21 +
  geom_smooth(data= t1_5_21, aes(x= Date, y= T1_5),color = "forestgreen", span = 0.07, se =
FALSE)
  #geom_Line(data= t1_5_21, aes(x= Date, y= T1_5),color = "forestgreen")

#g21<- g21+
  #geom_Line(data = t3_4_21, aes(x = Date, y = T3_4), color = "black" , linewidth = 0.2,
alpha = 0.3)
  #geom_Line(data = t3_4_21, aes(x = Date, y = T3_4), color = "black" )

g21 <- g21 +
  scale_x_date(labels = function(x) format(x, "%b %y"), date_breaks = "1 month")+
  labs(x = NULL,y= "WT depth to surface ", title = "Selected GW Wells - 2021")+
  theme_bw()+
  theme(plot.margin = margin(35,20,20,20), axis.text.x = element_text(angle = 45, hjust
=1))

g21 <- g21 +
  geom_hline(yintercept = 0, linewidth = 1)

g21 <- g21 +
  scale_color_identity(name = "Legend",
breaks = c("steelblue", "lightblue", "limegreen", "forestgreen"),
labels = c("T2_2 Fen South","T4_2 Fen South","T3_3 Fen North", "T1_5
Fen North"),
guide = "legend" )+
  labs()
g21

ggsave("gw_21seasonal_smooth.png", plot = g21, width = 21, height = 10, units = "cm", dpi =
300)

```

```

#plot 22

g22 <- ggplot(data= t2_2_22, aes(x= Date, y= T2_2))+
  geom_smooth(color = "steelblue", span = 0.07, se= FALSE)
#geom_line(color = "steelblue")

g22 <- g22 +
  geom_smooth(data = t4_2_22, aes(x= Date, y= T4_2), color = "lightblue", span = 0.07)
#geom_line(data = t4_2_22, aes(x = Date, y = T4_2), color = "lightblue")

g22 <- g22 +
  geom_smooth(data= t3_3_22, aes(x= Date, y= T3_3),color = "limegreen", span= 0.07, se =
FALSE)
#geom_line(data= t3_3_22, aes(x = Date, y = T3_3), color = "limegreen")

g22 <- g22 +
  geom_smooth(data= t1_5_22, aes(x= Date, y= T1_5),color = "forestgreen", span = 0.07, se =
FALSE)
#geom_line(data= t1_5_22, aes(x= Date, y= T1_5),color = "forestgreen")

g22<- g22+
  geom_line(data = t3_4_22, aes(x = Date, y = T3_4), color = "black" , linewidth = 0.2)
#geom_line(data = t3_4_22, aes(x = Date, y = T3_4), color = "black" )

g22 <- g22 +
  scale_x_date(labels = function(x) format(x, "%b %y"), date_breaks = "1 month")+
  labs(x = NULL,y= "WT depth to surface ", title = "Selected GW Wells - snow free period
2022")+
  theme_bw()+
  theme(plot.margin = margin(35,20,20,20), axis.text.x = element_text(angle = 45, hjust
=1))

g22 <- g22 +
  geom_hline(yintercept = 0, linewidth = 1)

g22 <- g22 +
  scale_color_identity(name = "Legend",
breaks = c("steelblue", "lightblue", "limegreen", "forestgreen"),
labels = c("T2_2 Fen South","T4_2 Fen South","T3_3 Fen North", "T1_5
Fen North"),
guide = "legend" )+
  labs()
g22

ggsave("gw_22seasonal_smooth.png", plot = g22, width = 21, height = 10, units = "cm", dpi =
300)

```

Eidesstaatliche Erklärung

Hiermit erkläre ich, dass die vorliegende Arbeit selbstständig verfasst worden ist, noch nicht anderweitig für Prüfungszwecke vorgelegt, keine anderen als die angegebenen Quellen oder Hilfsmittel benutzt, sowie Zitate als solche gekennzeichnet worden sind.

Westerheim, 21.06.2023

A handwritten signature in black ink, reading 'Heiß Niklas'. The signature is written in a cursive style, with the first name 'Heiß' and the last name 'Niklas' clearly legible.

Niklas Heiß